Spring 1-1-2012

# Application of UV/H2O2 Advanced Oxidation for Treatment of Pharmaceuticals in Wastewater

Olya S. Keen
*University of Colorado at Boulder*, olya.keen@gmail.com

# APPLICATION OF UV/$H_2O_2$ ADVANCED OXIDATION FOR TREATMENT OF PHARMACEUTICALS IN WASTEWATER

by

OLYA S KEEN

B.S., University of South Florida, 2008

M.S., University of South Florida, 2008

A thesis submitted to the

Faculty of the Graduate School of the

University of Colorado in partial fulfillment

of the requirement for the degree of

Doctor of Philosophy

Department of Civil, Environmental and Architectural Engineering

2012

This thesis entitled:
Application of UV/$H_2O_2$ Advanced Oxidation for Treatment of Pharmaceuticals in Wastewater
written by Olya S Keen
has been approved for the Department of Civil, Environmental and Architectural Engineering

Karl Linden

Fernando Rosario-Ortiz

Date 11/26/12

The final copy of this thesis has been examined by the signatories, and we find that both the content and the form meet acceptable presentation standards of scholarly work in the above mentioned discipline.

Keen, Olya S (Ph.D., Civil, Environmental and Architectural Engineering)

Application of UV/$H_2O_2$ Advanced Oxidation for Treatment of Pharmaceuticals in Wastewater

Thesis directed by Professor Karl G. Linden

Advanced oxidation processes (AOPs) are an effective treatment technology for a variety of organic pollutants. Hydroxyl radicals (HO•) are the main reactive species in the process. In this work, application of UV/$H_2O_2$ AOP for treatment of pharmaceuticals in wastewater was studied. Two aspects of the process were investigated: (1) the properties of the transformation products of the pharmaceutical pollutants, and (2) the effects of the background water matrix on the efficiency of the process.

Because AOP does not completely remove the parent molecule but rather transforms it into a product, it is important to understand whether the product retains the environmentally relevant properties of the parent molecule. This study evaluates the biodegradability of the products of biologically recalcitrant pharmaceuticals as well as changes in antibacterial activity of antibiotics, as they get transformed by AOP. Mass spectrometry, liquid scintillation counting and biological assays were used to quantify the effect of AOP on the properties of the transformation products.

Many background water matrix constituents in effluents are highly reactive with HO• and decrease the efficiency of the process. Effluent dissolved organic matter (EfOM) in particular is one of the major sinks of HO• in the urban water cycle. Because of the non-homogeneous nature of EfOM, its reactivity with HO• is variable and makes the process modeling more difficult. A statistical model was developed in this work to analyze correlations between the reactivity of EfOM with HO• and the bulk properties of EfOM, water quality

parameters, treatment train characteristics, and fluorescence derived data. The statistical analysis identified a set of dominant predictors for the reactivity between EfOM and HO•. In addition to HO• scavenging compounds, there are also background constituents that can generate HO•. Nitrate in particular is a common constituent in effluents known to generate HO• when exposed to UV. The efficiency of using nitrate rather than hydrogen peroxide for generation of HO• when using UV sources emitting in the 200-240 nm wavelength range was evaluated, and a model was devised to predict the outcome of the process.

Overall, the results of this work advance the fundamental scientific understanding of UV/$H_2O_2$ AOP and will help to guide engineering decisions in its applications to wastewater for the treatment of emerging contaminants.

## Acknowledgements

A great number of people and organizations made this research possible. The funding was provided by the US Environmental Protection Agency graduate fellowship Science to Achieve Results (STAR) grant No. 91713601 and by Water Environment Research Foundation grants INFR6SG09 and U2R11.

I would like to thank my advisor Professor Karl Linden for all the guidance he provided through my academic career at the University of Colorado, for all the tireless and detailed revisions, and the sincere interest and investment in my success. My thanks also go to the many people who provided collaboration and advice, to all of my mentors and mentees, to the committee members and to the collaborating utilities. I have learned a lot from all of you and would not be here if it wasn't for your help. Thanks to my undergraduate professors who inspired me to get a PhD and believed I could do it. Thanks to the Linden lab members for sharing the moments of joy and commiseration in the labwork and for the new friendships. And last but not least, thanks to my family and friends for their love and moral support through this sometimes grueling experience.

## Table of Contents

Chapter 1: Introduction ..... 1
Chapter 2: Biodegradability of the post-AOP products of recalcitrant pharmaceuticals ..... 9
2.1 Materials and Methods ..... 9
2.1.1 Chemicals, Samples and Cultures ..... 9
2.1.2 Analytical Methods and Experimental Protocols ..... 11
2.2 Results and Discussion ..... 20
Chapter 3: Degradation of antibacterial activity of antibiotics ..... 30
3.1 Materials and Methods ..... 30
3.1.1 Reagents ..... 30
3.1.2 Photolysis and advanced oxidation ..... 31
3.1.3 Antibacterial activity assays ..... 32
3.1.4 HPLC/MS analysis ..... 34
3.2 Results and Discussion ..... 34
3.2.1 Advanced oxidation ..... 34
3.2.2 Direct photolysis ..... 38
Chapter 4: Formation of hydroxyl radicals during photolysis of nitrate at 200-240 nm wavelength ..... 42
4.1 Materials and Methods ..... 42
4.1.1 Chemicals and reagents ..... 42
4.1.2 UV systems ..... 43
4.1.3 Test methods ..... 43
4.1.4 Experimental procedure ..... 44
4.1.5 Model Development ..... 44
4.2 Results and Discussion ..... 49
4.2.1 Degradation of carbamazepine in nitrified effluent ..... 49
4.2.2 HO• production from nitrite in clean water ..... 50
4.2.3 HO• production from nitrate in clean water ..... 52
4.2.4 Generation of HO• by nitrate in nitrified effluents ..... 54
4.2.5 Implications for wastewater treatment utilities ..... 62
Chapter 5: Reactivity of effluent organic matter with hydroxyl radical ..... 65
5.1 Materials and methods ..... 65
5.1.1 Effluent samples ..... 65
5.1.2 Reaction rate constants ..... 67

5.1.3 Variables ..... 69
5.1.4 Statistical analysis ..... 73
5.2 Results ..... 74
5.2.1 Model results and evaluation ..... 74
5.2.2 Treatment train effects ..... 79
Chapter 6: Summary and conclusions ..... 83
References ..... 85

## List of Tables

Table 1: Water quality measurements for the effluents ..... 11

Table 2: Summary of antibiotics used in the study ..... 30

Table 3: Effluent water quality ..... 30

Table 4: Water quality measurements for the two effluents used in the study ..... 55

Table 5: Hydroxyl radical scavengers and the corresponding reaction rate constants with HO• 58

Table 6: Wastewater treatment trains of the participating utilities ..... 65

Table 7: Water quality for the samples ..... 66

Table 8: Modeling parameters ..... 75

## List of Figures

Figure 1: Carbamazepine and iopromide structures and location of $^{14}C$ atom ..... 10

Figure 2: Experimental setup for assessing the biological stability of effluents treated with AOP versus those not treated with AOP. ..... 15

Figure 3: Oxidation products retained after rotary evaporation compared to solid phase extraction. ..... 17

Figure 4: Change in $SUVA_{254}$ during degradation of effluent with activated sludge, both with and without carbamazepine (CBZ). ..... 18

Figure 5: Radioactivity of effluents before and after AOP, before commencement of the biotransformation step ..... 20

Figure 6: Migration of radiolabeled $CO_2$ from the main sample bottle into the $CO_2$ traps during biodegradation of carbamazepine ..... 22

Figure 7: Comparison of abiotic mineralization of iopromide with and without sodium azide ..... 22

Figure 8: Carbamazepine Sample 1 mass balance ..... 23

Figure 9: Iopromide mass balance ..... 24

Figure 10: Radiochromatogram of untreated and AOP treated samples ..... 26

Figure 11: $UV_{254}$ absorbance chromatogram of the sample pretreated with AOP after 25 days of biodegradation ..... 27

Figure 12: Extracted ion chromatogram for tricyclic fragment of carbamazepine (m/z 194) of the sample pretreated with AOP after 25 days of biodegradation ..... 26

Figure 13: MS chromatogram of the AOP-treated carbamazepine in effluent before biotransformation and after 25 days of biotransformation ..... 27

Figure 14: Proposed products of carbamazepine advanced oxidation. ....28

Figure 15: Decrease of antibacterial activity of antibiotics (potency equivalent) with corresponding decrease in the concentration of the parent antibiotic after advanced oxidation treatment ....35

Figure 16: Decrease of antibacterial activity of antibiotics (potency equivalent) with corresponding decrease in the concentration of the parent antibiotic after photolysis without $H_2O_2$ addition ....39

Figure 17: Fraction of initial antibiotic still remaining in effluent after 1000 mJ/cm$^2$ and 2000 mJ/cm$^2$ with different treatment....41

Figure 18: Simplified photolysis pathway from nitrate to hydroxyl radical. ....46

Figure 19: Degradation of carbamazepine in wastewater effluent containing 16.2 mg-N/L of nitrate with and without 5 mg/L of $H_2O_2$ ....50

Figure 20: Formation of HO• during irradiation of varying nitrite concentrations with MP UV ....51

Figure 21: Formation of HO• at varying nitrate concentrations ....52

Figure 22: Formation of HO• per mg/L of $H_2O_2$ and $NO_3^-$ in clean water ....54

Figure 23: Molar absorption of nitrite, nitrate and hydrogen peroxide ....57

Figure 24: Degradation of methylene blue in the effluent with 10.3 mg-N/L nitrate and 4.04 mg-N/L nitrate with and without additional hydrogen peroxide ....57

Figure 25: Measured vs. predicted values of [HO•]ss ....60

Figure 26: (a) Correlation between the average germicidal irradiance normalized to absorbance at 223 nm (x-axis) and the specific rate of light absorption by

nitrate (y-axis); (b) Specific rate of light absorption by nitrate as a function of wavelength. ....62

Figure 27: Expected degradation of organic contaminants in nitrified effluents with high (≈$5.7 \cdot 10^{-14}$ M) and low (≈$3.0 \cdot 10^{-14}$ M) [HO•]ss generating potential, as a function of the contaminant's reaction rate constant with HO•. ....64

Figure 28: Principal component analysis results indicating the contribution to explaining the variability in the data by each additional variable ....76

Figure 29: (a) Predicted vs. measured values of $k_{OH,EfOM}$; (b) Cross-validated vs. measured values of $k_{OHEfOM}$ ....77

Figure 30: Percent error in predicting the fluence required for 90% removal of methylene blue in the effluent samples using the modeled $k_{HO,EfOM}$, the value determined for NOM isolates, and the average value for EfOM determined in this study ....79

Figure 31: $k_{HO,EfOM}$ after different biological treatment steps at a single wastewater treatment plant ....80

Figure 32: Variability of $k_{HO,EfOM}$ for different size utilities ....81

Figure 33: Average $k_{HO,EfOM}$ for plants with different SRT ranges....81

# Chapter 1: Introduction

Advanced oxidation process (AOP) is a treatment technology involving generation of hydroxyl radicals. These radicals non-selectively react with most organic and some inorganic compounds typically at diffusion control reaction rates. As a result, advanced oxidation processes present an attractive treatment technology for addressing organic pollutants in a variety of applications. Several processes fit into the category of advanced oxidation processes: combination of ozone ($O_3$) and hydrogen peroxide ($H_2O_2$), ultraviolet irradiation (UV) and $H_2O_2$, UV and $O_3$, Fenton reaction, photo-Fenton reaction, photocatalysis and gamma-radiolysis among the most commonly studied ones. The focus of this study is the UV/$H_2O_2$ AOP and its application for treatment of municipal wastewater for mitigation of environmental pollution with pharmaceuticals.

Wastewater treatment plants' effluent had been determined to be one of the major sources of pharmaceuticals entering the environment (Kümmerer 2001; Kolpin, Furlong et al. 2002). Many of the compounds detected in effluents have been since proven to cause environmental damage. Estrogenic compounds have been shown to cause endocrine system disruption in aquatic organisms (Lye, Frid et al. 1997; Routledge, Sheahan et al. 1998; Vajda, Barber et al. 2008), psychoactive compounds affect the predator avoidance behavior (Painter, Buerkley et al. 2009), some compounds have shown physiological effects (Fraker and Smith 2004), and a variety of pharmaceuticals are toxic to smaller organisms at environmental levels (Fent, Weston et al. 2006).

In addition to environmental effects, there are concerns about effects on human health. A connection between trace levels of antibiotics released by wastewater treatment facilities and

proliferation of antibiotic resistance has been demonstrated by multiple studies. These trends have been reported downstream of an antibiotic manufacturer discharge (Li, Qi et al. 2011), facility treating hospital wastewater (Galvin, Boyle et al. 2010; Chagas, Seki et al. 2011) and pharmaceutical manufacturing wastewater (Guardabassi, Petersen et al. 1998), conventional WWTP (Goni-Urriza, Capdepuy et al. 2000; Iwane, Urase et al. 2001; Watkinson, Micalizzi et al. 2007; Zhang, Marrs et al. 2009; Koczura, Mokracka et al. 2012) and a WWTP using tertiary treatment (LaPara, Burch et al. 2011). Surveys of wider watersheds also indicated that wastewater treatment plants along with runoff from animal husbandry are significant sources of antibacterial resistance genes in the environment (Pruden, Pei et al. 2006; Storteboom, Arabi et al. 2010). In addition to an increased presence of antibiotic resistant organisms downstream of WWTPs, there is also a shift in microbial representation (Li, Qi et al. 2011) and a broader spectrum of resistance (Chagas, Seki et al. 2011). The resistance genes found in wastewater impacted streams have been shown to be transferrable to non-resistant bacteria species introduced to samples in the lab (Malik and Aleem 2011; West, Liggit et al. 2011). In the samples impacted by WWTP effluents, bacteria have shown resistance not typical for the species (Heuer, Krögerrecklenfort et al. 2002). Bacteria exposed to trace levels of amoxicillin in bench-scale experiments also exhibited resistance to silver ion (Cunningham and Lin 2010).

A concern also exists regarding so-called persistent compounds: a number of pharmaceuticals that have shown remarkable resistance to conventional and advanced treatment processes. Among those are carbamazepine (Joss, Keller et al. 2005; Yang, Flowers et al. 2011) and iopromide (Ternes and Hirsch 2000; Joss, Keller et al. 2005). Some of the persistent pharmaceuticals do not have known environmental issues associated with them, e.g. iopromide is considered a non-toxic compound (Steger-Hartmann, Länge et al. 1999). However, their

accumulation in the environmental cycle is still undesirable. Some of the persistent compounds, such as carbamazepine, have the potential to cause issues. Studies have demonstrated bioaccumulation of carbamazepine in aquatic organisms (Zhang, Oakes et al. 2010). Carbamazepine, as part of a mixture with other pharmaceutically active compounds at environmentally relevant concentrations, affected the growth and morphology of human embryonic cells (Pomati, Castiglioni et al. 2006). Additionally, as a psychoactive drug, carbamazepine can potentially inhibit predator avoidance in fish. This effect has been previously shown for another group of psychoactive drugs – antidepressants – at concentrations detected in the environment (Painter, Buerkley et al. 2009).

Furthermore, several studies also present findings with implications for water reuse. For example, soil irrigated with treated wastewater effluent showed higher presence and broader spectrum of antibacterial resistance than soil watered with groundwater (Malik and Aleem 2011). Another study demonstrated that plants irrigated with recycled water can uptake some of the antibiotics (Jones-Lepp, Sanchez et al. 2010). Some antibiotics present in reclaimed water used for irrigation accumulate in soils and persist for months after the irrigation season (Kinney, Furlong et al. 2006). These results indicate that antibiotic-resistant human pathogens can be introduced to food crops which may have health implications and decrease acceptance of water reuse practices for crop irrigation. Additionally, some of the other persistent pharmaceuticals have demonstrated uptake by plants (Wu, Spongberg et al. 2010). Many drinking water utilities rely on sources impacted by wastewater treatment plant effluents and as a result have trace levels of pharmaceuticals in finished water due to resistance of many of them to the treatment processes (Heberer 2002; Ternes, Meisenheimer et al. 2002; Stackelberg, Furlong et al. 2004; Benotti,

Trenholm et al. 2009). This is a concern to drinking water customers. Pharmaceuticals are one of the main factors that hinder acceptance of potable water reuse (Toze 2006).

Treating wastewater for removal of pharmaceuticals has obvious environmental benefits and many processes have been studied for this potential application. While conventional treatment can attenuate some compounds (Joss, Keller et al. 2005), others require advanced treatment. Adsorption and membrane filtration have been studied for pharmaceutical removal in drinking water treatment (Snyder, Adham et al. 2007), but would not be feasible for wastewater treatment due to high organic content of the background water matrix. Many researchers proposed that transformative processes, such as oxidation, may be the best option for wastewater treatment (Klavarioti, Mantzavinos et al. 2009). Among the oxidative processes ozonation, oxidation by chlorine and potassium permanganate and Fenton advanced oxidation have been studied (Huber, Canonica et al. 2003; Sharma 2008; Dodd, Kohler et al. 2009; Neafsey, Zeng et al. 2009; Dodd, Rentsch et al. 2010; Hu, Martin et al. 2010; Bińk and Sobera-Madej 2012). All of these processes can be very effective for some compounds and not at all effective for others due to the selectivity of the oxidants.

Advanced oxidation processes (AOPs) generate the hydroxyl radical, which is a non-selective reactive species. Any engineered process that generates hydroxyl radicals falls into the category of AOPs. It should be noted that some hydroxyl radicals get generated during ozonation, but the concentrations are lower than in other types of AOP, and direct reaction with ozone is still a predominant route of contaminant transformation. This work focuses on UV/$H_2O_2$ AOP where hydroxyl radicals are generated by homolytic cleavage of hydrogen peroxide by UV. The resulting unpaired electron is the key to the non-selective reactivity of hydroxyl radicals. Oxidation by hydroxyl radicals happens at diffusion controlled rates for

majority of organic compounds. UV/$H_2O_2$ AOP selected as a subject of this investigation also includes photolysis and photo-initiated processes (e.g. singlet oxygen) as potential additional transformation routes for select compounds.

There are two major concerns with application of AOP for wastewater treatment: background scavenging of hydroxyl radicals by wastewater matrix and formation of unknown transformation byproducts.

First, the non-selective nature of the hydroxyl radicals makes many background constituents to be sinks for hydroxyl radicals. Major hydroxyl radical scavenging constituents are alkalinity and dissolved organic matter. To complicate the matters further, dissolved organic matter is a non-homogeneous substance with reaction rates that vary from sample to sample, which is particularly pronounced for so called effluent organic matter: a combination of dissolved organic matter, synthetic trace constituents and soluble microbial products (Rosario-Ortiz, Mezyk et al. 2008). It has been shown that the reaction rate between effluent organic matter depends on the average molecular size (Dong, Mezyk et al. 2010). Other factors can contribute to the variability. For example, the duration of the solid retention time during the treatment process can change the molecular size distribution as well as the percentage of the organic mass represented by soluble microbial products and the degree of oxidation, both of which have the potential to affect the reaction rate constant.

In addition to the sinks of hydroxyl radicals, background wastewater matrix also has potential sources of hydroxyl radicals. Nitrate is of particular interest in that respect. It forms during nitrification which is a common process at wastewater treatment plants (WWTPs). Even if not required by regulation, nitrification occurs in activated sludge WWTPs that operate at solids residence times beyond about three days, which is a typical operating range for most

activated sludge plants (Grady, Daigger et al. 2011). In some locations, nitrification is coupled with denitrification to remove nitrate and achieve higher levels of total nitrogen removal. Most plants that incorporate denitrification only achieve partial nitrogen removal such that effluent nitrate concentrations remain above 5 mg/L as N, and it is only in severely nitrogen sensitive regions (e.g., the Chesapeake Bay) where most plants operate at total nitrogen effluent levels below 5 mg/L. Therefore, most biological WWTPs contain at least 5 mg/L nitrate-N in the effluent. Formation of hydroxyl radicals from nitrate has been confirmed during irradiation with either solar spectrum light (Daniels, Meyers et al. 1968) or UV (Shuali, Ottolenghi et al. 1969). This indirect photolysis process has been long recognized as a source of additional degradation of pollutants in natural aquatic systems under sunlight (Zarifiou and Bonneau 1974; Zepp, Hoigné et al. 1987; Andreozzi, Raffaele et al. 2003). In the past decades researchers determined quantum yields for hydroxyl radicals formed from nitrite and nitrate exposed to irradiation wavelengths within the solar spectrum (Zarifiou and Bonneau 1974; Zepp, Hoigné et al. 1987; Zellner, Exner et al. 1990; Vaughan and Blough 1998), and at 254 nm UVC wavelength emitted by low mercury pressure lamps (Alif and Boule 1991; Mark, Korth et al. 1996), but much less information is available about the photolysis of nitrate at wavelengths below 240 nm. Previous studies about nitrate photolysis at wavelengths < 240 nm focused on nitrite formation (Warburg 1918; Bayliss and Bucat 1975; Sharpless and Linden 2001). Formation of hydroxyl radicals by photolysis of nitrite and nitrate at wavelengths <240 nm has not been studied to date. In the review paper on nitrate photochemistry by Mack and Bolton (1999) the authors state that advanced oxidation using UV and nitrate is not likely to be efficient at full scale due to nitrate's low hydroxyl radical quantum yield in the 350 to 250 nm range compared to the quantum yield of hydrogen peroxide – a chemical typically used in advanced oxidation processes for generation

of radicals. This statement is correct when applied to wastewater utilities that use low pressure lamps (LP UV) emitting monochromatic UV at 254 nm for disinfection. However, use of medium pressure lamps (MP UV) emitting polychromatic UV irradiation at wavelengths above 200 nm is becoming more widespread in the water and wastewater treatment industry. MP UV was shown to be more effective than LP UV for adenovirus inactivation (Linden, Thurston et al. 2007). In addition, MP UV systems require a smaller footprint due to the higher energy output per lamp (Bolton 1999), and because of that can be more economical in some situations than LP UV systems. Researchers have previously noted unexpected degradation of organic contaminants during UV disinfection processes at WWTPs (Sunkara and Wells 2010), however, the role of MP UV in formation of hydroxyl radicals in a nitrified wastewater effluent for in-situ degradation of trace organic chemicals has not been assessed nor appreciated.

The second aspect of AOP that requires attention, i.e. formation of unknown transformation products, can be addressed by developing assays that test for specific toxicity or biological activity endpoint rather than monitoring the disappearance of the parent molecule. In the past, studies have monitored such endpoints as the changes in estrogenic activity of the transformation products (Rosenfeldt and Linden 2004), toxicity (Schmitt-Jansen, Bartels et al. 2006) or antibacterial potency (Wammer, Lapara et al. 2006; Dodd, Kohler et al. 2009; Dodd, Rentsch et al. 2010; Paul, Dodd et al. 2010).

This work focuses on addressing the unknown aspects of UV/$H_2O_2$ AOP for wastewater treatment. The results are presented in 4 chapters, 2 of which address the transformation products of pharmaceuticals in wastewater treatment and another 2 address aspects of wastewater matrix effects. Chapter 2 focuses on the ability of advanced oxidation to create biodegradable transformation products from recalcitrant pharmaceuticals carbamazepine and iopromide.

Chapter 3 addresses the changes in antibacterial activity of antibiotics representative of main structural classes during advanced oxidation. Chapter 4 evaluates the potential to generate hydroxyl radicals from indigenous nitrate in lieu of adding $H_2O_2$ in effluents. And Chapter 5 shows the results of the model determining the main predicting factors in the variable reactivity between effluent organic matter and hydroxyl radicals. Each chapter includes a methodology section specific to the topic covered in the section. An overall conclusion of the research follows in Chapter 6.

# Chapter 2: Biodegradability of the post-AOP products of recalcitrant pharmaceuticals

Portions of the work presented in this chapter were previously published as Keen, O. S., Baik, S., Linden, K. G., Aga, D. S. and Love, N. G. (2012). "Enhanced Biodegradation of Carbamazepine after UV/$H_2O_2$ Advanced Oxidation." Environmental Science & Technology **46**(11): 6222-6227.

## 2.1 Materials and Methods

### 2.1.1 Chemicals, Samples and Cultures

All chemicals used in the study were reagent grade. Sodium azide (Alfa Aesar, Ward Hill MA) 1 M stock solution was prepared for deactivating microbial metabolism in abiotic controls. Hydrogen peroxide (J.T. Baker, Phillipsburg NJ) was used during advanced oxidation treatments to produce hydroxyl radicals. A stock solution of 1,000 mg/L (2950 units/mg) of bovine catalase (Sigma-Aldrich, St. Louis, MO) was prepared for hydrogen peroxide quenching before the activated sludge inoculum was added to AOP-treated samples. Non-radiolabeled (cold) carbamazepine was manufactured by Acros Organics (Geel, Belgium), and cold iopromide was purchased from (U.S. Parmacopeia, Rockville, MD). Radiolabeled (hot) carbamazepine was purchased from Sigma Radiochemicals (MO, USA) and iopromide was donated by the Laboratory for Diagnostics, Genetics & Ecotoxicology, Berlin, Germany. A stock solution of cold carbamazepine was prepared in methanol and stock solution of cold iopromide was prepared in water based on solubility. Hot carbamazepine was labeled with $^{14}C$ carbon in the amide group and hot iopromide was labeled on the aromatic ring structure as shown in Figure 1. The specific activity of the stock solutions was 22.6 mCi/mol and 24.5 mCi/mol for

carbamazepine and iopromide respectively. The stock concentrations were 1.11 mM for carbamazepine and 9.38 mM for iopromide.

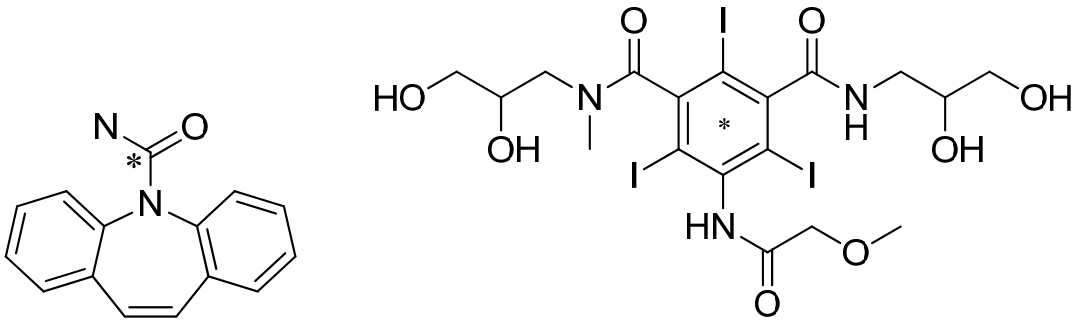


**Figure 1: Carbamazepine (left) and iopromide (right) structures and location of $^{14}C$ atom (marked with *)**

Mixed liquor (a mixture of wastewater and microorganisms in the activated sludge aeration tank) and pre-disinfected secondary effluent were obtained from a wastewater treatment facility that uses nitrifying activated sludge as a biological treatment process. The wastewater treatment plant (WWTP) effluent was filtered through a 0.2 μm nylon filter (Millipore, Billerica MA) to remove particulate matter and microbial cells that could interfere with the experimental procedure. A diluted activated sludge sample was spiked in at a known total suspended solids concentration to inoculate the biotransformation assay. The experiment was performed in duplicate using grab samples of effluents collected on two different days for carbamazepine and on two additional days for iopromide, because the experiments were conducted sequentially and not in parallel. The samples were collected in the junction box that received secondary clarifier overflows. Water quality characteristics for the effluents are available in the Table 2-1. For each duplicate, a number of measurements were taken to confirm the repeatability of the instrumental data.

**Table 1: Water quality measurements for the effluents**

| Water quality parameter | Method used | Units | Effluent 1 carbamazepine | Effluent 2 carbamazepine | Effluent 1 iopromide | Effluent 2 iopromide |
|---|---|---|---|---|---|---|
| Alkalinity | Hach digital titrator | mg/L as $CaCO_3$ | 88 | 86 | 62 | 106 |
| pH | Beckman pH meter | - | 6.3 | 6.6 | 6.3 | 6.0 |
| Ammonium | Hach colorimetric test kit | mg/L as N | 0.043 | < 0.015 | 0.058 | 0.018 |
| Nitrite | Hach colorimetric test kit | mg/L as N | < 0.015 | < 0.015 | 0.086 | 0.016 |
| Nitrate | Hach colorimetric test kit | mg/L as N | 16.2 | 9.9 | 14.6 | 7.8 |
| Dissolved organic carbon | Shimadzu TOC analyzer | mg/L as C | 7.5 | -* | 10.3 | 5.4 |

* TOC measurement was discarded due to analytical problems that were discovered later.

### 2.1.2 Analytical Methods and Experimental Protocols

Briefly, a solution of $^{14}C$ labeled pharmaceutical was split into two volumes, half of which received advanced oxidation treatment, and half of which did not. Both samples were allowed to biodegrade by heterotrophic bacteria in a biodegradability assay where a continuously aerated bottle was connected to bottles containing an alkaline solution trap to capture any $CO_2$ that formed during mineralization of organic compounds. The samples before the bioassay and at different stages of biodegradation were tested with liquid scintillation counting and liquid chromatography with radioactivity, mass spectrometry and UV detectors. Sections below describe each part of the experimental protocol in more detail.

#### *2.1.2 (a) UV-$H_2O_2$ advanced oxidation*

A solution containing 0.26 mg/L of hot carbamazepine or 0.74 mg/L of hot iopromide and 1.00 mg/L of the corresponding cold compound was prepared by evaporating methanol from a necessary volume of the stock solution under a nitrogen stream, followed by reconstituting the pharmaceutical residue with effluent. Cold pharmaceutical was added to facilitate the detection

of by-products using mass spectrometry. The resulting solution was sonicated until no aggregation of the residue was visible. The effluent was spiked with 10 mg/L of hydrogen peroxide prior to addition of the pharmaceutical. Hydrogen peroxide ($H_2O_2$) was measured using the triiodide method.(Klassen, Marchington et al. 1994) A preliminary study was conducted to determine an optimal concentration of hydrogen peroxide that would achieve a significant increase in hydroxyl radical production. Ten mg/L of hydrogen peroxide was selected based on the results.

Irradiations for AOP experiments were carried out using a medium pressure (MP) collimated beam system (Calgon Carbon, Pittsburg, PA) equipped with one 1 kW lamp quasi-collimated by a 6.4 cm diameter, 10 cm long cylindrical tube. The sample was held in a 150 mm diameter crystallization dish. The incident irradiance was 3.0 $mW/cm^2$ measured with International Light IL-1700 radiometer (Peabody, MA), Petri Factor was 0.60 and sample depth was 4.4 cm. The average irradiance was calculated using the procedure by Bolton and Linden (2003).

Preliminary studies were conducted with each compound using cold stock to determine the UV fluence + $H_2O_2$ combination necessary to achieve 1-log degradation of the parent compound. That fluence was established to be 1800 $mJ/cm^2$ at 10 mg/L $H_2O_2$ for carbamazepine and 2400 $mJ/cm^2$ at 10 mg/L $H_2O_2$ for iopromide. These experimental conditions are consistent with full scale UV/$H_2O_2$ AOP systems currently used in water reuse and industrial effluent treatment trains.

### *2.1.2. (b) Biotransformation Assay*

Biotransformation assays were conducted over 25-35 days in 250 mL amber bottles, which were continuously aerated and connected in series to two 60 mL amber glass bottles

holding 50 mL of 1 N potassium hydroxide (KOH) each. Mineralization of the radiolabeled molecules was assessed by measuring the amount of $^{14}CO_2$ captured in the KOH trap, combined with the disappearance of the $UV_{254}$-absorbing species in the chromatogram indicating the loss of aromaticity and the absence of the characteristic mass fragments of carbamazepine with m/z 194 in the mass spectra also indicating the loss of the core aromatic structure of carbamazepine. These additional ways of confirming the opening of the ring structure were not necessary for iopromide because of the ring location of the $^{14}C$ label.

The biotransformation assays were dosed with 100 mL effluent samples that either received AOP treatment or did not. All biotransformation assay bottles then received 1 mg/L bovine catalase to quench residual $H_2O_2$ and prevent potential inhibition of biomass during the incubation period. After catalase was added, the sample was stirred and allowed to sit for 30 min to make sure that $H_2O_2$ was reduced to levels below 0.1 mg/L. The dose of bovine catalase and the reaction time were determined in preliminary experiments.

Mixed liquor from the activated sludge basins at the WWTP was used as the microbial inoculum for the biotransformation assays. A mixed liquor sample was collected from the recycled activated sludge inlet the same day as effluent was collected. Enough biomass was added to the assay bottles so that the final biomass concentration was 32 ± 1 mg/L as volatile suspended solids (VSS), which was determined using Standard Method 2540E (20$^{th}$ ed.) and Pall type A/E glass fiber filters (Pall, Port Washington NY). Because of the slower rate of mineralization of iopromide observed in preliminary experiments and lower sorption potential onto the biomass (Khunjar and Love 2011), higher concentration of biomass was used in iopromide assays (67± 1 mg/L). The mixed liquor was shaken prior to inoculation into assay bottles to prevent settling and ensure a uniform starting biomass concentration in each sample.

Diluted biomass was used to keep the overall kinetics of biotransformation slow and to allow for biotransformation intermediates, if any, to be determined. Upon adding the biomass, samples were stirred, capped and the air supply was turned on to initiate the experiment.

Each sample had a corresponding abiotic control that contained the same effluent but the mixed liquor inoculum was inactivated by adding 0.01 M sodium azide, a strong respiratory inhibitor.(Barbot, Seyssiecq et al. 2010; Khunjar and Love 2011) The setup also contained a blank that consisted of effluent without carbamazepine and mixed liquor inoculum for baseline measurements. The complete experimental setup of the biotransformation study is shown in Figure 2.

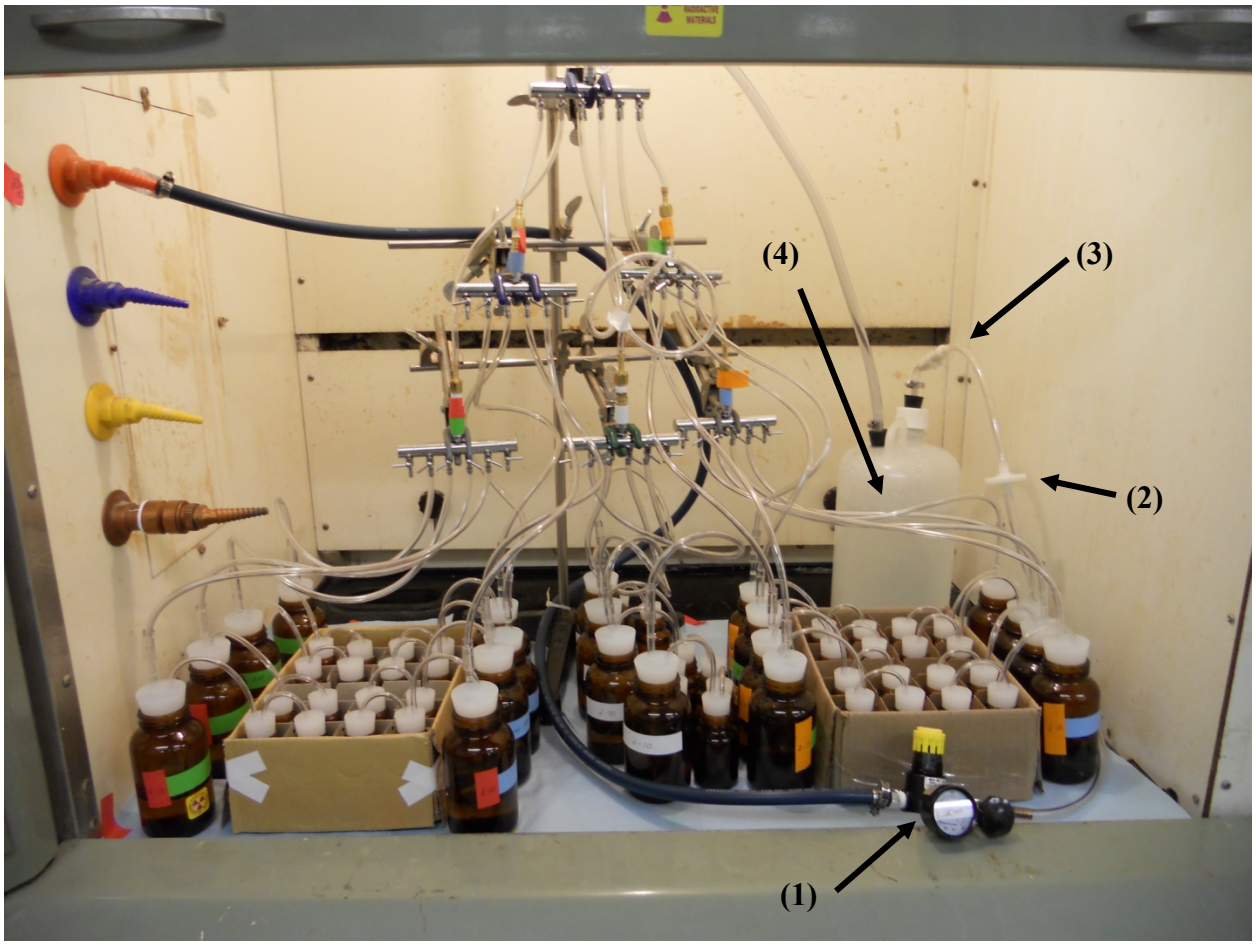


**Figure 2: Experimental setup for assessing the biological stability of effluents treated with AOP versus those not treated with AOP. The building air delivered to the system passed through a regulator which assured constant flow (1), a 0.2 micron filter removed non-gaseous particles (2), a check valve prevented backflow (3), and a wash bottle hydrated the air to minimize sample evaporation (4). Air was delivered to the samples through a series of manifolds. Each bottle had an individual regulator valve allowing for the gaseous flow rate to be adjusted.**

Throughout the study, evaporation from the samples was monitored to ensure that volume losses were taken into account. The extent of evaporation from each sample was measured by weighing each bottle at the beginning of the study and when the samples were collected. It was determined that over the 25 days, sample bottles lost at most 0.9 mL to evaporation (<1% of the total volume), and KOH traps lost 0.7 mL at most (<2% of the total volume). Most of the evaporation occurred in the second trap bottle, while most of the

radiolabeled $CO_2$ was captured in the first trap bottle. Therefore, no correction for evaporation was necessary.

After 9 or 25 days (9 and 19 for iopromide), aliquots from each assay bottle and from the KOH traps were tested for radioactivity by liquid scintillation counting (LSC) described in detail in Section 2.1.2. (c). Before each assay bottle was disconnected from the air supply line, it was purged with a high flow rate stream of air for several minutes to ensure that any radiolabeled $CO_2$ accumulated in the head-space of the sample bottle was pushed into the KOH trap. After the radioactivity was measured, samples were prepared for shipping to the University at Buffalo for LC/MS analysis. The preparation procedure included filtering the samples through a 0.2 μm nylon syringe filter (Fisherbrand, Fisher Scientific, Pittsburg PA) and reducing the volume by rotary evaporation (Buchi RE 111, Flawil, Switzerland) using a Buchi V-700 vacuum pump (150 mbar evaporation pressure) and Buchi 461 water bath set at 60°C. Rotary evaporation was chosen as a concentration method to prevent the loss of small hydrophilic products in solution which are not likely to be retained by solid phase extraction (SPE). Figure 3 shows examples of radiochromatograms comparing peaks recovered after rotary evaporation and after SPE. The details of the LC/MS analysis and SPE are described in Section 2.1.2. (d).

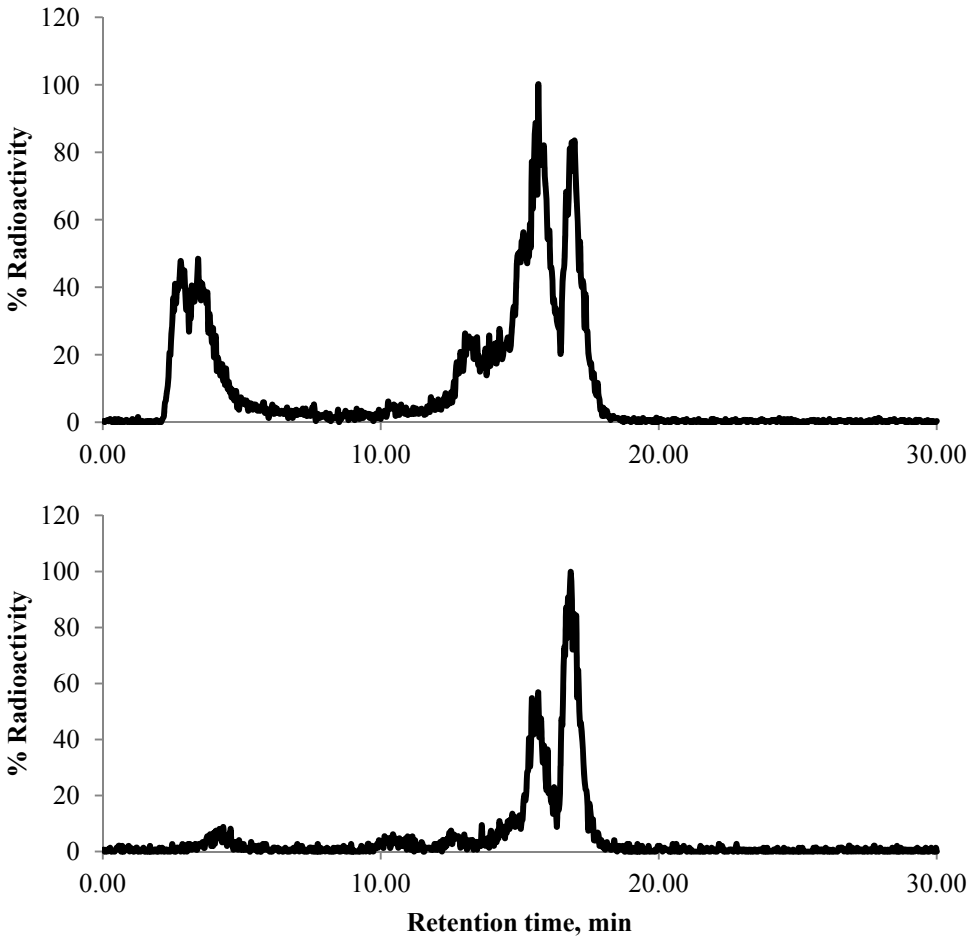


**Figure 3: Oxidation products retained after rotary evaporation (top) compared to solid phase extraction (bottom).**

A preliminary study was conducted to determine if the activated sludge inoculum was inhibited by the concentrations of carbamazepine used in this study. Specific UV absorbance $SUVA_{254}$ (Weishaar, Aiken et al. 2003) (UV absorbance at 254 nm divided by DOC) was used as an indicator of changes to organic matter present in the assay. $SUVA_{254}$ is a surrogate measure of the aromaticity of the dissolved organic carbon (Weishaar, Aiken et al. 2003) and decreases as a result of microbial activity due to biodegradation of aromatic rings in the organic matter and production of aliphatic microbial products (Jarusutthirak and Amy 2007). Two aerated bottles contained identical effluent and biomass, but only one of them was spiked with 1.26 mg/L

carbamazepine. SUVA $_{254}$ was monitored over 7 days. A decrease in $SUVA_{254}$ indicates a decrease in the aromatic content of organic compounds in solution (Weishaar, Aiken et al. 2003). If carbamazepine is not inhibitory at the concentrations used, the rate of change in $SUVA_{254}$ will be the same in both bottles. DOC for $SUVA_{254}$ calculation was measured with a Shimadzu TOC-$V_{CSH}$ organic carbon analyzer (Shimadzu America, Inc., Columbia, MD) and UV absorbance was measured with a Varian Cary-Bio100 spectrometer (Agilent Technologies, Santa Clara CA). As shown in Figure 4, $SUVA_{254}$ decreased at the same rate in effluent with and without carbamazepine, so no inhibition of the inoculum by carbamazepine was observed. Inhibition of biomass by iopromide was not tested because its lack of toxicity to bacteria has been documented in literature (Steger-Hartmann, Länge et al. 1999).

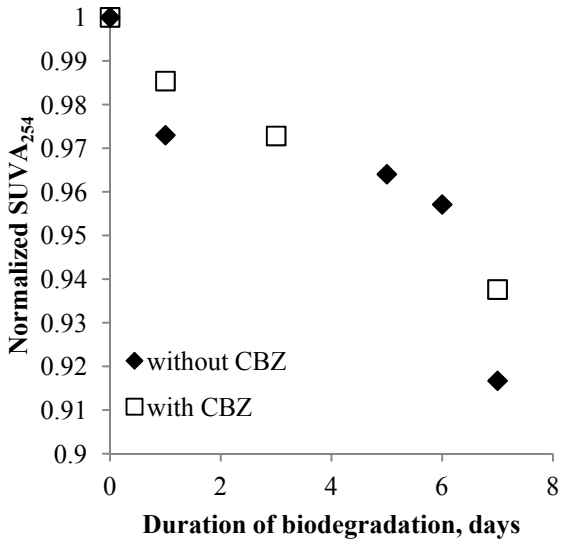


**Figure 4: Change in $SUVA_{254}$ during degradation of effluent with activated sludge, both with and without carbamazepine (CBZ).**

### *2.1.2. (c) Liquid scintillation counting*

Radioactive signal from the $^{14}C$-labeled compounds was measured using a liquid scintillation counter or LSC (Packard, 1600 TR or 2300TR). Ultima Gold scintillation cocktail

(Perkin Elmer, Waltham MA) was selected due to its efficiency for highly alkaline solutions, as reported by the manufacturer. Optimal sample to cocktail ratios for the sample and the alkaline trap were selected by testing several ratios: 2 mL of sample to 5 mL of cocktail, 1 mL to 6 mL and 0.2 mL to 6.8 mL. All ratios performed equally well, so the latter ratio was selected for the sample bottles. Because low concentrations of radiolabeled $CO_2$ were expected in the alkaline trap, 1 mL sample to 6 mL cocktail ratio was selected for the traps. One mL was the highest volume of the alkaline solution that did not result in cloudiness in the scintillation vials. The starting radioactivity in the samples was over 70 times above the limit of detection.

### *2.1.2 (d) Liquid chromatography/mass spectrometry analysis*

The analysis of carbamazepine and its by-products in samples were performed using liquid chromatograph with ion trap mass spectrometer (LC-ITMS) detection [LCQ Advantage™, Thermo Finnigan, CA, USA], which was also equipped with a UV 6000LP UV-Vis diode array detector. For radioactive samples, analysis was performed using Surveyor™ HPLC (Thermo Finnigan, San Jose, CA) equipped with an on-line radiochromatographic detector (IN/US Systems, Inc., Tampa, FL) that uses a flow-through cell with a volume of 0.5 mL and a 3:1 scintillation fluid: eluent ratio (Ecoscint, National Diagnostics, Atlanta, GA). The details of the LC-ITMS and the HPLC-radiochromatography conditions are described in the SI.

For qualitative analysis, 3 mL aliquots were taken from each sample and reduced to 0.2 mL under a gentle stream of nitrogen. Furthermore, selected samples were subjected to a clean-up procedure using Phenomenex® Strata™-X cartridges for solid phase extraction (SPE) to reduce the sample matrix that affects both separation and the signals of the analytes in the LC-ITMS. The SPE eluates were reduced in volume to 0.2 mL prior to analysis by LC-radiochromatography, and the results were compared with the samples that were concentrated by

direct evaporation (without SPE clean-up). At each step in the SPE procedure, a small aliquot was taken from the eluate and from the waste; radioactivity of each aliquot was measured by LSC in order to check for %recovery. SPE eluates were analyzed only to demonstrate the effect of SPE on the loss of polar carbamazepine products. For all quantitative analyses performed in this study, no SPE samples were used.

## 2.2 Results and Discussion

While UV-$H_2O_2$ AOP treatment transformed each of the pharmaceuticals into products, this process alone did not result in mineralization of either of them. As illustrated in Figure 5, all radioactivity remained in solution after UV-$H_2O_2$ AOP treatment.

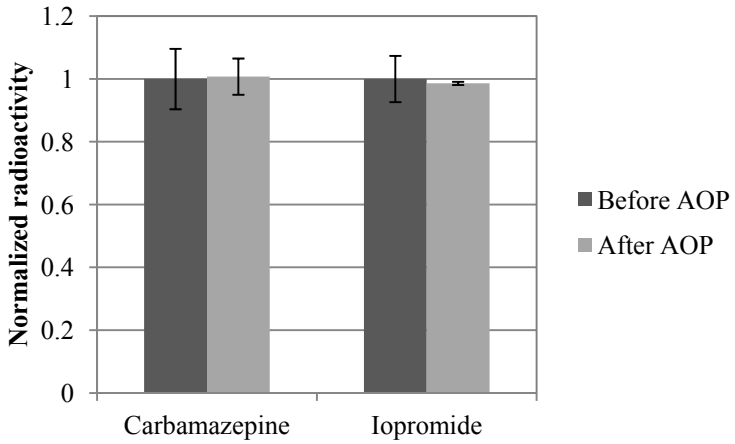


**Figure 5: Radioactivity of effluents before and after AOP, before commencement of the biotransformation step. The error bars represent the 95% confidence intervals of LSC instrumental measurement based on replicate readings of the same sample for carbamazepine and 95% confidence of single instrumental reading of 3 separate experiments for iopromide.**

In contrast, LSC analysis of AOP-treated samples that were later subjected to biotransformation showed that up to 45% of $^{14}$C-carbamazepine and up to 20% of $^{14}$C-iopromide was completely mineralized (biodegraded) to $CO_2$ in AOP-treated effluents over the course of 25 days, while no biotransformation occurred in the effluents that were not pre-treated with UV-$H_2O_2$ AOP (Figure 6). Statistical analysis of the carbamazepine results indicated that the faction

of radiolabeled carbon that migrated into the $CO_2$ trap after a 9-day or 25-day period of biodegradation was significantly different in all AOP pretreated samples compared to the samples that received no AOP pretreatment ($p < 0.05$). There was also a statistically significant difference ($p < 0.05$) between the post-AOP samples and post-AOP controls. The $CO_2$ released from the post-AOP controls was also statistically significant ($p < 0.05$) compared to the samples not treated with AOP for most of the samples excluding day 9 of sample 2 (Figure 6). This indicates that while some mineralization occurred in the post-AOP control sample, the degree of mineralization was significantly smaller than that in the sample with uninhibited bacterial growth. A small degree of biotransformation in the AOP-treated controls can be attributed to bacteria overcoming the inhibitor over time. Additionally, sodium azide can result in abiotic mineralization of the pharmaceuticals due to its strong nucleophilic properties, which was confirmed in a control study. The control study samples consisted of effluent filtered through 0.2 μm filter. The samples were spiked with $^{14}$C-iopromide and treated with AOP. No bacterial culture was added to the samples, and sodium azide was added to one of the two samples. Figure 7 shows the results of the control study with the sample spiked with sodium azide showing slightly increased rate of abiotic mineralization compared to the non-spiked sample. Figures 8 and 9 provide the mass balance for $^{14}$C for both pharmaceuticals. In all samples >95% of $^{14}$C was accounted for.

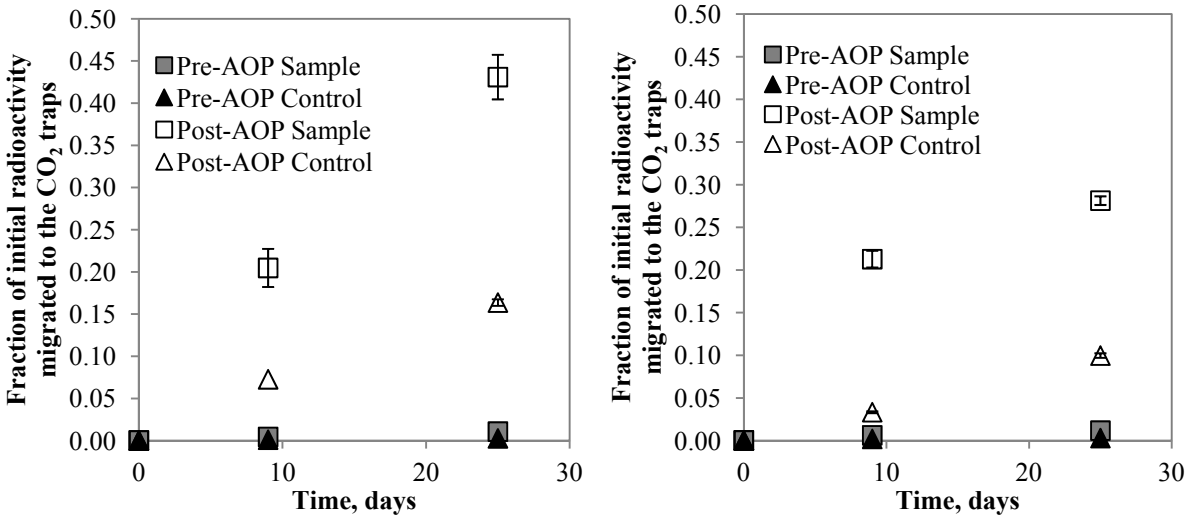


**Figure 6: Migration of radiolabeled $CO_2$ from the main sample bottle into the $CO_2$ traps during biodegradation of carbamazepine in Sample 1 (left) and Sample 2 (right). The values are the means of several measurements taken from the same trap bottle with error bars representing 95% confidence intervals for the measurements.**

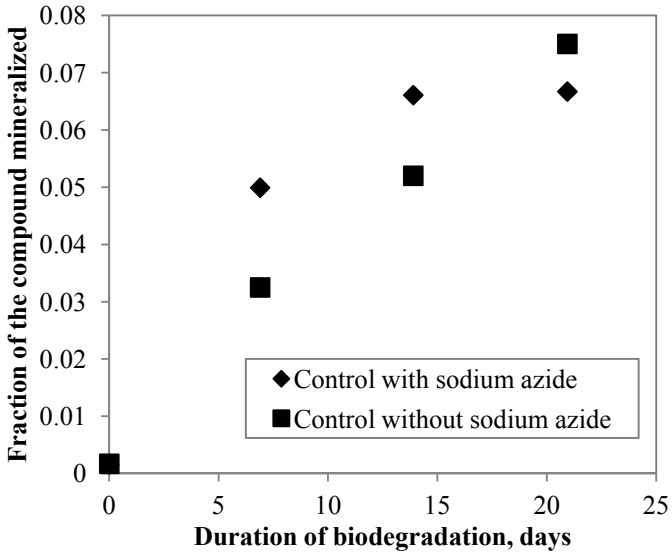


**Figure 7: Comparison of abiotic mineralization of iopromide with and without sodium azide**

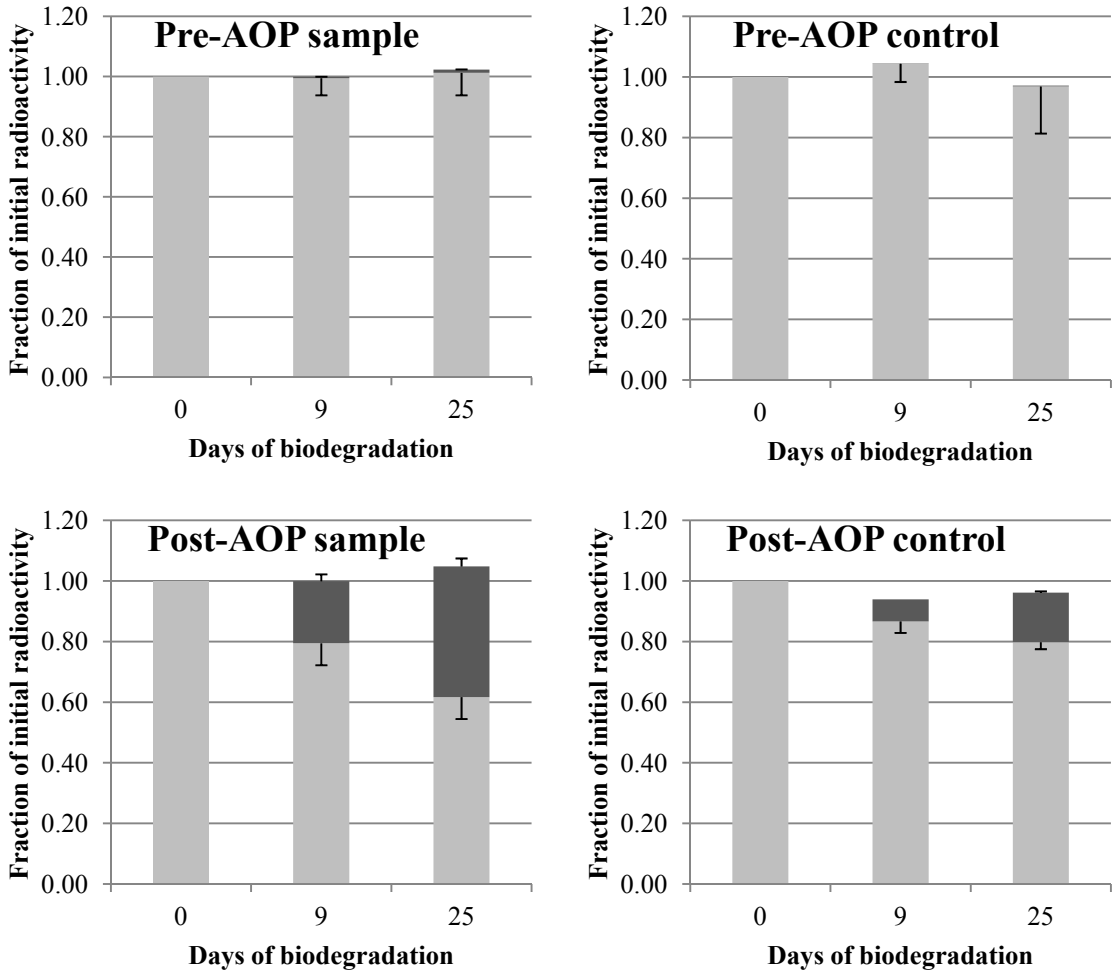


**Figure 8: Carbamazepine Sample 1 mass balance. Light gray color – fraction of radioactivity due to parent compound and products still in solution. Dark gray color – fraction of radioactivity that migrated into the KOH traps as $CO_2$, i.e. fraction of the radiolabeled compound fully mineralized. The results are for one of the two replicates. Left - samples; right - controls (Sample + $NaN_3$); top – before AOP; bottom – after AOP. The values are the means of several measurements taken from the same sample with error bars representing 95% confidence intervals for the measurements.**

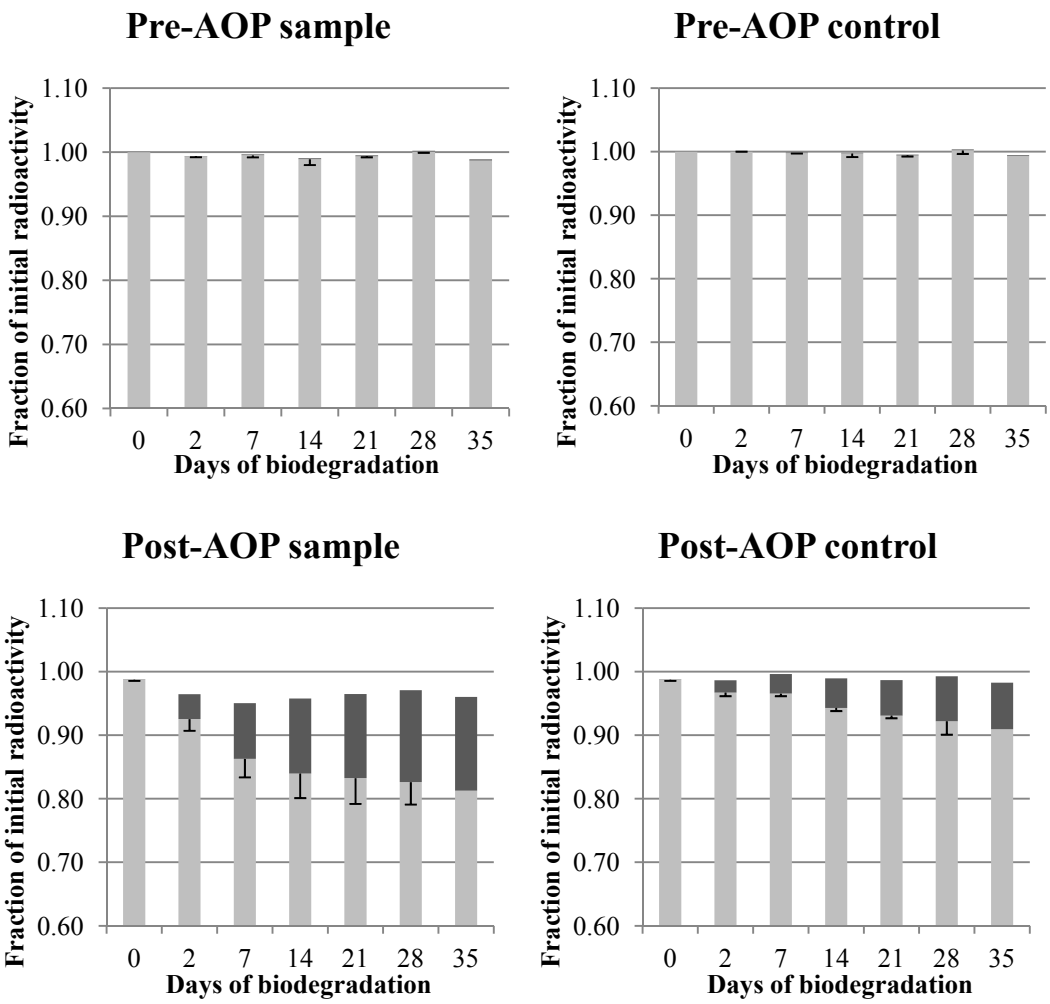


**Figure 9: Iopromide mass balance. Light gray color – fraction of radioactivity due to parent compound and products still in solution. Dark gray color – fraction of radioactivity that migrated into the KOH traps as $CO_2$, i.e. fraction of the radiolabeled compound fully mineralized. The results are for both replicates. Left - samples; right - controls (Sample + $NaN_3$); top – before AOP; bottom – after AOP. The values are the means of the two replicates with error bars representing the standard deviation between the two samples. The y-axis starts at 0.60 rather than 0 for a clearer view of the extent of biodegradation.**

Iopromide was labeled with $^{14}C$ on the ring structure so it did not require additional tools to confirm the ring opening. Carbamazepine, on the other hand, was labeled on the amide group that could have mineralized without the ring opening. To further confirm the opening of the ring, additional analysis was performed. Figure 10 shows radiochromatograms comparing samples with and without UV-$H_2O_2$ AOP treatment. Carbamazepine is unchanged in samples that were not exposed to UV-$H_2O_2$ AOP (pre-AOP) but were exposed to activated sludge for 25

days. In contrast, the radiochromatogram of samples that were exposed to UV-$H_2O_2$ AOP (post-AOP) show that some by-products formed during UV-$H_2O_2$ AOP (Day 0). Furthermore, after 25 days of exposure to activated sludge under aerobic conditions, there is a distinct decrease in the peak area associated with the early (more polar) eluting peaks, suggesting that these peaks were biotransformed and mineralized to $CO_2$. Mineralization was further supported by the absence of characteristic tricyclic fragment ion of carbamazepine (m/z 194) in the mass spectrum (Figure 11) obtained under both full-scan and selection mode. Furthermore, no new peaks with UV signal at 254 nm corresponding to a tricyclic carbamazepine product devoid of the $^{14}C$ labeled moiety were observed in the chromatograms, while the UV254 signal corresponding to an oxidation product disappeared during biodegradation (Figure 12).

The LC-ITMS data in Figure 13 show that carbamazepine (m/z 237) is stable over time, but after UV-$H_2O_2$ AOP treatment, by-products with m/z 251 and 253 were formed. After 25 days in the biotransformation assay, the by-product with molecular ion m/z 251 disappeared, and the other peak with m/z 253 was significantly reduced in size, such that the mixture predominantly contained non-degraded carbamazepine. The MS/MS data indicated that the by-products of AOP were carbamazepine with a hydroxyl or carbonyl group added (Figure 13). These are common by-products of AOP during which the main mechanism of the contaminant transformation is the reaction between the parent molecule and hydroxyl radicals.

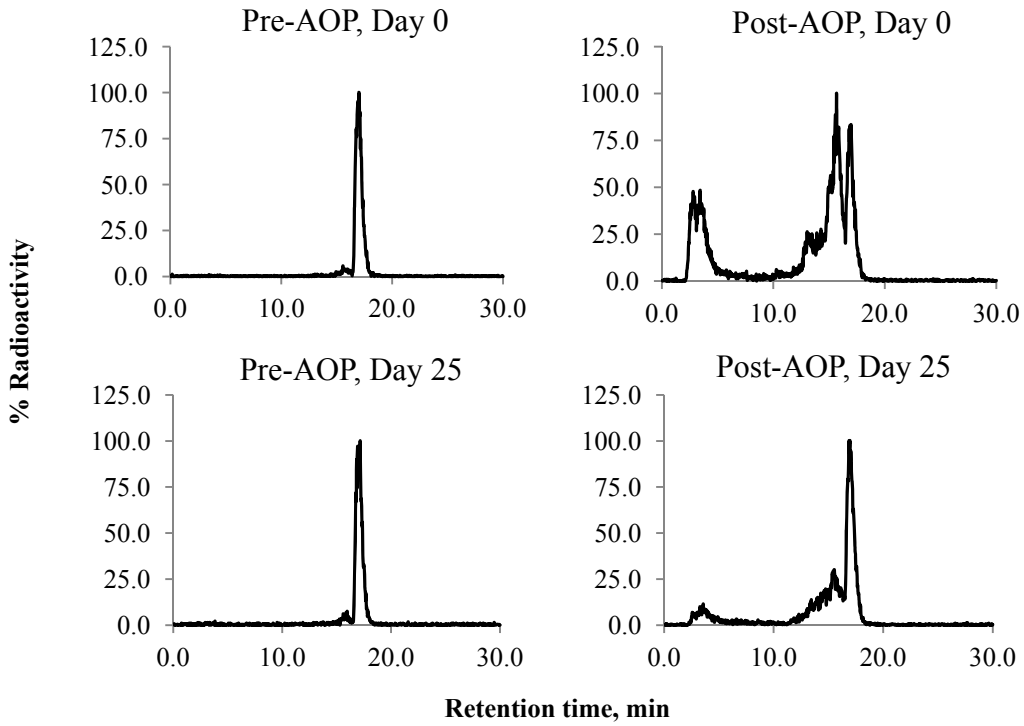


**Figure 10: Radiochromatogram of untreated (left) and AOP treated (right) samples before biotransformation (top) and after biotransformation (bottom). The peaks are normalized to the highest peak of the chromatogram.**

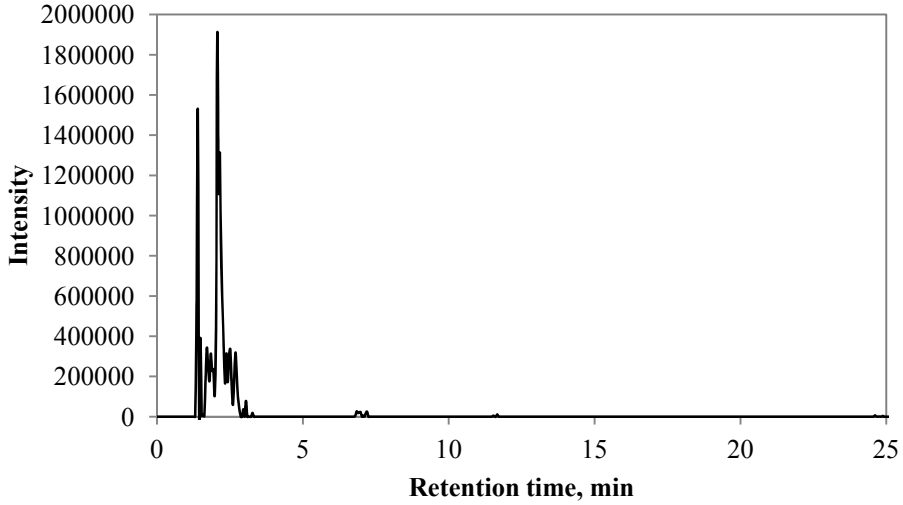


**Figure 11: Extracted ion chromatogram for tricyclic fragment of carbamazepine (m/z 194) of the sample pretreated with AOP after 25 days of biodegradation.**

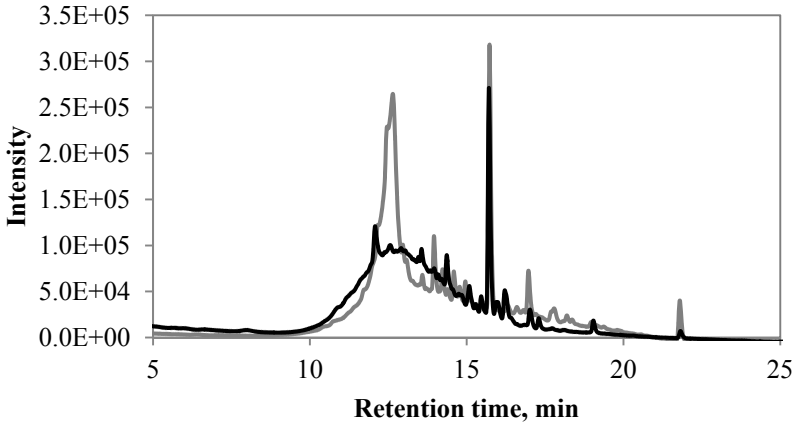


**Figure 12: $UV_{254}$ absorbance chromatogram of the sample pretreated with AOP before biodegradation (gray) and after 25 days of biodegradation (black). The main peak at 15.71 min retention time is the parent carbamazepine. All other minor peaks were overlapped with their full-scan mass spectra, but none of these peaks showed m/z peak that corresponds to a tricyclic by-product of carbamazepine devoid of the $^{14}CONH_2$ moeity.**

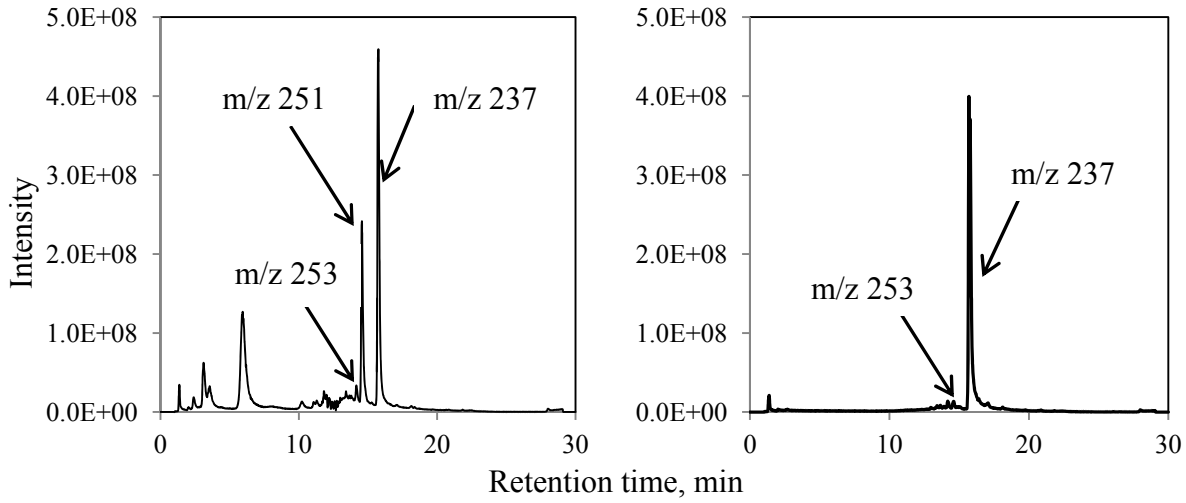


**Figure 13: MS chromatogram of the AOP-treated carbamazepine in effluent before biotransformation (left) and after 25 days of biotransformation (right).**

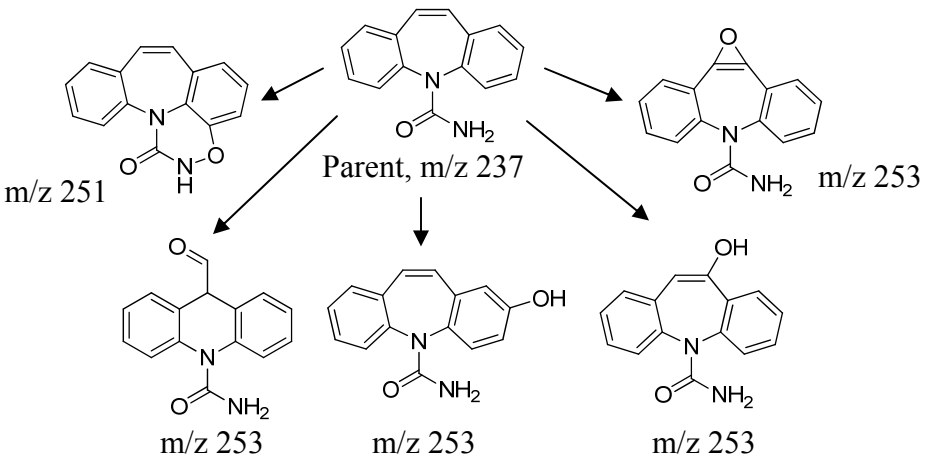


**Figure 14: Proposed products of carbamazepine advanced oxidation.**

Hydroxylation of aromatic rings to catechols makes the rings susceptible to cleavage by catechol dioxygenase enzymes produced by heterotrophic bacteria (Bugg and Winfield 1998), such as those typically found in activated sludge.(Ma and Love 2001) Once the ring is open, the molecule becomes less stable and therefore more amenable to mineralization.

The results of this study indicate that the AOP products of carbamazepine and iopromide – pharmaceuticals routinely found to be recalcitrant to biotransformation at wastewater treatment plants – become mineralized by microorganisms found in activated sludge processes. This synergy between advanced oxidation and biological decay indicates that UV-$H_2O_2$ AOP followed by some form of biological treatment can lead to mineralization of recalcitrant pharmaceuticals. Formation of smaller, more biotransformable compounds (known as assimilable organic carbon or AOC) during advanced oxidation creates conditions that promote biofilm growth (Hu, Wang et al. 1999; Metz, Reynolds et al. 2011). Consequently, and due to the very low organic load remaining in WWTP effluents, a biofilm-mediated biofiltration process (either a granular medium filtration system or a constructed wetland) rather than suspended growth process located downstream of a UV-$H_2O_2$ process would be most advantageous to facilitate subsequent biotransformation and, preferably, mineralization.

Previous research has indicated that the viability of biofilms can be enhanced when located downstream of a UV-based advanced oxidation process (Metz, Reynolds et al. 2011). The biofiltration polishing step can also reduce the AOC before the treated water is released into the environment or distribution network in the case of wastewater reuse or drinking water treatment scenarios. In addition to chemical oxidation activity, UV-$H_2O_2$ AOP at a wastewater treatment plant would provide very high levels of effluent disinfection, effectively eliminating the need for any additional disinfection step (United States Environmental Protection Agency 2006).

# Chapter 3: Degradation of antibacterial activity of antibiotics

## 3.1 Materials and Methods

### 3.1.1 Reagents

Antibiotics used in the study were reagent grade: erythromycin (MP Biomedicals, Solon, OH), clindamycin (Enzo Life Sciences, Farmingdale, NY), doxycycline, penicillin, ciprofloxacin and trimethoprim (all four manufactured by Sigma-Aldrich, St.Louis, MO). Table 2 summarizes some of the relevant details of the selected compounds.

**Table 2: Summary of antibiotics used in the study**

| Antibiotic | Class | Use (Kemper 2008) | Bacteria | m/z |
|---|---|---|---|---|
| Erythromycin | Macrolide | Humans, cattle, chicken | B. subtilis | 734.6, 716.6 (-$H_2O$) |
| Doxycycline | Tetracycline | Humans | E. coli | 445.2 |
| Clindamycin | Lincosamide | Humans, dogs | B. subtilis | 425.3 |
| Penicillin-G | Beta-lactam | Humans | B. subtilis | 335.2 |
| Ciprofloxacin | Fluoroquinolone | Humans | E. coli | 332.2 |
| Trimethoprim | Dihydrofolate reductase inhibitor | Humans | E. coli | 291.2 |

Experiments were performed in ultrapure water (arium611-VF, Sartorius Stedim, Bohemia, NY) and in secondary effluent of two wastewater treatment plants. The effluents were collected prior to disinfection and filtered through a 0.2 µm nylon filter (Millipore, Billerica, MA). Plant 1 uses solids contact activated sludge followed by nitrifying trickling filters followed by denitrifying trickling filters. Plant 2 uses Modified Ludzack-Ettinger biological treatment. Water quality parameters for both effluents are listed in Table 3.

**Table 3: Effluent water quality**

| Alkalinity, mg/L as $CaCO_3$ | pH, - | Nitrite, mg-N/L | Nitrate, mg-N/L | Dissolved organic carbon, mg-C/L | Total hydroxyl radical scavenging, $s^{-1}$ |
|---|---|---|---|---|---|
| 123 | 6.84 | <0.015 | 4.04 | 5.8 | 1.95E+05 |
| 88 | 6.58 | 0.021 | 10.3 | 4.9 | 1.77E+05 |

Bacterial culture was purchased from ATCC. B. subtilis Marburg strain was used as a gram-positive surrogate and E. coli B strain was used as a gram-negative surrogate. Both strains have no known resistance to the antibiotics selected. B. subtilis Difco™ nutrient broth was purchased from BD (Sparks, MD) and consisted of 3.0 g/L of beef extract and 5.0 g/L peptone. Difco™ nutrient agar contained the same ingredients plus 15 g/L of agar. E. coli nutrient broth was prepared with 10 g/L Bacto™ tryptone (BD, Sparks, MD), 5 g/L Bacto™ yeast extract and 5 g/L sodium chloride (BDH, West Chester, PA). Nutrient agar for E. coli was prepared by adding 15 g/L Bacto™ agar (BD, Sparks, MD) to the nutrient broth. Phosphate buffer saline (PBS) was prepared with 8 g/L sodium chloride (BDH, West Chester), 0.2 g/L potassium chloride (Fisher Scientific, Rochester, NY), 1.81 g/L of dibasic sodium phosphate dihydrate ($Na_2HPO_4 \cdot 2H_2O$) and 0.24 g/L of potassium phosphate monobasic $KH_2PO_4$ (EMD, Gibbstown, NJ).

### 3.1.2 Photolysis and advanced oxidation

Both low pressure mercury vapor and medium pressure mercury vapor UV sources were used in the study. Medium pressure lamp system was manufactured by Calgon Cabon Inc. (Pittsburg, PA) and consisted of a 1kW lamp emitting a polychromatic spectrum above 200 nm. The lamp was collimated with a 10cm X Ø6.4 cm cylindrical tube. Low pressure lamp system consisted of four 15 W lamps (ozone-free, General Electric #G15T8) collimated by two Ø10cm apertures 1.2 cm apart. Low pressure lamp emitted monochromatic UV at around 253.7 nm. Spectral irradiance of the lamps was measured with an Ocean Optics USB2000 spectrometer (Ocean Optics, Dunedin, FL), and incident irradiance at the sample surface was measured with an IL-1700 radiometer (International Light, Peabody, MA). Average UV fluence was calculated using the appropriate factors and was not germicidally weighted.(Bolton and Linden 2003) To

generate hydroxyl radicals, samples were spiked with 9-10 mg/L of reagent grade hydrogen peroxide (Sigma-Aldrich, St.Louis, MO). Hydrogen peroxide concentration was measured spectrophotometrically (Hach DR5000, Hach Corporation, Loveland, CO) using triiodide method.(Klassen, Marchington et al. 1994)

Incremental UV fluences up to 2000 mJ/cm$^2$ (levels reasonable for full scale advanced oxidation) were used in treatment. Irradiations were carried out in batch reactors using continuously stirred crystallization dish 50 mm in diameter.

When effluent was used, it was pre-disinfected using 300 mJ/cm$^2$ germicidal dose of UV prior to spiking an antibiotic. Pre-disinfection step was based on the preliminary experiments that had shown that filtration through 0.2 μm filter allows enough bacteria pass through to interfere with the assay.

### 3.1.3 Antibacterial activity assays

Preliminary studies were conducted to optimize the assays. Optical density (absorbance at 600 nm) was used as a measure of bacterial growth. Bacterial cultures were allowed to grow overnight to optical density ($OD_{600}$) to 0.8-1.0. At that point the overnight culture was rediluted by a factor of 1000 in fresh sterile broth. The increase in OD600 was monitored for the next 12 hours with cell culture dilutions plated on agar plates at the corresponding times as well. The bacterial counts and the $OD_{600}$ associated with them were used as the basis for estimating cell concentrations for the assays. For both B. subtilis and E. coli, $OD_{600}$ of 0.2 corresponded to approximately $10^7$ CFU/mL, and it took 5 hours and 1 hour respectively for each culture to reach that cell concentration. The growth curve generated in this preliminary work was also used to determine the duration of the incubation period of the assay. That period was established to be

8-10 hours for B. subtilis and 4-5 hours for E. coli. The duration was selected to reach sufficient $OD_{600}$ while remaining in the logarithmic growth phase.

The assays were carried out in sterile 96-well Cellstar plates (Greiner Bio-One, Monroe, NC) where a dilution series of the given antibiotic before and after treatment was prepared using PBS as a dilution medium. Residual hydrogen peroxide in AOP samples was quenched with thymine-free bovine catalase (Sigma-Aldrich, St. Louis, MO) to avoid any bacterial inhibition. Bovine catalase controls were performed to confirm that it does not interfere with the assay. The outside wells of the plate were filled with 100 µL of PBS and were not used in the analysis due to the evaporation effects. The dilution series was then spiked with 100 µL of bacterial culture at $10^6$ CFU/mL concentration. Positive and negative controls were used as well. Positive control (PC) consisted of 100 µL of PBS and 100 µL of bacterial culture (no antibiotic, unrestricted bacterial growth). Negative control (NC) consisted of 100 µL of PBS and 100 µL of sterile growth medium. Negative control served as a PBS and broth medium sterility check. The $OD_{600}$ of each well in the plate was measured before and after the incubation period appropriate for the culture as determined in the preliminary study described above. Epoch plate reader (BioTek Instruments, Inc., Winooski, VT) was used. Incubation occurred in a shaking incubator rotating at 150 rpm at 30°C for B. subtilis and 37°C for E. coli. The growth in each sample well was calculated using the following formula:

$$Growth = \frac{OD_{600}^{sample} - OD_{600}^{NC}}{OD_{600}^{PC} - OD_{600}^{NC}} \qquad [3\text{-}1]$$

Probability unit analysis(Finney 1977) was used to linearize the resulting data and determine the $LD_{50}$. The remaining antibacterial activity in the sample after treatment was calculated as a potency equivalency (PEQ):

$$PEQ = \frac{LD_{50}^{untreated}}{LD_{50}^{treated}} \qquad [3\text{-}2]$$

### 3.1.4 HPLC/MS analysis

Each treatment condition tested with an antibacterial activity assay was tested with high-performance liquid chromatography (HPLC) with ion trap mass spectrometry (MS) to determine the residual concentration of the parent antibiotic. The instruments used were Agilent 1100 series HPLC equipped with 4.6x50-XDB-C8 column and XCT Plus ion trap (Agilent, Santa Clara, CA). All compounds used in the study were detectable with the positive mode electrospray ionization. The mobile phase consisted of HPLC grade water (Honeywell Burdick & Jackson, Morristown, NJ) with 0.1% formic acid (Fluka, St. Louis, MO) and HPLC grade acetonitrile (Honeywell Burdick & Jackson, Morristown, NJ). The gradient elution started with 10% acetonitrile and 90% water and increased to 100% acetonitrile over 13 minutes after which it continued at 100% for 2 more minutes.

## 3.2 Results and Discussion

### 3.2.1 Advanced oxidation

Experimental results were grouped based on the water (clean water or effluent), type of UV source used (polychromatic or monochromatic), and whether hydrogen peroxide was added for hydroxyl radical generation. The plots show the normalized concentration of the parent antibiotic on the x-axis with the values in reverse order, so that values further right along the axis represent lower concentrations of the parent compound remaining after increasing treatment. These values are determined by HPLC/MS analysis. The y-axis shows the potency equivalent (PEQ) that remains in the sample after the corresponding level of treatment. Ideally, the values

should fall along the line where PEQ is equal to the fraction of the parent compound still remaining ($C/C_0$). That would indicate that the products that form do not retain the antibacterial activity. If some of the products retain the antibacterial activity, the point would fall above the PEQ=$C/C_0$ line. Figure 15 below shows the results of advanced oxidation experiments.

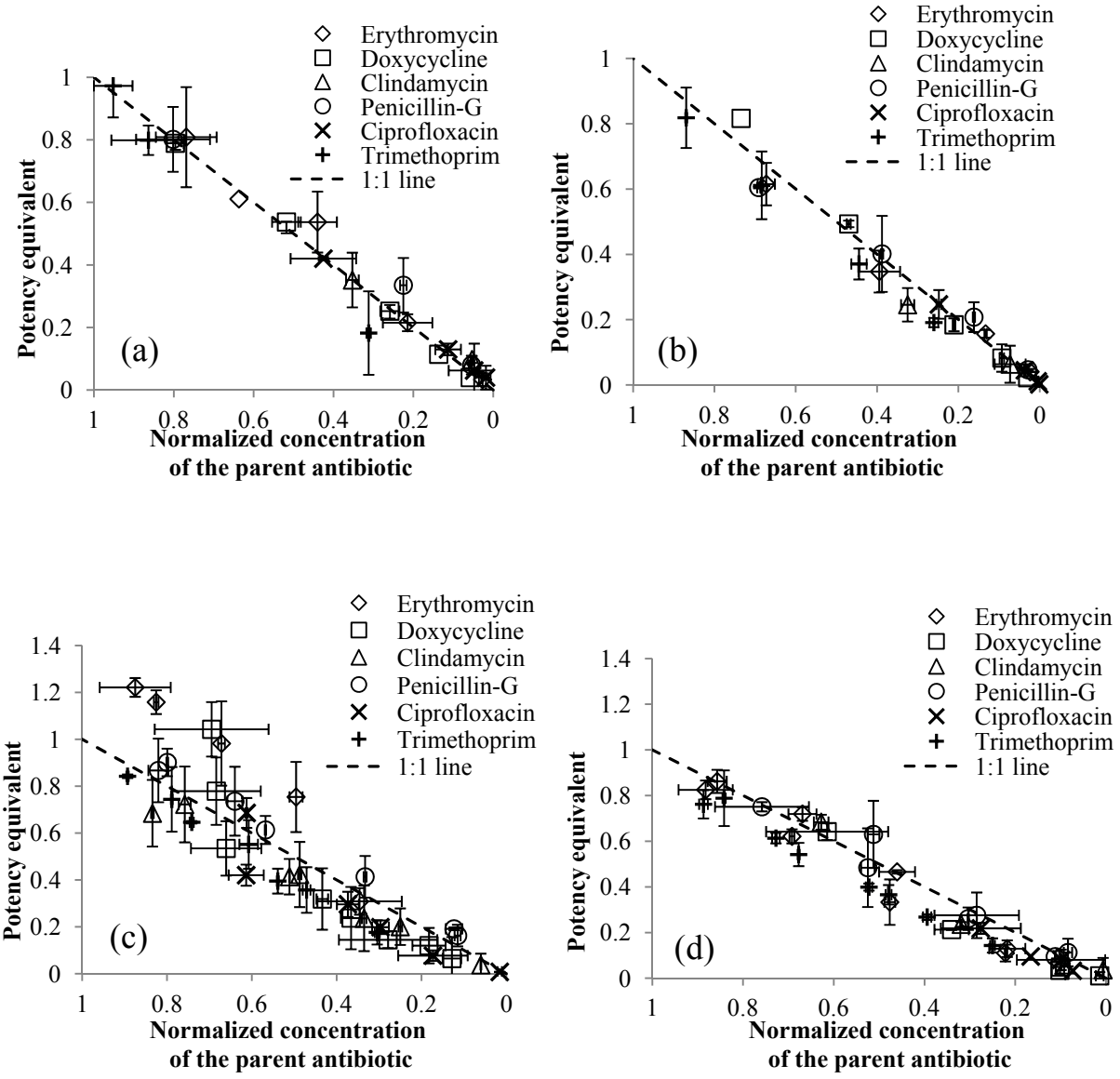


**Figure 15: Decrease of antibacterial activity of antibiotics (potency equivalent) with corresponding decrease in the concentration of the parent antibiotic after advanced oxidation treatment (a) using UV at 254nm in clean water, (b) using polychromatic UV above 200 nm in clean water, (c) using UV at 254 nm in effluent, and (d) using polychromatic UV in effluent**

As evident from the plots, a majority of the tested antibiotics showed no products exhibiting antibacterial activity in clean water, although doxycycline showed a very slight residual activity among early products of photolysis by polychromatic UV. In effluent, on the other hand, two of the antibiotics (erythromycin and doxycycline) showed early products that retained antibacterial activity. Another interesting finding is that those antibacterially active products only formed with UV at 254 nm, and were not observed when polychromatic UV was used. Because these active products were not detected in clean water experiments, it is reasonable to assume that those products do not form via reaction with hydroxyl radicals but rather by other photosensitized reactions common in natural waters with complex matrices, such as reaction with singlet oxygen or with triplet organic matter. The difference in the degradation pathways with the two different UV sources can be explained by the differences in the energy delivered by different wavelengths of the UV spectrum. Wavelength between 200 and 254 nm are not present in the spectrum of the monochromatic UV source. Much higher energy associated with those wavelengths can initiate additional photosensitized reactions and result in different reaction pathways being dominant. Additionally, nitrate photolysis occurring in effluents under wavelengths between 200 and 240 nm creates radicals other than HO• which could also participate in reactions with antibiotics. Nitrate photochemistry is discussed in greater detail elsewhere (Chapter 4). These results stress the importance of conducting bench-scale experiments in matrices representing full-scale conditions as close as possible. The experiments performed in clean water prove that hydroxyl radical pathway does not form active intermediates in any of the tested antibiotics, but the experiments in effluent revealed that other photosensitized pathways do. The results were consistent in both effluents.

It is important to note that continued treatment eventually resulted in enough transformation to the parent compound that no residual antibacterial activity remained. This point was achieved faster for doxycicline than for erythromycin. It is also notable that the potency equivalent for both compounds was > 1 indicating that the active products are more potent antibiotics than the parent antibiotic.

A few notes must be added on the analytical challenges associated with these two compounds. Erythromycin is easily dehydrated in water. Preliminary experiments were conducted to confirm that dehydrated erythromycin has the same antibacterial potency as the original erythromycin. Direct photolysis converts erythromycin to the dehydrated erythromycin. Samples with different ratios of one form or the other exhibited the same antibacterial activity. The parent antibiotic concentration for erythromycin is a sum of erythromycin and dehydrated erythromycin formed by photolysis. The two products appear on the same scale in the mass spectrometry analysis, as was confirmed by allowing a solution of erythromycin in clean water to dehydrate at room temperature so that no other products formed. The signals produced by each form of erythromycin added up to the mass balance.

An analytical challenge with doxycycline comes from its ability to form chelate complexes with divalent cations which are abundant in effluents. When it forms a chelate complex, it loses its ability to inactivate bacteria resulting in lower response.(Andrews and Magee) However, when the same sample is tested with mass spectrometry, some of those complexation bonds will be dissociated on impact in the ion source. As a result, the data points fall below the 1:1 line due to the apparent concentration of the parent compound measured by mass spectrometry being higher than the actual non-complexed molecules available for bacterial inactivation.

Additionally, penicillin-G reacted with hydrogen peroxide, so the samples collected for both antibacterial assays and for mass spectrometry had to be immediately quenched with bovine catalase after the advanced oxidation experiment.

### 3.2.2 Direct photolysis

Figure 16 shows the results of photolysis presented in the same manner as the results of advanced oxidation described in the previous section. Compounds that exhibited less than 15% transformation by direct photolysis at fluence of 2000 mJ/cm$^2$ were considered non-susceptible to photolysis and were not included in the analysis. Three out of the six tested antibiotics exhibited degradation by direct photolysis: doxycycline, penicillin-G and ciprofloxacin. In effluent, all compounds showed degradation with polychromatic UV due to hydroxyl radical generation via nitrate photolysis. With UV at 254 nm in effluent, apart from antibiotics degradable by direct photolysis, clindamycin showed degradation by photosensitized reactions. Clindamycin is not susceptible to direct photolysis by UV at 254 nm due to lack of absorbance at this wavelength, so the degradation observed in effluent is entirely due to photosensitized reactions.

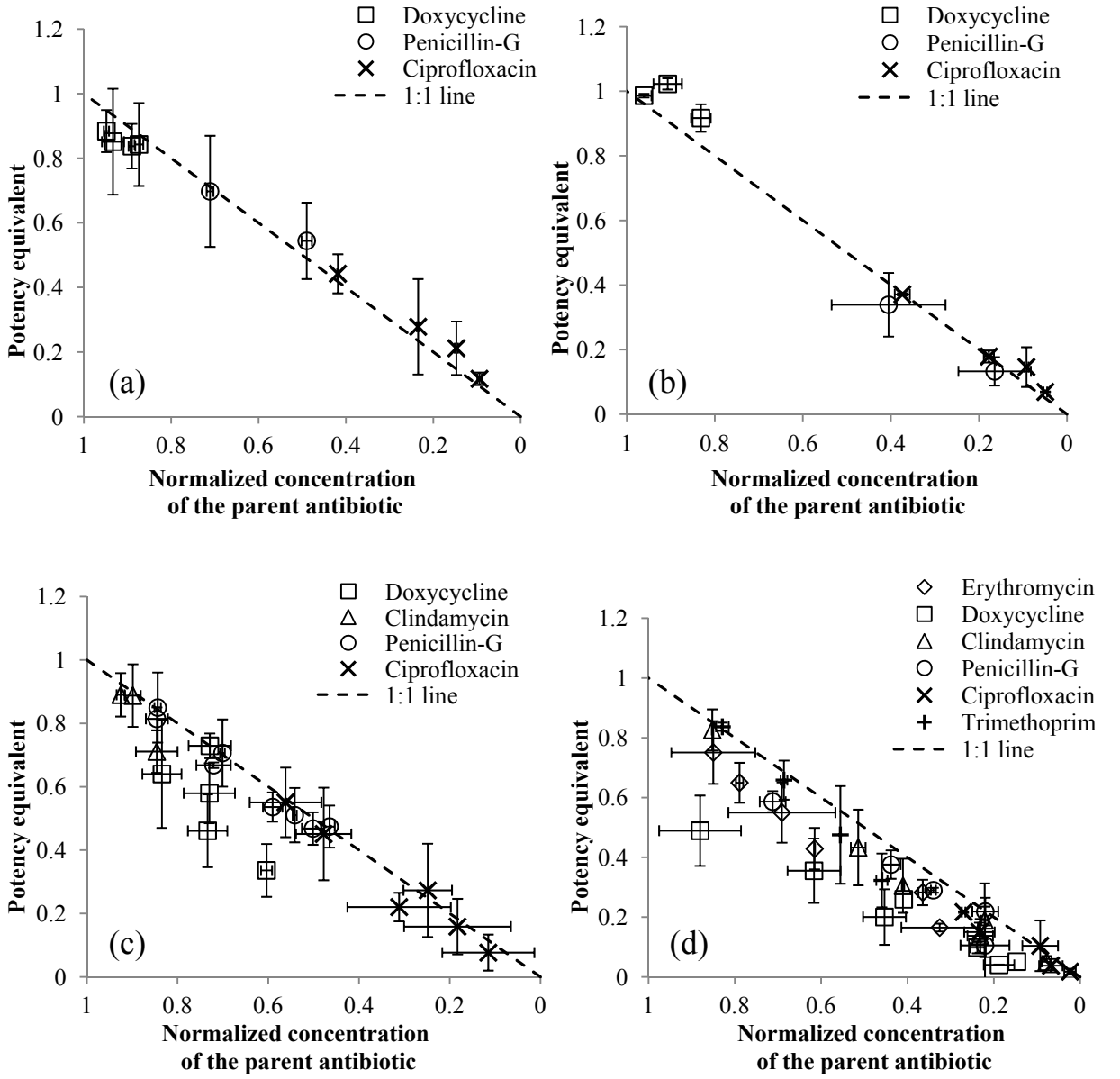


**Figure 16: Decrease of antibacterial activity of antibiotics (potency equivalent) with corresponding decrease in the concentration of the parent antibiotic after photolysis without $H_2O_2$ addition (a) using UV at 254nm in clean water, (b) using polychromatic UV above 200 nm in clean water, (c) using UV at 254 nm in effluent, and (d) using polychromatic UV in effluent**

Once again doxycycline appeared to form antibacterially active intermediates with polychromatic UV in clean water. This is consistent with the results for advanced oxidation in clean water. However, with advanced oxidation these active intermediates are observed only in the early stages of treatment and apparently get degraded further by hydroxyl radicals where they no longer retain the antibacterial activity. The effect of divalent cations forming chelate

complexes with doxycycline is again evident in effluent in the same manner as described in the previous section.

Overall, the results of advanced oxidation proved satisfactory for degradation of antibacterial activity in effluents. Although some active intermediates were detected for two of the six antibiotics (erythromycin and doxycycline), they eventually were degraded to products with no antibacterial activity. The highest doses of treatment applied for analysis were consistent with full-scale UV fluences and $H_2O_2$ concentrations. Figure 17 shows the extent of transformation for each tested antibiotic at 1000 mJ/cm$^2$ and 2000 mJ/cm$^2$ in effluent with and without $H_2O_2$. The results show that after treatment with 2000 mJ/cm$^2$ and 10 mg/L of $H_2O_2$, 4 out of 6 antibiotics dropped to less than 10% of the starting concentration. The degradation with medium pressure lamp in the absence of $H_2O_2$ is mainly due to hydroxyl radical formation via nitrate photolysis.

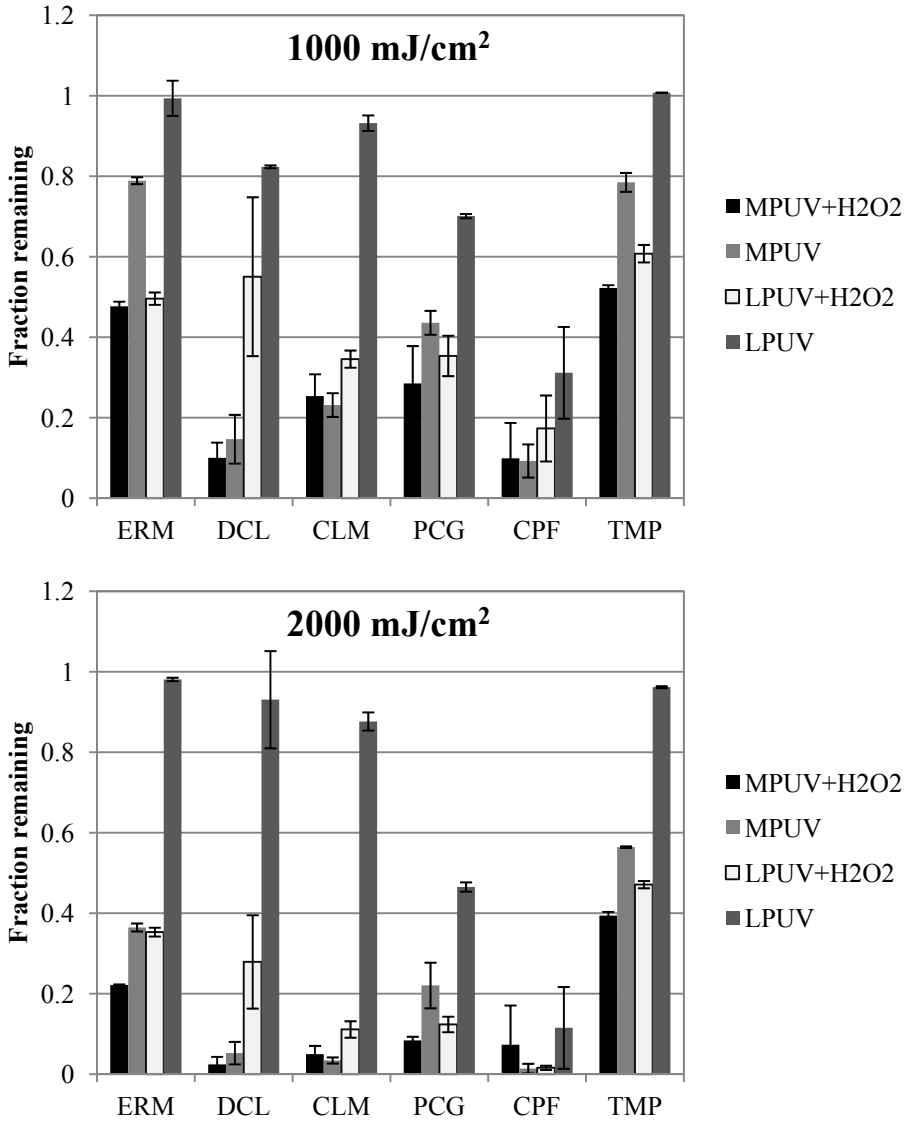


**Figure 17: Fraction of initial antibiotic still remaining in effluent after 1000 mJ/cm$^2$ (top) and 2000 mJ/cm$^2$ (bottom) with different treatment: medium pressure UV lamp (MPUV) or low pressure UV lamp (LPUV) with or without hydrogen peroxide for erythromycin (ERM), doxycycline (DCL), clindamycin (CLM), penicillin-G (PCG), ciprofloxacin (CPF) and trimethoprim (TMP)**

It can be concluded that when effluents are treated with AOP at full scale, active antibiotic transformation products will not present a concern. Two of the antibiotics (erythromycin and doxycycline) may form active intermediates during direct photolysis at lower doses of UV, such as those currently used for disinfection.

# Chapter 4: Formation of hydroxyl radicals during photolysis of nitrate at 200-240 nm wavelength

The work presented in this chapter was previously published as Keen, O. S., Love, N. G. and Linden, K.G. (2012). "The role of effluent nitrate in trace organic chemical oxidation during UV disinfection." Water Research **46**(16): 5224-5234.

## 4.1 Materials and Methods

### 4.1.1 Chemicals and reagents

Hydrogen peroxide and sodium nitrite (both J.T. Baker, Phillipsburg, NJ), methylene blue and t-butanol (both Sigma-Aldrich, St.Louis, MO), carbamazepine (Acros Organics, Geel, Belgium) and sodium nitrate (Fisher Chemical, Fair Lawn, NJ) used in the study were of reagent grade purity. Effluent was taken pre-disinfection from eight WWTPs. All plants achieve various degrees of nitrification and denitrification.. Plant 1 uses extended aeration with on/off aeration. Plant 2 is an activated sludge process with anoxic selector for filament control, followed by clarifiers and nitrifying trickling filters. Plant 3 has a solids contact tank followed by nitrifying trickling filters and denitrifying filters. Plant 4 has high purity oxygen high rate aerated sludge with short sludge age and does not achieve significant nitrification. Plants 5, 6 and 8 use Modified Ludzack-Ettinger (MLE) process. Plant 5 has additional sidestream partial removal of phosphorus, and Plant 8 has denitrifying filters following the MLE process. Plant 7 uses a 5-stage Bardenpho process for nutrient removal. Samples from Plants 7 and 8 were allowed to biodegrade further upon collection before being filtered and chilled. During this, additional decrease in nitrate was achieved, and the samples were used as low nitrate controls together with effluent from Plant 4. Therefore, it should be noted that low nitrate values for Plants 7 and 8 are not typical of the treatment process. All remaining samples were filtered immediately upon

collection through a 0.45µm nylon filter (Pall, Port Washington, NY) and stored at 4° C. Water quality parameters and treatment processes for each plant are listed in Table 1.

### 4.1.2 UV systems

The bench scale MP UV system (Calgon Carbon Corp., Pittsburgh, PA) was equipped with a 1 kW MP UV lamp quasi-collimated by a 6.4 cm diameter, 10 cm long cylindrical tube. The irradiations at fluences of up to 2000 mJ/cm$^2$ were carried out in a crystallization dish, continuously stirred. The lamp irradiance was measured with a calibrated International Light IL-1700 radiometer (Peabody, MA) and corrected according to the method outlined in Bolton and Linden (2003), including absorbance and depth of sample. The fluence was calculated as the product of 200-300 nm average irradiance and exposure time, and was not germicidally weighted except when stated otherwise. The lamp emission spectrum was measured by an Ocean Optics spectrometer USB2000 (Ocean Optics, Dunedin, FL).

### 4.1.3 Test methods

Hydrogen peroxide was measured prior to UV/$H_2O_2$ AOP exposure using the triiodide method by Klassen et al. (1994). Alkalinity was measured using Hach digital titrator, and nitrate and nitrite were measured colorimetrically using Hach kits TNT835 and TNT839 respectively (Hach Corporation, Loveland, CO). Beckman Φ 340 pH meter (Beckman Coulter, Inc., Brea, CA) was used to measure pH. Dissolved organic carbon was measured with a Shimadzu TOC-$V_{CSH}$ organic carbon analyzer (Shimadzu America, Inc. Columbia MD). Methylene Blue was measured spectrophotometrically at 664 nm wavelength using Varian Cary100Bio spectrophotometer (Agilent, Santa Clara, CA). The concentration of Methylene Blue was determined based on the manufacturer specifications for the reagent, and molar extinction coefficient for the solution at 664 nm was 64000 $M^{-1}cm^{-1}$. Carbamazepine (4.2 µM) was spiked

into effluents and subsequently measured by high performance liquid chromatography with mass spectrometry analysis (HPLC/MS) using an Agilent 1100 Series HPLC with XCT Plus ion trap (Agilent Technologies, Inc., Santa Clara, CA). Mobile phases were acetonitrile (HPLC grade, Honeywell Burdick & Jackson, Morristown, NJ) and ultrapure water (arium611-VF, Sartorius Stedim, Bohemia, NY) with 0.1% formic acid (Fluka, St. Louis, MO). Acetonitrile concentration was increased from 30% to 100% over 6 minutes. Positive ion mode was used.

### 4.1.4 Experimental procedure

A solution of methylene blue was spiked into ultrapure water at a concentration 10 μM to act as an HO• radical probe. Different concentrations of $H_2O_2$ and $NO_3^-$ were added to aliquots of the solution and exposed to increasing fluence up to 2000 mJ/cm$^2$. Controls for the experiment were as follows: a) the photolysis of methylene blue (MB) without added $H_2O_2$ or $NO_3^-$; b) degradation of MB without UV in the presence of $H_2O_2$ or $NO_3^-$; c) sample spiked with 200 μM of t-butanol – a hydroxyl radical scavenger – with added nitrate or hydrogen peroxide. This scavenger was added to determine whether the main degradation pathway for methylene blue is indeed oxidation by hydroxyl radicals and to measure the contribution to contaminant degradation by direct photolysis or by other reactive species that may form during UV exposure.

### 4.1.5 Model Development

When nitrate is irradiated with UV, the formation of hydroxyl radicals follows a more complex pathway than formation from hydrogen peroxide irradiation. When a molecule of hydrogen peroxide absorbs a photon of UV, it splits into two hydroxyl radicals with a quantum yield (Φ) of reaction of 1.0. When a molecule of nitrate absorbs a photon of UV, it can either form nitrite and oxygen as shown in Eq.4-1a or a nitrite radical and an oxygen radical (Eq.4-1b). Oxygen radical forms a hydroxyl radical by reacting with water (Eq. 4-2) (Zepp et al. 1987).

Nitrite radical can either get oxidized by a hydroxyl radical back to nitrate or react with water and another nitrite radical to form more nitrite ion. The quantum yield of nitrite formation by all pathways during nitrate photolysis has been established for sunlight-relevant wavelengths and for UV irradiation over a range of conditions with values from many studies summarized in Mack and Bolton (1999). In the wavelength range below 240 nm only a few studies are available where Φ of nitrite formation from nitrate photolysis has been established. Warburg (1918) and Bayliss and Bucat (1975) determined the Φ to be 0.25 at 207 nm and 0.23 at 229 nm. These data indicate that the quantum yield does not vary significantly between 200-240 nm. However, in both studies Φ was determined at a high pH (11.7 and 11.5 respectively), which is not representative of the neutral pH of most wastewater effluents. The dependence of the nitrite quantum yield on pH has been demonstrated for nitrate photolysis at 254 nm (Mark et al. 1996). Sharpless and Linden (2001) determined Φ for nitrite formation at pH 6 and pH 8 (representative of natural water samples) to be in the range of 0.053-0.028 at 228 nm, about 6 times lower than the values measured at high pH in other studies.

$$NO_3^- \xrightarrow{h\nu} NO_2^- + \frac{1}{2}O_2 \qquad \text{(a)} \qquad \Phi = 0.053\text{-}0.028 \qquad [4\text{-}1]$$

$$NO_3^- \xrightarrow{h\nu} NO_2^{\bullet} + O^{\bullet -} \qquad \text{(b)}$$

$$O^{\bullet -} + H_2O \leftrightarrow HO^{\bullet} + OH^- \qquad k = 1.7 \cdot 10^6\ M^{-1}s^{-1} \text{ (Buxton et al. 1988)} \qquad [4\text{-}2]$$

Nitrite that forms during nitrate photolysis can in turn absorb another photon and produce a nitric oxide radical and an oxygen radical (Eq.4-3). The quantum yield for that reaction for low wavelength (<240 nm) UV has not been established.

$$NO_2^- \xrightarrow{h\nu} NO^{\bullet} + O^{\bullet -} \qquad \Phi = ? \qquad [4\text{-}3]$$

The oxygen radical immediately reacts with water to form a hydroxyl radical (Eq.4-2).

The nitric oxide radical and nitrite are strong hydroxyl radical scavengers.

$$NO^{\bullet} + HO^{\bullet} \rightarrow HNO_2 \qquad k = 1.0 \cdot 10^{10}\ M^{-1}s^{-1}\ \text{(Buxton et al. 1988)} \qquad [4\text{-}4]$$

$$NO_2^- + HO^{\bullet} \rightarrow NO_2^{\bullet} + OH^- \qquad k = 1.0 \cdot 10^{10}\ M^{-1}s^{-1}\ \text{(Buxton et al. 1988)} \qquad [4\text{-}5]$$

Nitrate is also a scavenger, but with a rate constant $k < 1.0 \cdot 10^5\ M^{-1}s^{-1}$ its contribution is negligible relative to other HO• scavenging compounds in solution. A simplified diagram of HO• sources and sinks during photolysis of nitrate is presented in Figure 18. In short, upon irradiation nitrate produces hydroxyl radicals as well as nitrite ions and radicals and other photoproducts. Many of these products lead to formation of nitrite ion as well. Nitrite can produce more hydroxyl radicals as well act as a radical scavenger. Nitrite and other nitrate photolysis products are hydroxyl radical scavengers as well as sources.

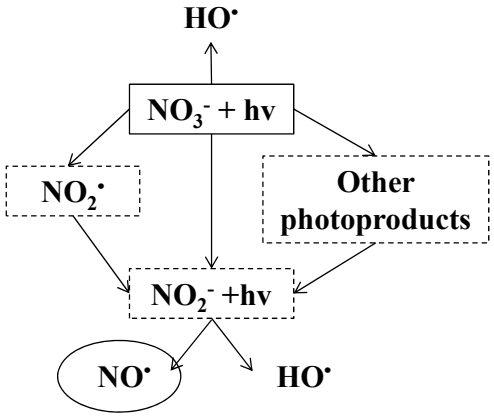


**Figure 18: Simplified photolysis pathway from nitrate to hydroxyl radical. Solid rectangle indicates a source of HO•, oval – sink, and dashed rectangle indicates that the compound is a source as well as a sink of HO•.**

To calculate the production of HO• from nitrite, the steady-state hydroxyl radical concentration model (Eq. 4-6) developed by Glaze et al. (1995) for UV/hydrogen peroxide was adapted as:

$$[HO\bullet]ss = \frac{E_\lambda \varepsilon_{NO2,\lambda} [NO_2^-] \Phi_{HO}}{U_\lambda \sum k_{S,HO}[S]} \qquad [4\text{-}6]$$

where

[HO•]ss = steady-state hydroxyl radical concentration, M

$E_\lambda$ = irradiance at the given wavelength, mW $cm^{-2}$

$\varepsilon_\lambda$ = molar absorption coefficient of nitrite at the given wavelength, $M^{-1}cm^{-1}$

$\Phi_{HO}$ = quantum yield of HO• production from nitrite, -

$U_\lambda$ = is the energy of the given wavelength, J $Es^{-1}$

$k_{S,HO}$ = reaction rate constant of a given HO• scavenging compound with HO•, $M^{-1}$ $s^{-1}$

[S] = concentration of the given HO• scavenging compound, M

As was noted above, the quantum yield for production of HO• from the photolysis of nitrate (Eq.4-2) is not available. However, the steady-state concentration of hydroxyl radicals is readily measured using a probe compound with a well established HO• scavenging rate constant. Methylene blue (MB) was used as a probe compound in this study. It is not susceptible to direct UV photolysis above 200 nm as has been determined in control experiments for this study, and its reaction rate constant with HO• has been reported as $2.1 \cdot 10^{10}$ $M^{-1}$ $s^{-1}$ (Buxton et al. 1988). The major scavenging compounds included MB, $NO_2^-$ and NO•, the latter being a function of $[NO_2^-]$ and $\Phi_{HO}$. It is difficult to estimate the concentration of NO• in solution. But because its concentration depends on the concentration of $NO_2^-$ and both have the same reaction rate with HO• equal to $1.0 \cdot 10^{10}$ $M^{-1}s^{-1}$ (Buxton et al. 1988), the two scavengers can be combined together as $[NO_2^-]_*$. Therefore, the expression for $[HO\bullet]_{ss}$ formed from photolysis of nitrite in clean water can be written as follows:

$$[HO\bullet]_{SS} = \frac{E_\lambda \varepsilon_{NO2,\lambda} [NO_2^-] \Phi_{HO}}{U_\lambda (k_{MB,HO}[MB] + k_{NO2,HO}[NO_2^-] + k_{NO\bullet,HO}[NO\bullet])} \qquad [4\text{-}7]$$

where $k_{NO2,HO} = k_{NO\bullet,HO}$

and $[NO_2^-] + [NO\bullet] = [NO_2^-]_* = \text{constant}$

Equation 4-7 simplifies to the following form:

$$[HO\bullet]_{SS} = \frac{E_\lambda \varepsilon_{NO2,\lambda} [NO_2^-] \Phi_{HO}}{U_\lambda (k_{MB,HO}[MB] + k_{NO2,HO}[NO_2^-]_*)} \quad [4\text{-}8]$$

In nitrified effluents, HO• is produced from nitrite, via nitrate as a starting compound through a multitude of concurrent and intermediate reactions. In addition, a certain percentage of HO• is produced directly from nitrate. It is therefore more practical to fit an empirical model that would tie the production of HO• to nitrate concentration rather than nitrite because (1) nitrate is the starting point and more stable in wastewater, and (2) it would combine the complex elements of the overall process into a more useful and experimentally measurable format. Equation 4-8 would then become:

$$[HO\bullet]_{SS} = \frac{E_\lambda \varepsilon_{NO3,\lambda} [NO_3^-] \Phi'_{HO}}{U_\lambda (k_{MB,HO}[MB] + k'_{NO3,HO}[NO_3^-])} \quad [4\text{-}9]$$

where $\Phi'_{HO}$ is a pseudo-quantum-yield that combines all the intermediate reactions that eventually lead to formation of HO• from nitrate as a starting compound. $k'_{NO3,HO}$ is an overall HO• scavenging rate between all of the HO• scavenging compounds that form during photolysis of nitrate with the nitrate concentration as a surrogate measure of combined concentrations of the nitrate-derived scavenging intermediates.

To find coefficients of best fit for both models (Eq.4-8 and Eq.4-9), several $[HO\bullet]_{SS}$ values were measured by tracking the decay of the probe compound MB at different starting nitrate or nitrite concentrations with all other parameters being held constant. The coefficients of best fit for Eq.4-8 are the quantum yield of HO• production from nitrite ($\Phi_{OH}$) and the reaction

rate constant for scavenging of HO• by nitrite and nitrite ion combined ($k_{NO2,HO}$). The coefficients of best fit for Eq.4-9 are the quantum yield of HO• production from nitrate via all reaction pathways ($\Phi'_{OH}$) and the reaction rate constant for scavenging of HO• by all nitrate photolysis products ($k'_{NO3,HO}$). The coefficients were determined by using a linearization similar to Langmuir isotherm fitting (Benjamin 2002).

## 4.2 Results and Discussion

### 4.2.1 Degradation of carbamazepine in nitrified effluent

When carbamazepine was spiked in nitrified effluent containing 16.2 mg-N/L of nitrate with and without addition of 5 mg/L of $H_2O_2$ and irradiated with MP UV, the loss of the compound was nearly identical in both instances as seen in Figure 19. The level of carbamazepine degradation observed in the sample with no $H_2O_2$ would not be achievable by direct photolysis alone because of the extremely low quantum yield of the compound: 0.00039 in the 200-300 nm range of the typical MP UV spectrum (Linden, Keen et al. 2011). Therefore, the production of radicals from an indigenous species during UV photolysis of the effluent was suspected. The most likely reactive species was HO• generated by nitrate photolysis, mediated by intermediate nitrite formation during UV irradiation.

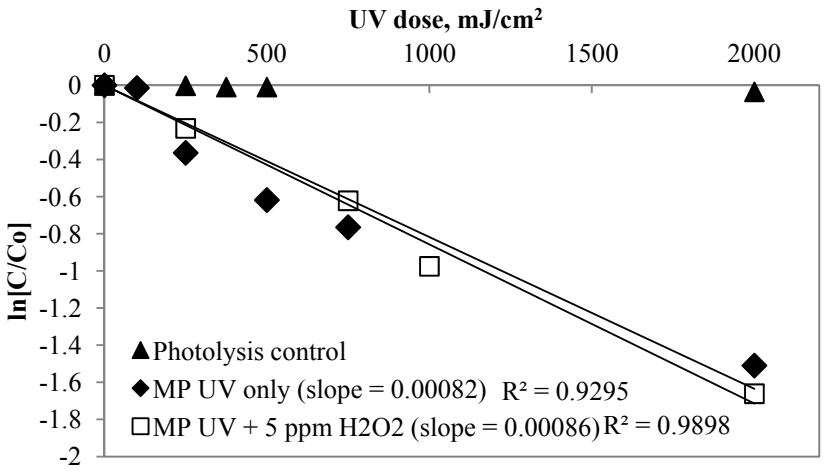


**Figure 19: Degradation of carbamazepine in wastewater effluent containing 16.2 mg-N/L of nitrate with and without 5 mg/L of $H_2O_2$**

### 4.2.2 HO• production from nitrite in clean water

Experiments were conducted using clean water and MB as a hydroxyl radical probe to establish a relationship between the initial nitrite concentration and the steady-state concentration of hydroxyl radicals ([HO•]ss) generated by nitrite photolysis described in Equations 4-2 and 4-3. The procedure for calculating [HO•]ss from a different probe compound was described by Rosenfeldt and Linden (2007). In short, the following equation was used:

$$\ln\frac{[MB]_t}{[MB]_0} = \frac{-k_{HO,MB}[HO\bullet]_{SS}}{E_0}\cdot F_0 \qquad [4\text{-}10]$$

where $E_0$ is the average fluence rate ($mW/m^2$), $F_0$ is the fluence ($mJ/m^2$) and $k_{HO,MB}$ is a time-based reaction rate constant between probe MB and hydroxyl radicals ($M^{-1}s^{-1}$). As illustrated in Figure 20, the production of HO• increased rapidly with nitrite concentration, then slowed, indicating that the additional nitrite acted as a scavenger of the HO• it produced.

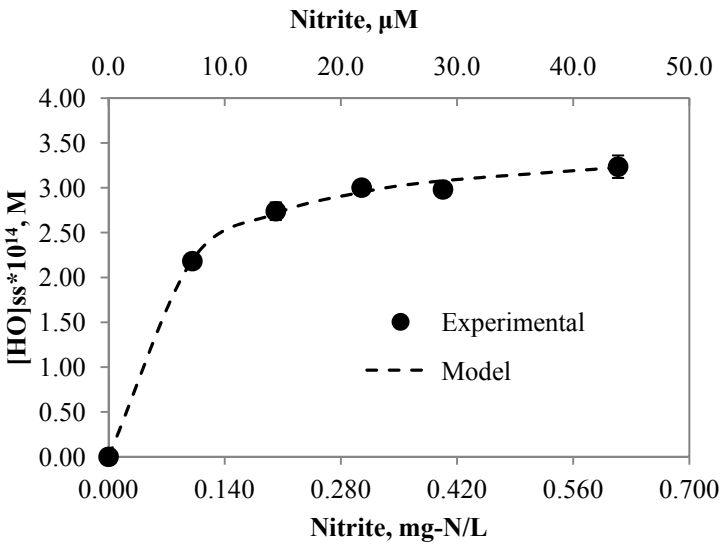


**Figure 20: Formation of HO• during irradiation of varying nitrite concentrations with MP UV**

The best fit model of Equation 4-8 describing a relationship between nitrite and [HO•]ss returned the following coefficients:

$$[HO\bullet]_{SS} = \frac{1.7\cdot10^{-3}[NO_2^-]}{1.0\cdot10^{-5}\cdot2.1\cdot10^{10} + 4.7\cdot10^{10}[NO_2^-]} \qquad [4\text{-}11]$$

In the expression above, $1.0\cdot10^{-5}$M is the concentration of the probe (MB) and $2.1\cdot10^{10}M^{-1}s^{-1}$ is its reaction rate constant with HO•. The best fit coefficient $1.7\cdot10^{-3}$ in the numerator represents the following term from equation 8: $\sum \frac{E_\lambda \varepsilon_{NO2,\lambda} \Phi_{HO}}{U_\lambda}$. From here average $\Phi_{HO}$ for the 200-240 nm range of wavelengths can be calculated by dividing the coefficient by the sum of the $\frac{E_\lambda \varepsilon_{NO2,\lambda}}{U_\lambda}$ terms for each wavelength, based on measured data for $E_\lambda$, $\varepsilon_{NO2,\lambda}$, and $U_\lambda$. The resulting value of $\Phi_{HO}$ is 0.65±0.06. The contribution to the photolysis by other wavelengths can be assumed negligible because of the low absorbance of nitrite above 240 nm (Figure S1). The other empirical coefficient in the denominator represents $k_{NO2,HO}$ which includes the scavenging by nitrite itself and any of its photoproducts. The value of $4.7\cdot10^{10}$ $M^{-1}s^{-1}$ is higher than the

reaction rate constant between HO• and nitrite reported in the literature ($1.0 \cdot 10^{10}$ $M^{-1}s^{-1}$). This high reaction rate can be explained by the fact that diffusion is not playing the same role in the recombination reactions as it does in scavenging of HO• by the nitrite in the bulk solution. In the case of the recombination, the radical and its parent are still in the so called "solvent cage" facilitating a faster reaction than between the molecules in the bulk solution.

### 4.2.3 HO• production from nitrate in clean water

When HO• is generated during irradiation of nitrified effluent, nitrite is often initially at a very low concentration and is generated by the photolysis of nitrate which is typically more abundant. Therefore a relationship between the HO• generation and starting nitrate rather than nitrite concentration is more useful for practical purposes. Figure 21 shows the experimental data for HO• generation as a function of the starting nitrate concentration with each point determined in a fully separate experiment, using MB as a probe compound. The dashed line represents the best fit model for the experimental data.

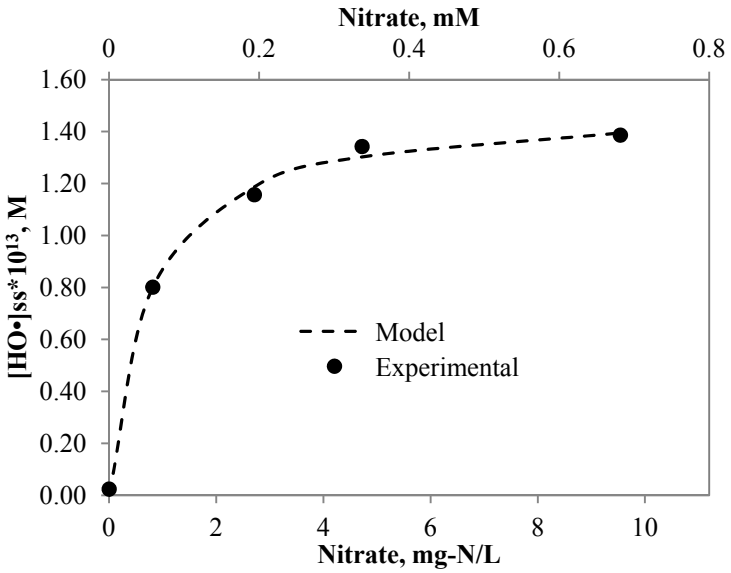


**Figure 21: Formation of HO• at varying nitrate concentrations**

The best fit model of the Equation 4-9 on the data returned the following coefficients:

$$[HO\bullet]_{SS} = \frac{6.2 \cdot 10^{-4}[NO_3^-]}{1.0 \cdot 10^{-5} \cdot 2.1 \cdot 10^{10} + 4.1 \cdot 10^{9}[NO_3^-]} \quad [4\text{-}12]$$

where $1.0 \cdot 10^{-5}$M is the concentration of the probe (MB) and $2.1 \cdot 10^{10}$M$^{-1}$s$^{-1}$ is its reaction rate constant with HO•. The best fit coefficient $6.2 \cdot 10^{-4}$ in the numerator represents $\sum \frac{E_\lambda \varepsilon_{NO3,\lambda} \Phi'_{HO}}{U_\lambda}$ The value of $\Phi'_{HO}$ was calculated as 0.24±0.03 using the measured values for $E_\lambda$, $\varepsilon_\lambda$, $U_\lambda$, [HO•]ss and $[NO_3^-]$. Based on the reported values for the quantum yield of nitrite formation during nitrate photolysis (0.028-0.053 as per Sharpless and Linden (2001)), and the quantum yield of HO• from nitrite calculated above (0.65±0.06), about 6-18% of HO• produced during nitrate photolysis forms via nitrite as an intermediate. The majority of HO• forms directly from nitrate or via intermediates other than nitrite, e.g. peroxynitrite. The other empirical coefficient in the denominator represents $k'_{NO3,HO}$. The value of $4.1 \cdot 10^9$ M$^{-1}$s$^{-1}$ is within the typical range of reaction rate constants for most compounds with HO•. This value combines all the HO• scavenging products of nitrate photolysis. Nitrite ion and nitric oxide are the fastest reacting scavengers with $k_{OH} = 1.0 \cdot 10^{10}$ M$^{-1}$s$^{-1}$. But their relative representation among the products is small with the quantum yield of nitrite of 0.028-0.053. This indicates that the majority of HO• scavenging comes from other photoproducts of nitrate, such as nitrite radical with $k_{OH} = 1.3 \cdot 10^9$ M$^{-1}$s$^{-1}$ (Buxton et al. 1988). Additionally, solvent cage effects make the scavenging rates observed here higher than what would be expected when the reaction occurs between two molecules in the well-mixed bulk solution.

When $[HO\bullet]_{SS}$ generation is compared for a typical range of $H_2O_2$ used in advanced oxidation (5 to 15 mg/L) and for a range of $NO_3^-$ typically measured in effluents (5 to 15 mg-

N/L, see Table 4), nitrate at concentrations up to 5 mg/L is more effective for generation of HO• than when $H_2O_2$ is present at similar concentrations. As illustrated in Figure 22, when both $NO_3^-$ and $H_2O_2$ are present in the 5 to 10 mg/L range, both produce comparable [HO•]ss. Concentrations higher than 10 mg/L of $H_2O_2$ can be more efficient in generating hydroxyl radicals than concentrations of $NO_3^-$ above 10 mg/L (due to high HO• scavenging by nitrite) but eventually will also reach a plateau due to HO• scavenging by $H_2O_2$ (Glaze et al. 1995). For comparison, $k_{OH,NO2} = 1.0 \cdot 10^{10} M^{-1}s^{-1}$ and $k_{OH,H2O2} = 2.7 \cdot 10^{7} M^{-1}s^{-1}$ (Buxton et al. 1988).

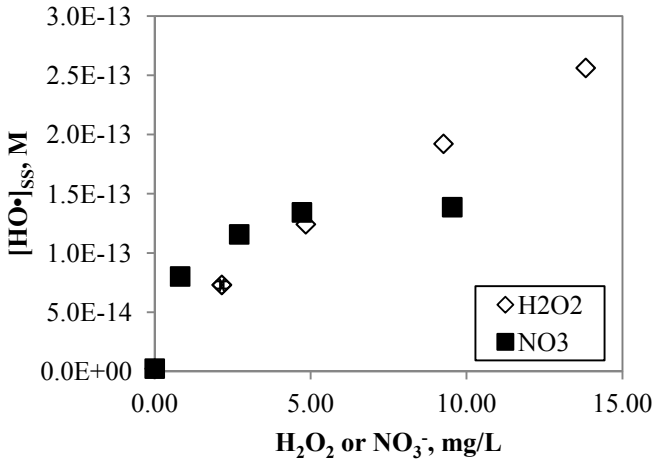


**Figure 22: Formation of HO• per mg/L of $H_2O_2$ and $NO_3^-$ in clean water**

### 4.2.4 Generation of HO• by nitrate in nitrified effluents

To validate the model, grab samples of effluents from 8 different facilities, each achieving a different level of nitrification, were used. Effluents from 3 of the facilities either contained levels of nitrate below the detection limit of the experimental method or were allowed to further biodegrade to achieve lower nitrate levels, and were used as low nitrate controls. Two of the facilities were sampled twice on separate occasions (WWTPs 3 and 6). Additionally, one of the samples was collected on the same day at different locations in a treatment train: from the denitrifying filters and final effluent before disinfection (WWTP 3). The rest of the samples

were collected as final effluent before disinfection, typically from secondary clarifiers. Water quality characteristics of each effluent as well as measured [HO•]ss are listed in Table 4.

**Table 4: Water quality measurements for the two effluents used in the study**

| Utility | Treatment process | Alkalinity, mg/L as $CaCO_3$ | pH, - | Nitrite, mg-N/L | Nitrate, mg-N/L | Dissolved organic carbon, mg-C/L | Measured $[HO•]_{ss}$, M |
|---|---|---|---|---|---|---|---|
| WWTP1 | Activated sludge with biological nutrient removal | 82 | 6.40 | 0.171 | 5.49 | 9.2 | 2.96E-14 |
| WWTP2 | Activated sludge with biological nutrient removal | 51 | 6.32 | 0.242 | 14.36 | 9.8 | 4.19E-14 |
| WWTP3 (1) [df] | Solids contact activated sludge + nitrifying trickling filters + denitrifying filters | 96 | 6.43 | 0.099 | 12.8 | 13.9 | 4.58E-14 |
| WWTP3 (1) [fe] | - | 91 | 6.57 | 0.116 | 12.6 | 10.6 | 4.80E-14 |
| WWTP3 (2)[df] | - | 123 | 6.84 | <0.015* | 4.04 | 5.8 | 4.26E-14 |
| WWTP4 | High rate activated sludge | 232 | 6.98 | 0.026 | 0.079* | 25.3 | 4.77E-15 |
| WWTP5 | Activated sludge with biological nutrient removal | 108 | 7.04 | 0.077 | 3.76 | 12.1 | 3.77E-14 |
| WWTP6 (1) | Activated sludge with biological nutrient removal | 84 | 7.07 | 0.017 | 13.1 | 11.9 | 5.65E-14 |
| WWTP6 (2) | - | 88 | 6.58 | 0.021 | 10.3 | 4.9 | 5.51E-14 |
| WWTP7 | Activated sludge with biological nutrient removal + sand filters | 238 | 6.96 | 0.197 | 0.153* | 19 | 6.95E-15 |
| WWTP8 | Activated sludge with biological nutrient removal + denitrifying filters + sand filters | 219 | 6.99 | 0.1 | 0.175* | 11.9 | 4.71E-15 |

[df] = denitrifying filter effluent; [fe] = final effluent; * = below detection limit

Two of the samples were selected to represent lower (4.04 mg-N/L from WWTP 3 denitrifying filter effluent) and higher (10.3 mg-N/L from WWTP 6) concentrations of nitrate in a nitrified effluent. Degradation of probe compound methylene blue (MB) was measured without $H_2O_2$ and with 5 and 10 mg/L of $H_2O_2$. In addition, a control experiment with a sample spiked with HO• scavenger t-butanol was performed to determine the contribution of non-OH radical reactive pathways of MB degradation in the effluent matrix. The results in Figure 6 (left) show that in the effluent with 10.3 mg-N/L nitrate, additional hydrogen peroxide does not contribute considerably to the generation of OH radical (decay of MB). In this effluent the difference between MB degradation with no $H_2O_2$ and with 5 mg/L of $H_2O_2$ was not statistically significant with $p > 0.05$, while the difference was statistically significant ($p<0.05$) for addition of 10 mg/L $H_2O_2$. This means that little additional [HO•]ss is generated due to $H_2O_2$ addition beyond what is generated by nitrate photolysis in wastewater effluents. At high nitrate concentrations, the absorbance of nitrate is much higher than the absorbance of $H_2O_2$ in the 200-240 nm wavelength range (Figure 23). As a result, additional $H_2O_2$ becomes a minor source of HO• compared to nitrate yet the additional $H_2O_2$ is also an HO• scavenger. In effluents with lower concentrations of nitrate, addition of 5 mg/L or more of $H_2O_2$ can appreciably increase the [HO•]ss as seen from MB degradation experiments in the effluent containing 4.04 mg-N/L nitrate (Figure 24). The difference in MB degradation with no $H_2O_2$ and with both 5 and 10 mg/L of $H_2O_2$ was statistically significant with $p < 0.05$. As seen in Figure 24, samples with t-butanol as a hydroxyl radical scavenger showed more carbamazepine loss than would be expected from direct photolysis. This loss can be attributed to other reactive species generated by nitrate photolysis or photosensitization of dissolved oxygen, among other processes. Because

radicals other than HO• form during nitrate photolysis, some products that form may be different than in the UV/$H_2O_2$ process.

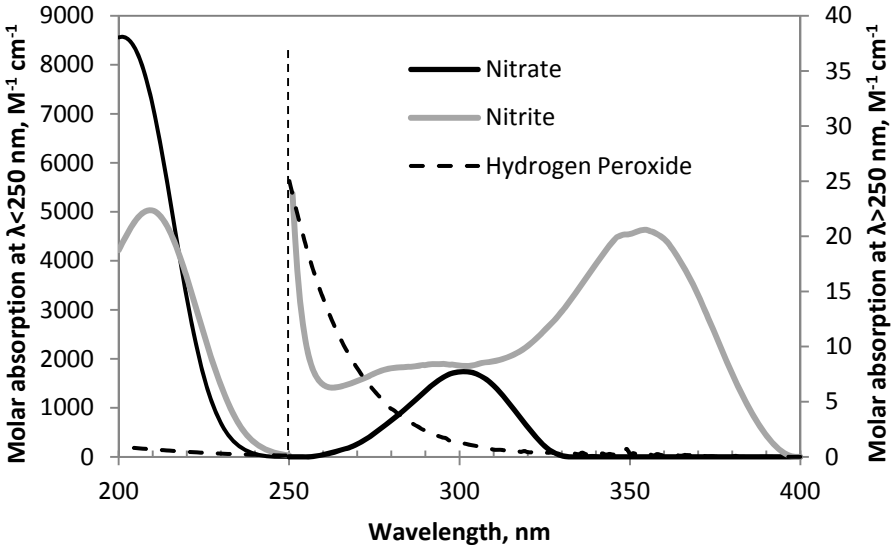


**Figure 23: Molar absorption of nitrite, nitrate and hydrogen peroxide**

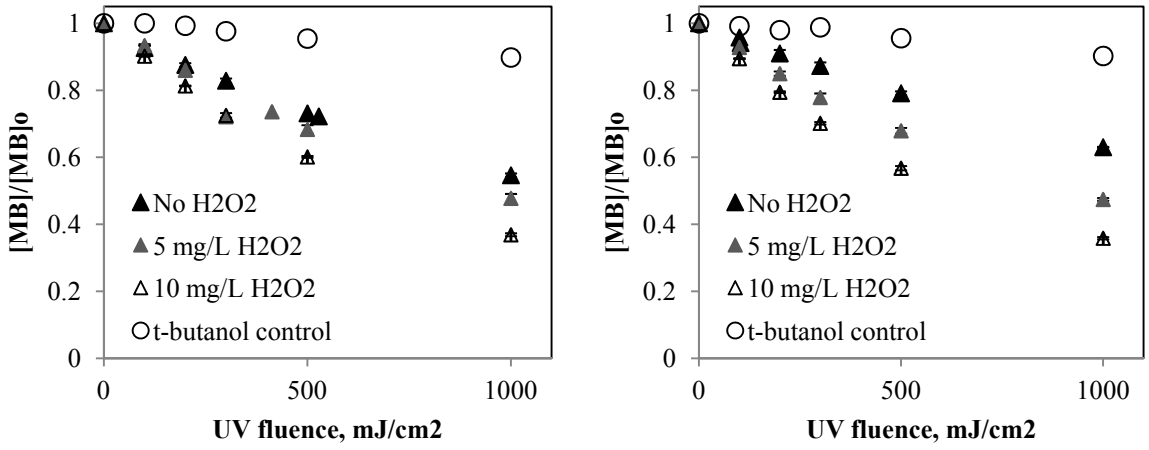


**Figure 24: Degradation of methylene blue in the effluent with 10.3 mg-N/L nitrate (left) and 4.04 mg-N/L nitrate (right) with and without additional hydrogen peroxide**

To predict the [HO•]ss that can be generated from the indigenous nitrate in a wastewater effluent, Eq. 4-9 was expanded to include other major known scavenging species in the effluent matrix. The resulting equation is:

$$[HO\bullet]_{SS} = \frac{E_\lambda \varepsilon_{NO3,\lambda}[NO_3^-]\Phi'_{HO}}{U_\lambda (k_{MB,HO}[MB] + k'_{NO3,HO}[NO_3^-] + k_{HCO3}[HCO_3^-] + k_{CO3}[CO_3^{2-}] + k_{NH3}[NH_3] + k_{DOC}[DOC])} \quad [4\text{-}13]$$

Reaction rate constants between these scavengers and OH radicals are summarized in Table 5.

**Table 5: Hydroxyl radical scavengers and the corresponding reaction rate constants with HO•**

| Scavenger | $k_{OH}$, $M^{-1}s^{-1}$ | Reference |
|---|---|---|
| $HCO_3^-$ | $8.5 \cdot 10^6$ | (Buxton, Greenstock et al. 1988) |
| $CO_3^{2-}$ | $3.9 \cdot 10^8$ | (Buxton, Greenstock et al. 1988) |
| MB | $2.1 \cdot 10^{10}$ | (Buxton, Greenstock et al. 1988) |
| $NH_4^+$ | $\sim 0$ | (Neta, Maruthamuthu et al. 1978) |
| $NH_3$ | $9.0 \cdot 10^7$ | (Neta, Maruthamuthu et al. 1978) |
| DOC | $3.6 \cdot 10^8$ | (Westerhoff, Aiken et al. 1999) |
| $NO_2^-$ | $1.0 \cdot 10^{10}$ | (Buxton, Greenstock et al. 1988) |

Several considerations are important for applying the model to calculate production of hydroxyl radicals in nitrified effluents. First, it has been noted by researchers previously, that with increasing concentrations of background scavengers the quantum yield of nitrite from nitrate increases because the background matrix consumes HO• and thus prevents newly formed nitrite from recombining with HO• back to nitrate (Sharpless and Linden, 2001). Because of high HO• scavenging potential, increased nitrite would decrease HO• formation potential in effluents compared to clean water. In addition, by increasing the yield of nitrite, these matrix effects would also change the balance between the yields of other nitrate photolysis products, including HO•. To improve the model performance for actual effluent samples, the model was amended with coefficients α and β, where $\alpha\Phi'_{HO}$ is the quantum yield of HO• in water matrices with heavy background scavenging, and β is the coefficient reflecting the change in HO• scavenging products that form during nitrate photolysis as a result of the change in the background matrix interactions. Equation 4-13 then becomes:

$$[\mathrm{HO\bullet}]_{SS} = \frac{E_\lambda \varepsilon_{\mathrm{NO3},\lambda} [\mathrm{NO_3^-}] \alpha \Phi'_{\mathrm{HO}}}{U_\lambda (\sum_i k_{\mathrm{S,HO}} [\mathrm{S}]_i + \beta k'_{\mathrm{NO3,HO}} [\mathrm{NO_3^-}])} \qquad [4\text{-}14]$$

In this equation

$$\sum_i k_{\mathrm{S,HO}} [\mathrm{S}]_i = k_{\mathrm{MB,HO}} [\mathrm{MB}] + k_{\mathrm{HCO3,HO}} [\mathrm{HCO_3^-}] + k_{\mathrm{CO3,HO}} [\mathrm{CO_3^{2-}}] + k_{\mathrm{NH3,HO}} [\mathrm{NH_3}] + k_{\mathrm{DOC,HO}} [\mathrm{DOC}]$$

Using MB as a probe, the measured [HO•]ss varied from $2.96 \cdot 10^{-14}$ M to $5.65 \cdot 10^{-14}$ M in the 8 samples that contained nitrate. Equation 4-14 was rearranged into its linear form using the procedure similar to the Langmuir isotherm fitting (Benjamin 2002) and coefficients α and β were calculated. The values of Φ'OH = 0.24 and k'OH = $4.1 \cdot 10^9$ $M^{-1}s^{-1}$ were determined in the experiments with clean water described above. The resulting value of α is 0.83, bringing down the yield of HO• by all pathways of nitrate photolysis from 0.24 observed in clean water to 0.20 in samples with high background scavenging. This difference is the result of the background matrix effects on nitrate photolysis. Changes in the quantum yield of nitrite in the presence of organic carbon were reported by Sharpless and Linden (2001), and other, previously unreported matrix effects on nitrate photolysis are possible. The value of β is a function of the rate at which nitrate absorbs UV energy in the given sample ($\sum(E_\lambda \cdot \varepsilon_{NO3,\lambda}/U_\lambda)$) and was calculated to be $515 \cdot \sum(E_\lambda \cdot \varepsilon_{NO3,\lambda}/U_\lambda)$ which put β in the range of 0.11-0.22 for the samples tested. This unitless coefficient (β) reflects the overall change in HO• scavenging species that form during photolysis of nitrate. Contrary to what was expected, the number is < 1 indicating that even though more nitrite may be forming, formation of other HO• scavenging products may be inhibited by the effluent matrix constituents resulting in smaller overall HO• scavenging potential of the products of nitrate photolysis. For example, nitrite radical (one of the major HO• scavenging photoproducts of nitrate) was possibly quenched by one of the background matrix constituents.

Indeed, the observed overall reaction rate between nitrate photoproducts and HO• in effluents is in the range of 4.5 to $9.0 \cdot 10^8$ $M^{-1}s^{-1}$, which is consistent with the expected scavenging by nitrite based on its quantum yield and its $k_{OH}$, i.e. $k'_{OH,NO3}[NO_3^-] \approx k_{OH,NO2}\Phi_{NO2}[NO_3^-]$ using the $\Phi_{NO2}$ reported by Sharpless and Linden (2001) for waters with high organic carbon.

The model amended with the coefficients predicted the [HO•]ss formation quite well (Figure 25). The discrepancy between the measured and the predicted [HO]ss is ≤ 10% in 5 out of 8 samples with measurable nitrate and < 15% in 7 out of 8 samples. The biggest error is 24%. The sample with 24% error had an unexpectedly low [HO•]ss generation. This sample may have had in its matrix another unexpected major scavenger not included in Eq.4-14. The residuals of the model showed no correlation as a function of nitrate, [HO•]ss generated, or background scavenging, indicating that the model is a good fit with randomly distributed residuals.

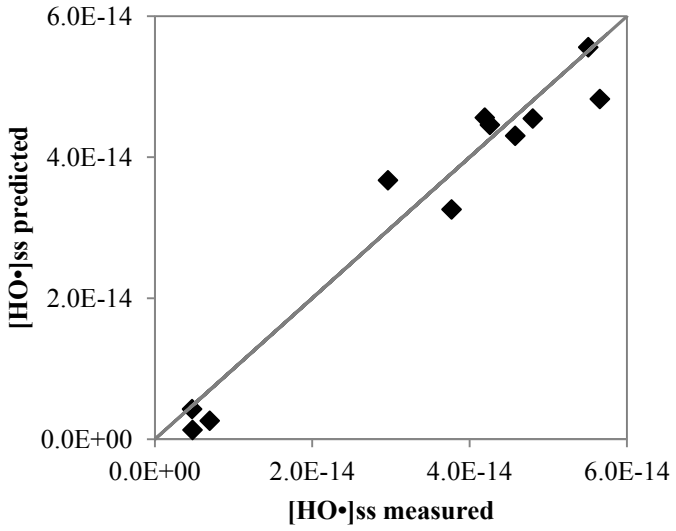


**Figure 25: Measured vs. predicted values of [HO•]ss**

Another consideration for future modeling of the HO• generation process at full scale is estimating the UV energy absorbed by nitrate. While the value of $\varepsilon_{NO3,\lambda}$ is published (including in the Supporting Information to this article) or easily measurable in the lab spectrophotometrically, and the value of $U_\lambda$ can be calculated from wavelength and fundamental

constants, obtaining the $E_\lambda$ requires specialized equipment not typically available at wastewater treatment plants. However, for a medium pressure mercury vapor lamp, the spectrum of irradiance is a fundamental physicochemical property of mercury gas and is similar for all lamps of that kind. As a result, the quantity of $\sum_\lambda \frac{E_{0,\lambda}}{E_0} \cdot \frac{\varepsilon_{NO3,\lambda}}{U_\lambda}$ is approximately the same for any medium pressure mercury vapor lamp. In this expression, $E_{0,\lambda}/E_0$ is the fraction of overall incident irradiance ($E_0$) emitted at each given wavelength $\lambda$. It is related to the average irradiance at each wavelength ($E_\lambda$) though the following expression:

$$E_\lambda = \frac{E_{0,\lambda}(1-\exp(-A_\lambda \cdot 2.303 \cdot L))}{A_\lambda \cdot 2.303 \cdot L} \quad [4\text{-}15]$$

where $A_\lambda$ is the decadic absorption of the sample at the given wavelength, 2.303 is a conversion factor from decadic absorption to exponential absorption, and L is the sample depth. As a result of this relationship, the overall average irradiance delivered by the lamp can be related to the $\sum_\lambda \frac{E_{0,\lambda}}{E_0} \cdot \frac{\varepsilon_{NO3,\lambda}}{U_\lambda}$ quantity and sample absorbance at a representative wavelength. Figure 8a below shows the correlation between $\sum_\lambda \frac{E_\lambda \cdot \varepsilon_{NO3,\lambda}}{U_\lambda}$ and the overall germicidally weighted irradiance for the 200-300 nm range normalized to the absorbance at 223 nm delivered by the lamp to each sample. The absorbance at 223 nm was chosen because $\sum_\lambda \frac{E_\lambda \cdot \varepsilon_{NO3,\lambda}}{U_\lambda}$ peaks at that wavelength (Figure 26b), so the absorbance at 223 nm has the most impact on the energy transferred to nitrate.

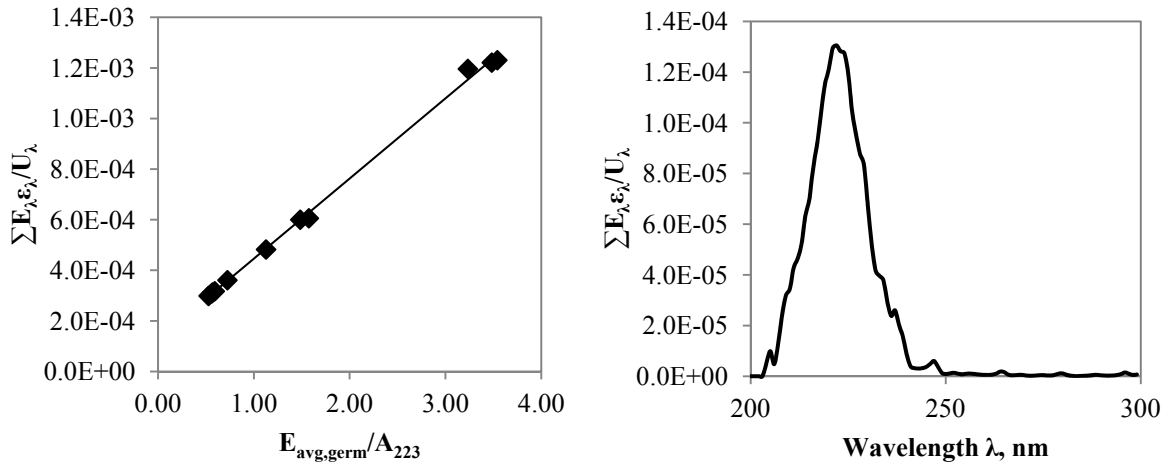


**Figure 26: (a) Correlation between the average germicidal irradiance normalized to absorbance at 223 nm (x-axis) and the specific rate of light absorption by nitrate (y-axis); (b) Specific rate of light absorption by nitrate as a function of wavelength.**

Therefore, the quantity $\sum_{\lambda} \frac{E_\lambda \cdot \varepsilon_{NO3,\lambda}}{U_\lambda}$ (in Es·mol$^{-1}$·s$^{-1}$) can be estimated from average germicidal irradiance measured by biodosimetry at the wastewater treatment plant (in mW/cm$^2$) and from water absorbance at 223 nm (cm$^{-1}$) using the relationship derived from the data in Figure 26a:

$$\sum_{\lambda} \frac{E_\lambda \cdot \varepsilon_{NO3,\lambda}}{U_\lambda} = 0.000317 \cdot \frac{E_{avg,germ}}{A_{223}} + 0.000129 \qquad [4\text{-}16]$$

Once this quantity is estimated, Equation 4-12 can be used to estimate the [HO•]ss generation expected given the nitrate concentration and water quality.

### 4.2.5 Implications for wastewater treatment utilities

Wastewater treatment utilities that use MP lamps for disinfection have the advantage of achieving some micropollutant degradation via advanced oxidation if the effluent contains nitrate. Figure 27 provides estimates of contaminant degradation based on OH radical rate constants at typical germicidally-weighted disinfection doses for bacterial and viral inactivation (40 and 186 mJ/cm$^2$ respectively) as well as an advanced oxidation dose of 2000 mJ/cm$^2$. Note

that a germicidally weighted dose is the average dose delivered by 200-300 nm UV wavelengths (used throughout the analysis above) weighted by the DNA absorbance spectrum. This DNA weighting results in germicidal UV doses being about 70% of the total unweighted dose and is the way doses are typically reported for polychromatic emission UV disinfection systems such as MP UV. At the UV doses used for disinfection, 5-30% degradation can be expected for most contaminants, based on the narrow range of diffusion controlled reaction rate constants for most organic contaminants with HO•. Compounds susceptible to direct photolysis would show even higher degradation. If micropollutant discharge becomes regulated, increasing the UV reactor residence time may be a sufficient adjustment for nitrifying utilities using MP UV. Adjusting the dose to 2000 mJ/cm$^2$ would achieve at least 20-70% oxidation for contaminants in most effluents. Contaminants with higher $k_{OH}$ can achieve over 95% transformation. Hydrogen peroxide cost is a major operational expense of advanced oxidation systems. Therefore, using indigenous nitrate in combination with MP UV would result in a cheaper advanced oxidation alternative for wastewater treatment and water reuse plants than MP UV/$H_2O_2$ systems. Note that radicals other than HO• are generated in the process and may result in formation of oxidation products different from those that form in the UV/$H_2O_2$ process. Studies are currently under way to evaluate whether nitrogen carrying radicals are incorporated into the parent molecule and whether it changes the biological effects of the resulting products.

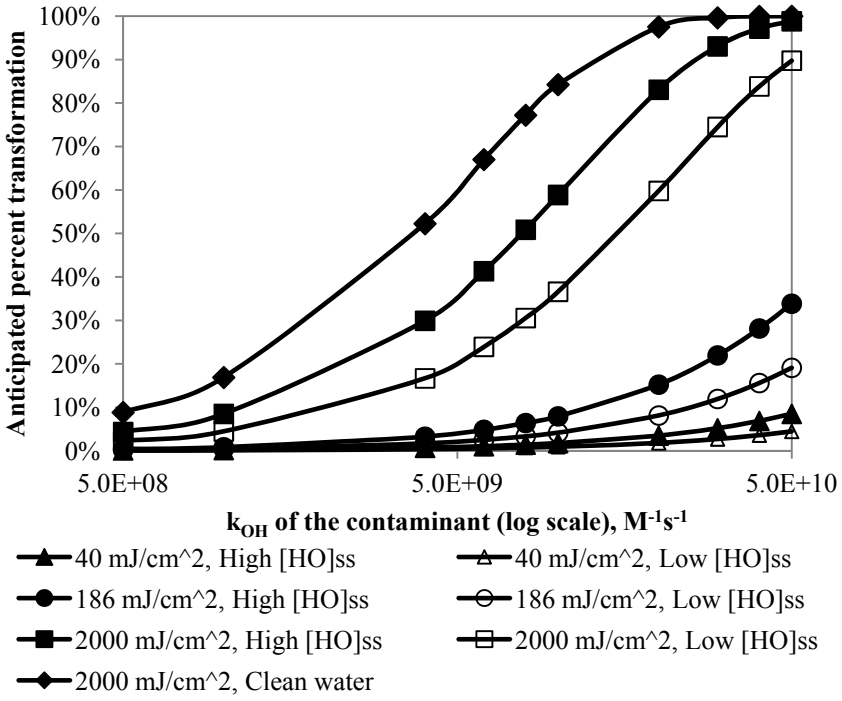


**Figure 27: Expected degradation of organic contaminants in nitrified effluents with high (≈$5.7 \cdot 10^{-14}$ M) and low (≈$3.0 \cdot 10^{-14}$ M) [HO•]ss generating potential, as a function of the contaminant's reaction rate constant with HO•.**

Effluents containing as little as 5 mg/L nitrate will create advanced oxidation conditions comparable to a typical UV/$H_2O_2$ process. Except for WWTPs that are regulated to meet total effluent nitrogen levels below 5 mg-N/L, most effluents from nitrifying plants have enough nitrate (up to 20 mg-N/L) to achieve advanced oxidation. Adding $H_2O_2$ to those effluents will produce a small increase in HO• production while introducing an additional HO• scavenger and may not justify the additional cost of the chemical.

# Chapter 5: Reactivity of effluent organic matter with hydroxyl radical

## 5.1 Materials and methods

### 5.1.1 Effluent samples

The samples were collected from 8 different wastewater treatment utilities, 6 out of which were sampled multiple times. All utilities were sampled at the point in the treatment train right before disinfection. The sampling location would be representative of the location of the AOP process in the treatment train. One of the utilities was sampled at several different points along the treatment train to determine how different biological processes affect the reactivity of EfOM. That particular plant was sampled after the secondary clarifier following the solids contact activated sludge, after the nitrifying trickling filter, after the denitrifying trickling filter and the final effluent before disinfection consisting of a blend of water that passed through the denitrifying filters and the water that bypassed the denitrification. Table 6 is the summary of the utilities and the corresponding treatment processes. Table 7 details the water quality characteristics of the samples.

**Table 6: Wastewater treatment trains of the participating utilities**

| Utility | Treatment process | Average plant flow, MGD | Solids retention time, days |
|---|---|---|---|
| 1 | Activated sludge with biological nutrient removal | 12 | 12 |
| 2 | Activated sludge with biological nutrient removal | 80 | 5 |
| 3 | Solids contact activated sludge + nitrifying trickling filters + denitrifying filters | 23 | 0.7 |
| 4 | Activated sludge with biological nutrient removal | 55 | 10 |
| 5 | Activated sludge with biological nutrient removal | 6.3 | 10 |
| 6 | Activated sludge with biological nutrient removal + denitrifying filters + sand filters | 22.5 | 15 |
| 7 | Extended aeration lagoon | 0.04 | 100 |
| 8 | Membrane bioreactor | 0.014 | - |

**Table 7: Water quality for the samples**

| Utility-Sample | pH, - | Nitrate, mg-N/L | Ammonia, mg-N/L | DOC, mg-C/L | Alkalinity, mg/L as $CaCO_3$ | Nitrite, mg-N/L | UV254, $cm^{-1}$ |
|---|---|---|---|---|---|---|---|
| 1-1 | 7.07 | 13.1 | BDL | 5.81 | 84.00 | 0.10 | 0.109 |
| 1-2 | 7.22 | 15.18 | BDL | 5.67 | 80 | BDL | 0.101 |
| 1-3 | 6.89 | 11.2 | 0.024 | 5.96 | 82.4 | 0.038 | 0.111 |
| 2-1 | 7.04 | 3.76 | 0.063 | 6.49 | 102.00 | 0.03 | 0.105 |
| 2-2 | 7.29 | 6.81 | 0.058 | 6.63 | 105.6 | 0.064 | 0.113 |
| 2-3 | 6.72 | 5.63 | 0.166 | 7.97 | 120 | 0.022 | 0.149 |
| $3\text{-}1^{fe}$ | 6.57 | 12.6 | 0.283 | 6.79 | 70.00 | BDL | 0.13 |
| $3\text{-}2^{fe}$ | 7.33 | 15.4 | 1.66 | 6.69 | 84.4 | BDL | 0.141 |
| $3\text{-}3^{fe}$ | 6.97 | 12.2 | 2.295 | 8.41 | 92.4 | BDL | 0.158 |
| $3\text{-}4^{fe}$ | 6.89 | 8.79 | 1.56 | 8.36 | 108 | 0.066 | 0.146 |
| $3\text{-}1^{dn}$ | 6.43 | 12.8 | 0.217 | 6.34 | 65.20 | BDL | 0.129 |
| $3\text{-}2^{dn}$ | 7.36 | 2.32 | 0.375 | 6.28 | 130.4 | BDL | 0.121 |
| $3\text{-}3^{dn}$ | 7.06 | 4.23 | 0.319 | 8.13 | 125.6 | BDL | 0.155 |
| $3\text{-}4^{dn}$ | 6.83 | 4.04 | 0.398 | 8.60 | 123.2 | 0.07 | 0.147 |
| $3\text{-}1^{sc}$ | 7.11 | 1.31 | 21.35 | 8.91 | 168 | 0.07 | 0.13 |
| $3\text{-}2^{sc}$ | 6.92 | 2.03 | 18.1 | 8.97 | 80.8 | 0.04 | 0.163 |
| $3\text{-}3^{sc}$ | 6.86 | 3.62 | 10.45 | 8.43 | 100 | BDL | 0.148 |
| $3\text{-}1^{tnf}$ | 7.39 | 19.92 | 2.065 | 7.80 | 72 | BDL | 0.137 |
| $3\text{-}2^{tnf}$ | 6.71 | 19.56 | 1.04 | 8.87 | 72.4 | 0.02 | 0.162 |
| $3\text{-}3^{tnf}$ | 6.71 | 15.4 | 0.091 | 9.51 | 93.2 | 0.095 | 0.147 |
| 4-1 | 6.28 | 13.3 | 0.067 | 5.34 | 149.6 | BDL | 0.106 |
| 4-2 | 7.39 | 2.26 | 0.078 | 5.76 | 188.4 | 0.021 | 0.115 |
| 4-3 | 6.88 | 0.946 | 0.046 | 5.41 | 191.2 | 0.025 | 0.105 |
| 5-1 | 6.32 | 14.36 | 0.12 | 6.41 | 45.20 | 0.00 | 0.127 |
| 5-2 | 7.01 | 13.1 | 0.024 | 7.46 | 51.2 | 0.067 | 0.158 |
| 6-1 | 6.99 | 0.175 | 0.123 | 7.75 | 200.00 | 0.11 | 0.174 |
| 7-1 | 6.69 | 2.7 | 0.745 | 3.82 | 207.2 | 0.026 | 0.081 |
| 8-1 | 7.23 | 2.43 | 0.285 | 5.29 | 60.40 | BDL | 0.115 |
| 8-2 | 6.84 | 6.4 | 0.035 | 7.20 | 52 | BDL | 0.124 |
| 8-3 | 6.85 | 4.46 | BDL | 5.62 | 56.8 | BDL | 0.115 |

$^{sc}$ = secondary clarifyer effluent; $^{tnf}$ = trickling nitrifying filter effluent; $^{dn}$ = denitrifying filter effluent; $^{fe}$ = final effluent; BDL = below detection limit (0.015 for nitrite and ammonia)

All samples were filtered upon collection through a 0.45 μm nylon filter (Nalgene, Rochester, NY) and stored at 4°C to stop any further bacterial processes. Nitrate, nitrite and

ammonia concentrations were measured using Hach DR5000 spectrophotometer (Hach Corporation, Loveland, CO) and the corresponding Hach kits (TNT835, TNT839 and TNT830 respectively). Dissolved organic carbon was measured using Shimadzu $V_{CSH}$ TOC analyzer (Shimadzu Scientific Instruments, Columbia, MD). Inorganic carbon was eliminated from solution by brining the pH to about 2.0 with hydrochloric acid (Mallinckrodt, Hazelwood, MO), after which the sample was purged with ultra-zero air during the TOC analysis. Sample pH was measured with a calibrated pH meter (Φ340, Beckman Coulter, Indianapolis, IN), alkalinity was measured with a Hach digital titrator (Hach Corporation, Loveland, CO), and absorbance scan was taken with Cary100Bio spectrophotometer (Agilent Technologies, Santa Clara, CA).

### 5.1.2 Reaction rate constants

Experiments measuring the overall hydroxyl radical scavenging of the water samples were performed with 5 μM of reagent-grade methylene blue (Sigma-Aldrich, St.Louis, MO) as a probe. Hydroxyl radicals were generated by irradiating with UV samples containing 10 mg/L of reagent-grade hydrogen peroxide (J.T.Baker, Phillipsburg, NJ). Low pressure mercury vapor UV lamp emitting near 253.7 nm and collimated through two 10 cm diameter opening in plates spaced 1.2 cm apart was used in the experiment. The experiments were performed in stirred crystallization dishes 5 cm in diameter with a Petri factor of 0.99. Average dose delivered to the sample was calculated using all appropriate correction factors (Bolton and Linden 2003). Hydrogen peroxide was measured by triiodide method (Klassen, Marchington et al. 1994) prior to adding methylene blue to the sample to avoid interference. Methylene blue was measured spectrophotometrically at 664 nm. Although methylene blue is a photostable compound under UV > 200 nm, blank run without hydrogen peroxide was performed to account for non-hydroxyl radical reaction pathways in wastewater matrix. The difference between the sample and the

blank was used to measure the extent of the probe degradation due to hydroxyl radicals alone. Concentration of the hydroxyl radicals [HO•] was then calculated using the following relationship:

$$\ln\frac{[\mathrm{MB}]_t}{[\mathrm{MB}]_0} = \frac{-k_{\mathrm{HO,MB}}[\mathrm{HO}\bullet]_{SS}}{E_0}\cdot F_0 \qquad [5\text{-}1]$$

where $E_0$ is the average fluence rate ($mW/m^2$), $F_0$ is the fluence ($mJ/m^2$) and $k_{HO,MB}$ is a time-based reaction rate constant between probe methylene blue (MB) and hydroxyl radicals ($M^{-1}s^{-1}$).

In this equation, the quantity $\frac{-k_{HO,MB}[HO\bullet]_{ss}}{E_0}$ is the slope of the plot of $\ln\frac{[MB]_t}{[MB]_0}$ vs $F_0$, and [HO•] can be calculated as

$$[HO\bullet] = \frac{-slope\cdot E_0}{k_{HO,MB}} \qquad [5\text{-}2]$$

The value for $k_{HO,MB}$ is $2.1\cdot10^9$ $M^{-1}s^{-1}$.(Buxton, Greenstock et al. 1988)

The UV/$H_2O_2$ model by Glaze et al. (1995) was then rearranged to calculate the total hydroxyl radical scavenging coming from the sample background:

$$\sum k_s[S] = \frac{E_0\varepsilon_{254}\Phi[H_2O_2]}{U_{254}}\cdot\frac{1}{[HO\bullet]} \qquad [5\text{-}3]$$

where $k_s$ is the hydroxyl radical reaction rate constant for a given scavenging compound ($M^{-1}s^{-1}$), [S] is the concentration of the corresponding scavenging compound (M), $\varepsilon_{254}$ is molar absorption of hydrogen peroxide at 254 nm ($M^{-1}cm^{-1}$), Φ is quantum yield of hydroxyl radical formation by photolysis of hydrogen peroxide at 254 nm (-), [$H_2O_2$] is the concentration of hydrogen peroxide (M), and $U_{254}$ is the wavelength energy (J/Es)

Substituting Eq. 5-2 into Eq. 5-3 yields

$$\sum k_s[S] = \frac{E_0 \varepsilon_{254} \Phi [H_2O_2]}{U_{254}} \cdot \frac{k_{HO,MB}}{-slope \cdot E_0} = \frac{\varepsilon_{254} \Phi [H_2O_2]}{U_{254}} \cdot \frac{k_{HO,MB}}{-slope} \qquad [5\text{-}4]$$

Typical scavengers in wastewater backgrounds are EfOM, bicarbonate and occasionally nitrite, although the levels at most properly operating wastewater treatment plants are very low. Table 5 in Chapter 4 has the summary of the rate constants between each of these compounds with HO•. If hydrogen peroxide is added for hydroxyl radical generation, then hydrogen peroxide is a scavenger as well. In the samples used in this study, the probe compound was also added to the scavenging compounds. Carbonate and ammonium are also scavengers of hydroxyl radicals, however all of the effluents had pH around 7, making the concentrations of either species negligible. A theoretical contribution by the scavenging compounds other than EfOM was calculated using the published values for reaction rates between hydroxyl radicals and bicarbonate, nitrite, hydrogen peroxide and methylene blue: $8.5 \cdot 10^6$, $1.0 \cdot 10^{10}$, $2.7 \cdot 10^7$ and $2.1 \cdot 10^{10}$ $M^{-1}s^{-1}$ respectively (Buxton, Greenstock et al. 1988). The difference between the measured scavenging (Eq.4) and the calculated scavenging by compounds other than EfOM was assumed to be the scavenging by EfOM. EfOM accounted for 41-70% of scavenging in the experiments, so the difference was measurable. The EfOM scavenging value was then divided by the organic carbon concentration to find the rate constant. The experiments were performed in duplicates.

### 5.1.3 Variables

#### *5.1.3 (a) Bulk EfOM parameters:*

Size exclusion chromatography was used to measure average molecular weight. Agilent 1200 HPLC (Agilent Technologies, Santa Clara, CA) equipped with a Biax 250x20mm column packed with Toyopearl HW-50S 30 mm resin was used. The eluent was 0.024 M sodium

monobasic phosphate (Sigma-Aldrich, St.Louis, MO), 0.0016 M sodium dibasic phosphate (EMD, Gibbstown, NJ) and 0.025 M sodium sulfate (BDH, West Chester, PA). The conductivity of the sample was increased to match that of the eluent using the concentrated eluent spike. The relative abundance of the molecules of a certain size was measured by using UV254 absorbance signal as a surrogate. Weight average molecular weight was determined using a calibration curve of retention times for different size polyethylene glycols (Fisher Scientific, Rochester, NY) with molecular weights between 232 and 17900 m.u. Dispersity was calculated as the ratio of the weight average molecular weight to the number average molecular weight.

Retention coefficient onto the $C_{18}$ and $NH_2$ media was measured using solid phase extraction cartridges (100mg/1.5mL Extract Clean$^{TM}$, Grace Davison Discovery Sciences, Deerfield, IL). The sample was run through the cartridge at the rate of 1 mL/min. Fraction of the sample eluting between 4 and 8 minutes was collected and absorbance at 254 nm was measured. Retention coefficient (RC) was calculated as follows:

$$RC = 1 - \frac{A_{254,br}}{A_{254}} \qquad [5\text{-}5]$$

where $A_{254,br}$ is the absorbance of the breakthrough fraction of the EfOM at 254 nm and $A_{254}$ is the absorbance of the original sample at the same wavelength. Samples with low breakthrough values will have higher RC indicating higher affinity for the cartridge medium. High RC for $C_{18}$ cartridges indicates prevalence of hydrophobic moieties in the bulk organic matter, and high RC for $NH_2$ cartridges indicates a prevalence of charged hydrophilic moieties. The response is proportional to the relative hydrophobicity or charge density. Analysis is described in greater detail in other sources (Rosario-Ortiz, Snyder et al. 2007). In addition a ratio of the two retention

coefficients ($NH_2/C_{18}$) was used as a predictor. Higher value of the ratio would indicate that the molecule is dominated by the hydrophilic groups which could affect the spatial configuration of the molecule making it less likely to shield potential reactive sites.

### *5.1.3 (b) Water quality parameters:*

Chemical oxygen demand (COD) was measured using Hach TNT820 method with a Hach DR200 digester and Hach DR5000 spectrophotometer (Hach Corporation, Loveland, CO). Chemical oxygen demand shows how much oxygen is required to oxidize the sample and was considered as a potential measure of how reactive organic carbon in the sample will be with another oxidizer: hydroxyl radical.

Specific UV absorbance at 254 nm ($SUVA_{254}$) was used as a measure of aromatic character of the organic matter as conjugated bonds dominate the absorbance at this wavelength (Weishaar, Aiken et al. 2003). It is calculated by normalizing the absorbance at 254 nm to the concentration of dissolved organic carbon and multiplying the value by 100 (Weishaar, Aiken et al. 2003). Conjugated bonds have different susceptibility to reactions with oxidants than non-conjugated bonds, making it a potential predictor for the reactivity of EfOM. It has been previously used to demonstrate the correlation between the reactivity of dissolved organic matter from non-effluent sources with hydroxyl radical (Westerhoff, Aiken et al. 1999).

### *5.1.3 (c) Treatment train characteristics:*

Solids retention time (SRT) information for the collection day of each sample was obtained from the utility. It must be noted that utilities may use different methods for calculating SRT. The values were used to group utilities into classes of low, medium and high SRT rather than as an exact predictor. Average reaction rate constants were compared for each range of

SRT duration to determine whether a relationship exists. SRT as a predictor of EfOM reactivity was previously suggested by Dong et al. (Dong, Mezyk et al. 2010) based on the effects SRT has on molecular weight distribution of the organic matter.

### *5.1.3 (d) Fluorescence-derived data:*

Fluorescence is commonly used to characterize the heterogeneous organic matter samples (Mopper and Schultz 1993; McKnight, Boyer et al. 2001; Chen, Westerhoff et al. 2003; Stedmon, Markager et al. 2003). The following fluorescence indicators were used in the model: fluorescence index (McKnight, Boyer et al. 2001), humification index (Ohno 2002), redox index (Miller, McKnight et al. 2006) and fluorescence intensity of protein-like compounds (Chen, Westerhoff et al. 2003). Fluorescence data was collected for 240-440 nm excitation wavelength range in 10 nm increments and 300-550 nm emission range in 2 nm increments using a Horiba F4 spectrofuorometer (Horiba Scientific, Edison, NJ). Fluorescence index is defined as the ratio of emission at 450 nm to emission at 500 mn with excitation at 370 nm (McKnight, Boyer et al. 2001). It has been determined to be a measure of microbially-derived vs. plant-derived organic matter. Microbially-derived organic matter tends to be more aliphatic while plant-derived organic matter is more aromatic in character. Different chemical structure prevalence would result in different reactivity of the EfOM. Lower fluorescence index is indicative of more microbially-derived organic matter.

Humification index is defined as the sum of emission intensities in the 435-480 nm range over the sum of emission intensities in the 300-345 nm range with excitation at 254 nm (Ohno 2002). Humification index was proposed as a measure of stability of organic matter.

Redox index is defined as the fluorescence signal of the reduced quinone-like compounds divided by the signal of both reduced and oxidized quinone-like compounds (Miller, McKnight

et al. 2006). Prevalence of oxidized species within the EfOM could indicate that further oxidation by hydroxyl radical would be more difficult than for EfOM dominated by reduced species. However, redox index is calculated based on quinone-like and hydroquinone-like fluorescence signature ratios, both of which are relatively oxidized species.

Protein-like fluorescence signal is associated with wastewaters (Chen, Westerhoff et al. 2003). It has shown a clear decrease trend with increased solids retention time in preliminary data analysis and was used as a surrogate for the extent of biological treatment. The decrease in protein-like signal is likely due to breakdown of the proteins during microbial processes. Longer biological treatment results in smaller average molecular weights and different distribution between the aliphatic microbial products and aromatic substrate, all of which could affect the reactivity of the bulk organic matter with the hydroxyl radicals. Protein-like compounds (specifically tryptophan and tyrosine) have maximum fluorescence at 270 and 280 nm excitation wavelengths with maximum emission occurring at about 430-440 nm (Chen, Westerhoff et al. 2003). The average highest intensity at 270 and 280 nm excitation wavelengths with emission at 430-440 nm was used as protein-like peak signal intensity.

### 5.1.4 Statistical analysis

Statistical software R was used to perform the statistical analysis described in this section.

The predictors described above were analyzed using principal component analysis (PCA). The analysis determined the number of predictors necessary to account for a certain percentage of variability within data. The values of each variable were scaled prior to the analysis by subtracting the mean of the variable and dividing the result by the standard deviation. This assured that the variable with the highest magnitude of the values did not bias the results.

Akaike Information Criterion (AIC) was used to identify the variables with the best predicting power. Step AIC was performed using a MASS library in R. Once the variables were identified, a generalized linear model (GLM) was fitted on the selected set of predictors. Because gamma distribution rather than normal distribution is more typical for environmental measurements, the data was transformed using a built-in "inverse" link function option in the GLM prior to fitting the model. The model was then tested by a cross-validation technique where each point is predicted by the model that did not use that point in developing the coefficients. Residuals were analyzed for normality of their distribution and lack of correlation with the function being predicted, which is expected from a well-fitting model.

## 5.2 Results

### 5.2.1 Model results and evaluation

All the variables measured for each sample and the corresponding $k_{OH,EfOM}$ are summarized in Table 8.

**Table 8: Modeling parameters**

| COD, mg/L | $SUVA_{254}$ | MW, Da | d, - | RC $C_{18}$, - | RC $NH_2$, - | $NH_2/C_{18}$ | FI, - | RI, - | PS, - | HIX, - | kOH, $M^{-1}s^{-1}$ |
|---|---|---|---|---|---|---|---|---|---|---|---|
| 19.6 | 1.88 | 1263 | 1.19 | 0.046 | 0.147 | 3.200 | 1.89 | 0.30 | 1.21 | 2.73 | 3.03E+08 |
| 17.7 | 1.78 | 1296 | 1.17 | 0.149 | 0.277 | 1.867 | 1.94 | 0.28 | 1.12 | 3.04 | 2.89E+08 |
| 19.5 | 1.86 | 1396 | 1.21 | 0.225 | 0.441 | 1.960 | 1.90 | 0.26 | 1.14 | 3.06 | 2.52E+08 |
| 19 | 1.62 | 1177 | 1.41 | 0.124 | 0.219 | 1.769 | 1.96 | 0.39 | 1.38 | 2.50 | 2.43E+08 |
| 21.3 | 1.70 | 1326 | 1.28 | 0.159 | 0.106 | 0.667 | 1.97 | 0.29 | 1.39 | 2.55 | 5.37E+08 |
| 26.8 | 1.87 | 1460 | 1.51 | 0.195 | 0.463 | 2.379 | 1.87 | 0.30 | 1.58 | 2.49 | 3.34E+08 |
| 23.3 | 1.92 | 1372 | 1.23 | 0.185 | 0.315 | 1.708 | 1.95 | 0.31 | 1.6 | 2.77 | 2.54E+08 |
| 27.6 | 2.11 | 1170 | 1.20 | 0.277 | 0.447 | 1.615 | 1.98 | 0.29 | 1.53 | 2.65 | 2.20E+08 |
| 32.1 | 1.88 | 1439 | 1.28 | 0.361 | 0.424 | 1.175 | 1.91 | 0.30 | 1.68 | 2.68 | 2.16E+08 |
| 29.4 | 1.75 | 1514 | 1.30 | 0.219 | 0.452 | 2.063 | 1.91 | 0.31 | 1.63 | 2.62 | 2.04E+08 |
| 17.5 | 1.98 | 1468 | 1.19 | 0.170 | 0.377 | 2.222 | 1.93 | 0.26 | 1.46 | 2.43 | 2.60E+08 |
| 17.4 | 2.00 | 1564 | 1.56 | 0.357 | 0.435 | 1.220 | 1.87 | 0.28 | 1.36 | 2.47 | 3.23E+08 |
| 16.7 | 1.94 | 1456 | 1.79 | 0.200 | 0.505 | 2.524 | 1.89 | 0.29 | 1.3 | 2.36 | 3.19E+08 |
| 23.6 | 1.98 | 1410 | 1.21 | 0.157 | 0.291 | 1.850 | 1.92 | 0.29 | 1.43 | 2.62 | 3.21E+08 |
| 26.8 | 2.12 | 1506 | 1.28 | 0.304 | 0.519 | 1.708 | 1.87 | 0.29 | 1.42 | 2.88 | 2.04E+08 |
| 21.8 | 2.24 | 1974 | 1.89 | 0.086 | 0.471 | 5.467 | 1.67 | 0.30 | 2.35 | 4.79 | 2.68E+08 |
| 13.4 | 2.12 | 1473 | 1.47 | 0.136 | 0.111 | 0.818 | 1.85 | 0.28 | 0.938 | 3.39 | 3.31E+08 |
| 21 | 2.18 | 1355 | 1.32 | 0.270 | 0.322 | 1.194 | 1.87 | 0.30 | 1.51 | 3.30 | 2.35E+08 |
| 21.3 | 1.72 | 1843 | 1.42 | 0.331 | 0.419 | 1.268 | 1.89 | 0.29 | 1.27 | 2.91 | 2.93E+08 |
| 19.5 | 2.05 | 1487 | 1.39 | 0.278 | 0.487 | 1.750 | 1.84 | 0.26 | 1.21 | 2.95 | 2.73E+08 |
| 26.7 | 2.03 | 1430 | 1.24 | 0.155 | 0.279 | 1.800 | 1.96 | 0.31 | 1.57 | 2.83 | 2.48E+08 |
| 26.1 | 1.93 | 1166 | 1.56 | 0.223 | 0.364 | 1.630 | 1.97 | 0.32 | 1.54 | 3.03 | 1.84E+08 |
| 32.3 | 1.91 | 1467 | 1.58 | 0.374 | 0.445 | 1.190 | 1.91 | 0.29 | 1.69 | 2.75 | 2.30E+08 |
| 29.6 | 1.71 | 1544 | 1.60 | 0.238 | 0.408 | 1.714 | 1.90 | 0.29 | 1.64 | 2.66 | 2.27E+08 |
| 30.7 | 1.46 | 1126 | 1.36 | 0.231 | 0.369 | 1.600 | 1.99 | 0.30 | 1.6 | 2.51 | 1.63E+08 |
| 35.4 | 1.82 | 1390 | 1.27 | 0.239 | 0.429 | 1.795 | 1.92 | 0.29 | 1.79 | 2.54 | 2.12E+08 |
| 32 | 1.76 | 1419 | 1.24 | 0.243 | 0.439 | 1.806 | 1.91 | 0.38 | 1.75 | 2.38 | 3.98E+08 |
| 29.5 | 1.76 | 1083 | 1.18 | 0.234 | 0.358 | 1.531 | 1.96 | 0.29 | 1.48 | 2.76 | 2.61E+08 |
| 33.1 | 1.83 | 1491 | 1.28 | 0.346 | 0.438 | 1.268 | 1.91 | 0.29 | 1.62 | 2.65 | 1.98E+08 |
| 30.4 | 1.55 | 1509 | 1.25 | 0.150 | 0.442 | 2.955 | 1.91 | 0.31 | 1.55 | 2.53 | 2.16E+08 |

PCA results are presented in Figure 28. The figure shows the fraction of variability explained by each additional variable in the model. A single variable model would account for only about 21% of variability. At least 5 variables are required to account for 70% of variability within data.

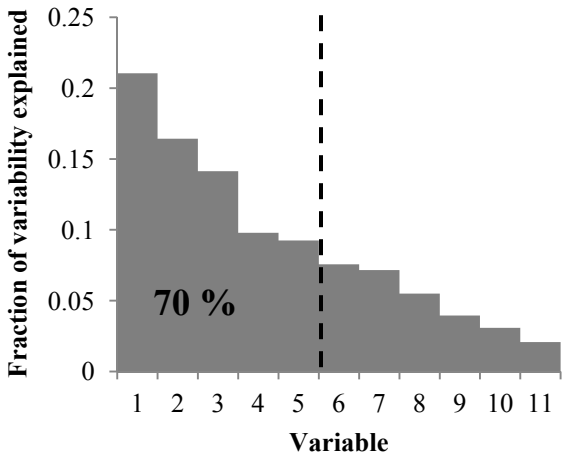


**Figure 28: Principal component analysis results indicating the contribution to explaining the variability in the data by each additional variable**

Step AIC analysis revealed that those variables are COD, the ratio of RCs $NH_2/C_{18}$, FI, intensity of the protein-like fluorescence signal (PS) and HIX. Some of the variables carried certain built-in redundancy, e.g. molecular weight distribution is likely correlated with solids retention time in biological treatment and so is protein-like fluorescence signature, or HIX and SUVA both can be surrogates for degree of bond conjugation. The statistical analysis performed in this study takes into account internal correlations among the variables to drop the redundant ones. The variables selected by the model account for many factors potentially influencing the reactivity. COD is a measure of the oxidation potential of the EfOM. The ratio of RC on $NH_2$ medium and RC on $C_{18}$ medium is a measure of the prevalence of hydrophilic vs. hydrophobic functional groups and could be related to the spatial folding of the molecules which would determine how easily accessible some parts of the molecule are for the reaction with hydroxyl radicals. FI is a measure of prevalence of more aliphatic microbial products. Protein signal (PS) is indicative of the duration of biological treatment and, as a result, of average molecular weight of EfOM. And humification index (HIX) is a measure of conjugated bonds.

The following model coefficients were determined:

$$\frac{1}{k_{HO,EfOM}\cdot 10^{-8}} = 0.01075\cdot COD + 0.03019\cdot\frac{RC_{NH2}}{RC_{C18}} + 0.4265\cdot FI - 0.1188\cdot PS + 0.08106\cdot HIX - 0.858$$

[5-6]

Figure 29(a) shows the predicted vs. observed values for all 30 samples, and Figure 29(b) shows the results of cross-validation where each point is predicted by the model, the coefficients for which were calculated without that point being part of the data set. Cross-validation measures the ability of the model to accurately predict the rate constant for the samples that were not part of the data set, e.g. if a water reuse or wastewater treatment utility wanted to evaluate the reactivity of their EfOM with hydroxyl radicals for AOP design. In addition, it can spot if any data points have particular influence on the coefficients. Those points would show more deviation from the 1:1 line in cross-validation then when predicted by the model that uses those points in coefficient determination.

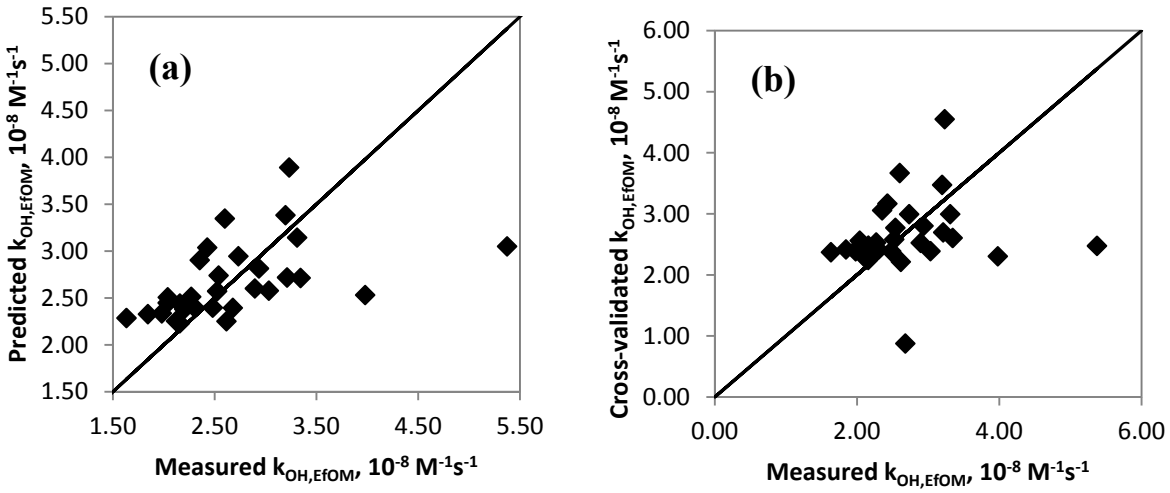


**Figure 29: (a) Predicted vs. measured values of $k_{OH,EfOM}$; (b) Cross-validated vs. measured values of $k_{OHEfOM}$**

It appears that the model is reasonably good at predicting the rate constants in the 2.0-3.5·$10^8$ $M^{-1}s^{-1}$ range. However, it is the outlying numbers that would benefit from better prediction. The average rate constant measures for the 30 samples was 2.7·$10^8$ $M^{-1}s^{-1}$ which is lower than the average value of 3.6·$10^8$ $M^{-1}s^{-1}$ currently used in modeling (Westerhoff, Aiken et al. 1999). The minimum and the maximum values were 1.6·$10^8$ $M^{-1}s^{-1}$ and 5.4·$10^8$ $M^{-1}s^{-1}$ respectively. These values certainly would result in the process under- or over-performing, but they were not well captured by the model.

To compare the benefit of using the model vs. using the average value measured for natural organic matter isolates (3.6·$10^8$ $M^{-1}s^{-1}$) vs. using the average value calculated for EfOM in this study (2.7·$10^8$ $M^{-1}s^{-1}$), degradation of methylene blue in the 30 samples was modeled using each scenario. Figure 30 shows the % error in the calculated UV fluence compared to the measured results (arranged in the order of increasing measured $k_{OH,EfOM}$). When the value predicted by the model is used, the percent error in estimation of the fluence required for 90% transformation of methylene blue was <15% for 27 out of 30 samples, with the outliers on either end fairing the worst. Highest percent error was 28%. In contrast, when the reaction rate constant established for natural organic matter (NOM) isolates was used, only for 9 out of 30 samples the predicted fluence was within 15% of the measured. The highest percent error was 49%. Using the average of the values measured in this study for $k_{OH,EfOM}$, 25 out of 30 predicted fluences were within 15%, and the highest error was 32%. The conclusion that follows is that both using the modeled value or the average value measured for EfOM rather than NOM isolates is a big improvement in modeling AOP in effluents. However, the model offers a modest improvement compared to just using the average value of $k_{OH,EfOM}$ presented in this study. The innate variability within the EfOM is more complex than the variables used in the study were

capable of capturing. The notable result, however, is that the average reaction rate constant between EfOM and HO• is lower than the one determined for NOM isolates. Organic matter was responsible for 63-95% of background HO• scavenging in the samples used in this study (81% on average), so the fact that it is only 75% as reactive with HO• than NOM isolates is an encouraging result for the future of AOP for water reuse or wastewater treatment applications.

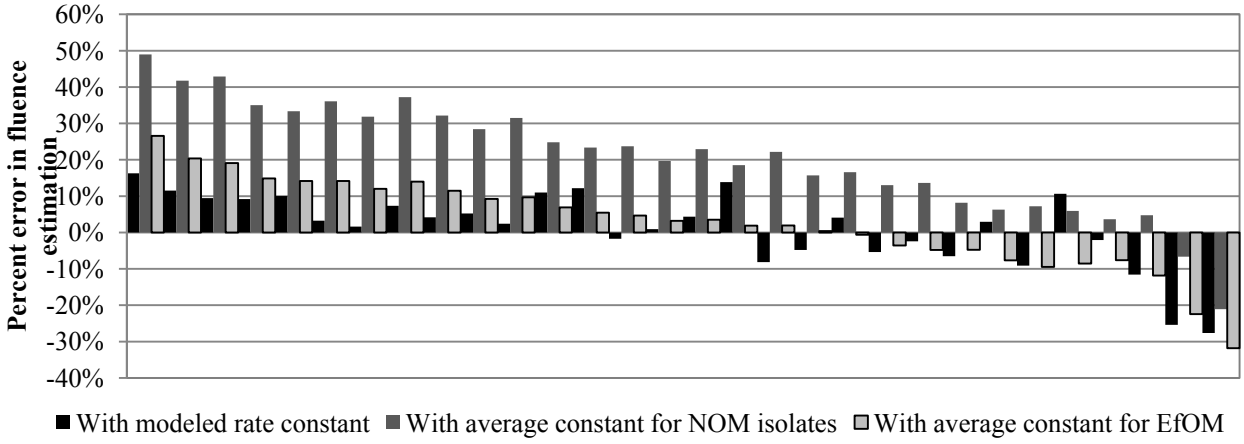


**Figure 30: Percent error in predicting the fluence required for 90% removal of methylene blue in the effluent samples using the modeled $k_{HO,EfOM}$, the value determined for NOM isolates, and the average value for EfOM determined in this study. The values are ranked in the order of increasing measured $k_{HO,EfOM}$**

### 5.2.2 Treatment train effects

When the reaction rate constants across the treatment train of a single facility were compared, the average reaction rate constant stayed largely unaffected by the nitrification or denitrification processes. Figure 31 below shows the reaction rate constant after the short SRT solids contact time from secondary clarifiers (SC), then after the trickling nitrifying filters (TNF) followed by the denitrifying filters (DN) and in final effluent (FE). It is clear from the figure that different types of biological processes at this facility did not cause significant changes in $k_{HO,EfOM}$. However, these processes appear to stabilize the rate constant, as seen from the decrease of the error bars representing 95% confidence intervals with progressing treatment. It is

not surprising, as utilities have variability in the influent, but the treatment processes are adjusted to meet the effluent goals, which are kept relatively constant.

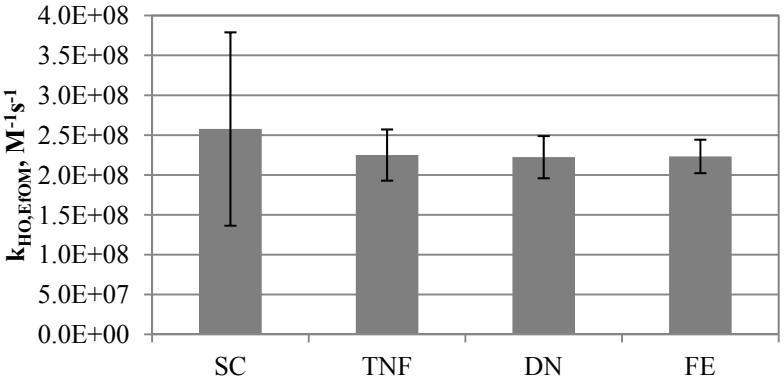


**Figure 31: $k_{HO,EfOM}$ after different biological treatment steps at a single wastewater treatment plant: after aerobic biodegradation and secondary clarification (SC), followed by trickling nitrifying filters (TNF), followed by denitrifying filters (DN), and in final effluent (FE). The values are the averages with error bars representing 95% confidence intervals.**

It is also notable that the smaller ones of the participating utilities had less variability in the $k_{HO,EfOM}$ of the samples from one sampling event to another (Figure 32). The wide range of the rate constants at the largest facility used in the study could be the result of a wide variability in the influent with high percent of industrial input compared to the smaller utilities treating mainly domestic waste. Some of the smallest utilities (community scale) could experience some variability due to limited operator oversight. However, more utilities would need to be surveyed for any conclusions to be drawn.

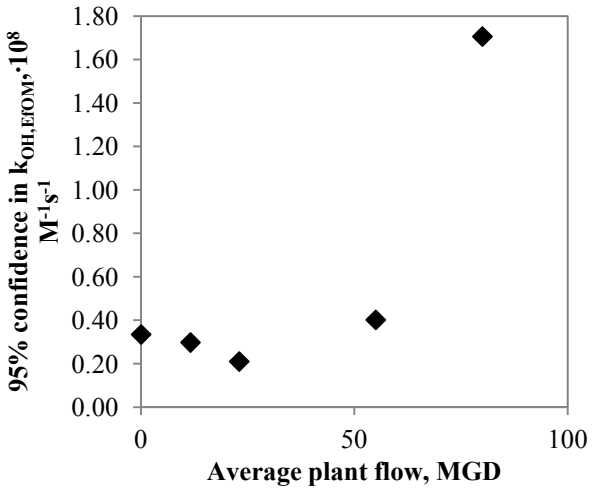


**Figure 32: Variability of $k_{HO,EfOM}$ for different size utilities**

Solids retention time did not show a clear correlation across all the utilities, but when separated into the short (<1 day), medium (9-15 days) and long (100 days) SRT bins, a trend for increasing $k_{HO,EfOM}$ with increasing SRT was seen (Figure 33). The difference is statistically significant ($p<0.05$) for the low and medium SRT bins. Only one long SRT sample was available, and although the $k_{HO,EfOM}$ for that sample was above the average $k_{HO,EfOM}$ at the plants with medium SRT, no conclusion about the statistical significance can be made.

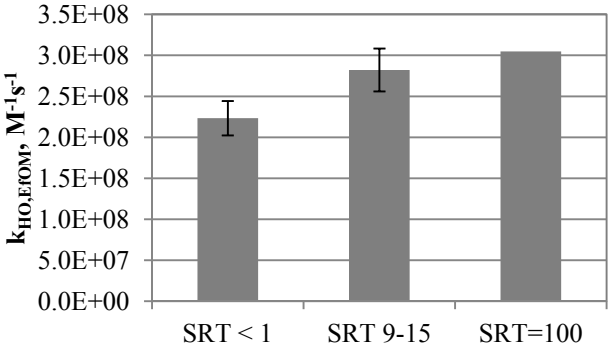


**Figure 33: Average $k_{HO,EfOM}$ for plants with different SRT ranges**

In conclusion, the average reaction rate constant was measured to be $2.7 \cdot 10^8$ $M^{-1}s^{-1}$ for effluent organic matter. The value is only about 75% of the previously established average value for organic matter isolates from natural systems such as rivers and lakes. EfOM is oxidized by

biological processes, so lower reactivity with oxidants compared to natural organic matter isolates is expected. In addition, the values for EfOM were variable with the range of (1.6-5.4)·$10^8$ $M^{-1}s^{-1}$. A model was proposed that captured some of the variability in $k_{HO,EfOM}$ values as a function of COD, $RC_{NH2}/RC_{C18}$, FI, protein-like fluorescence intensity and HIX. The model was a considerable improvement in predicting the outcomes of AOP, compared to using the $k_{OH}$ established for NOM isolates. However, it offered a modest improvement compared to using the average $k_{HO,EfOM}$ measured in this study. It is possible that some of the outliers had other scavengers not taken into account in this model. It is also possible that relationships between $k_{HO,EfOM}$ and some variables are non-linear, resulting in the poor fit for the outliers. Therefore, it is recommended that modeling of hydroxyl radical processes for wastewater treatment uses the average value for $k_{OH,EfOM}$ reported in this study (2.7·$10^8$ $M^{-1}s^{-1}$). It can be further improved by using a value adjusted for SRT: 2.2·$10^8$ $M^{-1}s^{-1}$ for SRT <1 day, and 2.8·$10^8$ $M^{-1}s^{-1}$ for plants operating at longer SRT.

Analysis of the variability of the constants across different utilities and treatment trains indicated that the rate constant does not change significantly across biological processes, although it shows more variability earlier in the treatment process. Additionally, plants with higher flow had larger fluctuations in $k_{HO,EfOM}$, potentially due to the variability of the influent at larger plants receiving industrial wastewater.

## Chapter 6: Summary and conclusions

The goals of the work presented above were to determine the effects of advanced oxidation on transformation products of pharmaceuticals and to gain a better understanding of the sources and sinks of hydroxyl radicals. The following conclusions can be made based on the results of the research:

1. Advanced oxidation at practical levels can cause sufficient transformation for the pharmaceuticals to lose their properties of concern
    a) As demonstrated in Chapter 2, two of the most recalcitrant pharmaceuticals with different physico-chemical properties were shown to form products that could be biodegraded to complete mineralization by conventional activated sludge bacteria.
    b) Of the six antibiotics tested, only two exhibited early transformation products that still retained their antibacterial activity. Those products formed early in the treatment and were transformed further to the point of no antibacterial activity at fluences up to 2000 $mJ/cm^2$.
2. Wastewater treatment utilities using medium pressure lamps for disinfection can generate advanced oxidation conditions without hydrogen peroxide addition, if they have > 5 mg-N/L nitrate. The level of hydroxyl radicals generated via nitrate photolysis is comparable to that generated by irradiation of 10 mg/L of hydrogen peroxide. Nitrate levels above 5 mg-N/L are typical for wastewater treatment plants, indicating that *in situ* UV/$NO_3$ AOP may be considered a viable technology.
3. Effluent organic matter accounts for majority of the hydroxyl radical scavenging in effluents. However, the average value of the scavenging rate constant is 2.7 x $10^8$ $M^{-1}s^{-1}$, which is about 25% lower than was originally assumed based on the numbers derived

from natural organic matter isolates. The value increased with increasing solids retention time, but the type of biological process (e.g. nitrification, denitrification) did not affect the constant.

## References

Alif, A. and P. Boule (1991). "Photochemistry and environment Part XIV. Phototransformation of nitrophenols induced by excitation of nitrite and nitrate ions." Journal of Photochemistry and Photobiology A: Chemistry **59**(3): 357-367.

Andreozzi, R., M. Raffaele, et al. (2003). "Pharmaceuticals in STP effluents and their solar photodegradation in aquatic environment." Chemosphere **50**(10): 1319-1330.

Andrews, W. H. and L. A. Magee Divalent Cation Reversal of Tetracycline-Inhibited Respiration of Klebsiella pneumoniae.

Barbot, E., I. Seyssiecq, et al. (2010). "Inhibition of activated sludge respiration by sodium azide addition: Effect on rheology and oxygen transfer." Chemical Engineering Journal **163**(3): 230-235.

Bayliss, N. and R. Bucat (1975). "The photolysis of aqueous nitrate solutions." Australian Journal of Chemistry **28**(9): 1865-1878.

Benjamin, M. M. (2002). Water Chemistry. New York, McGraw-Hill.

Benotti, M. J., R. A. Trenholm, et al. (2009). "Pharmaceuticals and Endocrine Disrupting Compounds in US Drinking Water." Environmental Science & Technology **43**(3): 597-603.

Biń, A. K. and S. Sobera-Madej (2012). "Comparison of the Advanced Oxidation Processes (UV, UV/H2O2 and O3) for the Removal of Antibiotic Substances during Wastewater Treatment." Ozone: Science & Engineering **34**(2): 136-139.

Bolton, J. R. (1999). Ultraviolet applications handbook. Ayr, Canada, Bolton Photosciences, Inc.

Bolton, J. R. and K. G. Linden (2003). "Standardization of methods for fluence (UV dose) determination in bench-scale UV experiments." ASCE Journal of Environmental Engineering: 209-215.

Bugg, T. D. H. and C. J. Winfield (1998). "Enzymatic cleavage of aromatic rings: mechanistic aspects of the catechol dioxygenases and later enzymes of bacterial oxidative cleavage pathways." Natural Product Reports **15**(5).

Buxton, G. V., C. L. Greenstock, et al. (1988). "Critical review of rate constants for reactions of hydrated electrons, hydrogen atoms and hydroxyl radicals ($^{\cdot}OH/^{\cdot}O^{-}$) in aqueous solution." Journal of Physical and Chemical Reference Data **17**: 513-886.

Chagas, T. P. G., L. M. Seki, et al. (2011). "Multiresistance, beta-lactamase-encoding genes and bacterial diversity in hospital wastewater in Rio de Janeiro, Brazil." Journal of Applied Microbiology **111**(3): 572-581.

Chen, W., P. Westerhoff, et al. (2003). "Fluorescence excitation-emission matrix regional integration to quantify spectra for dissolved organic matter." Environmental Science & Technology **37**(24): 5701-5710.

Cunningham, J. H. and L.-S. Lin (2010). "Fate of Amoxicillin in Mixed-Culture Bioreactors and Its Effects on Microbial Growth and Resistance to Silver Ions." Environmental Science & Technology **44**(5): 1827-1832.

Daniels, M., R. V. Meyers, et al. (1968). "Photochemistry of the aqueous nitrate system, I. Excitation in the 300-mμ band." Symposium on inorganic photochemistry **72**(2): 389-399.

Dodd, M. C., H.-P. E. Kohler, et al. (2009). "Oxidation of Antibacterial Compounds by Ozone and Hydroxyl Radical: Elimination of Biological Activity during Aqueous Ozonation Processes." Environmental Science & Technology **43**(7): 2498-2504.

Dodd, M. C., D. Rentsch, et al. (2010). "Transformation of β-Lactam Antibacterial Agents during Aqueous Ozonation: Reaction Pathways and Quantitative Bioassay of Biologically-Active Oxidation Products." Environmental Science & Technology **44**(15): 5940-5948.

Dong, M. M., S. P. Mezyk, et al. (2010). "Reactivity of Effluent Organic Matter (EfOM) with Hydroxyl Radical as a Function of Molecular Weight." Environmental Science & Technology **44**(15): 5714-5720.

Fent, K., A. Weston, et al. (2006). "Ecotoxicology of human pharmaceuticals." Aquatic Toxicology **76**(2): 122-159.

Finney, D. J. (1977). Probit analysis. Cambridge [u.a.], Cambridge Univ. Press.

Fraker, S. L. and G. R. Smith (2004). "Direct and interactive effects of ecologically relevant concentrations of organic wastewater contaminants on Rana pipiens tadpoles." Environmental Toxicology **19**(3): 250-256.

Galvin, S., F. Boyle, et al. (2010). "Enumeration and Characterization of Antimicrobial-Resistant Escherichia coli Bacteria in Effluent from Municipal, Hospital, and Secondary Treatment Facility Sources." Applied and Environmental Microbiology **76**(14): 4772-4779.

Glaze, W. H., Y. Lay, et al. (1995). "Advanced oxidation processes. A kinetic model for the oxidation of 1,2-dibromo-3-chloropropane in water by the combination of hydrogen peroxide and UV radiation." Industrial & Engineering Chemistry Research **34**(7): 2314-2323.

Goni-Urriza, M., M. Capdepuy, et al. (2000). "Impact of an urban effluent on antibiotic resistance of riverine Enterobacteriaceae and Aeromonas spp." Applied and Environmental Microbiology **66**(1): 125-132.

Grady, C. P. L., G. T. Daigger, et al. (2011). Biological Wastewater Treatment, International Water Association.

Guardabassi, L., A. Petersen, et al. (1998). "Antibiotic resistance in Acinetobacter spp. isolated from sewers receiving waste effluent from a hospital and a pharmaceutical plant." Applied and Environmental Microbiology **64**(9): 3499-3502.

Heberer, T. (2002). "Tracking persistent pharmaceutical residues from municipal sewage to drinking water." Journal of Hydrology **266**(3–4): 175-189.

Heuer, H., E. Krögerrecklenfort, et al. (2002). "Gentamicin resistance genes in environmental bacteria: prevalence and transfer." FEMS Microbiology Ecology **42**(2): 289-302.

Hu, J. Y., Z. S. Wang, et al. (1999). "The effect of water treatment processes on the biological stability of potable water." Water Research **33**(11): 2587-2592.

Hu, L., H. M. Martin, et al. (2010). "Oxidation Kinetics of Antibiotics during Water Treatment with Potassium Permanganate." Environmental Science & Technology **44**(16): 6416-6422.

Huber, M. M., S. Canonica, et al. (2003). "Oxidation of Pharmaceuticals during Ozonation and Advanced Oxidation Processes." Environmental Science & Technology **37**(5): 1016-1024.

Iwane, T., T. Urase, et al. (2001). "Possible impact of treated wastewater discharge on incidence of antibiotic resistant bacteria in river water." Water Science and Technology **43**(2): 91-99.

Jarusutthirak, C. and G. Amy (2007). "Understanding soluble microbial products (SMP) as a component of effluent organic matter (EfOM)." Water Research **41**(12): 2787-2793.

Jones-Lepp, T. L., C. A. Sanchez, et al. (2010). "Method Development and Application To Determine Potential Plant Uptake of Antibiotics and Other Drugs in Irrigated Crop Production Systems." Journal of Agricultural and Food Chemistry **58**(22): 11568-11573.

Joss, A., E. Keller, et al. (2005). "Removal of pharmaceuticals and fragrances in biological wastewater treatment." Water Research **39**(14): 3139-3152.

Kemper, N. (2008). "Veterinary antibiotics in the aquatic and terrestrial environment." Ecological Indicators **8**(1): 1-13.

Khunjar, W. O. and N. G. Love (2011). "Sorption of carbamazepine, 17α-ethinylestradiol, iopromide and trimethoprim to biomass involves interactions with exocellular polymeric substances." Chemosphere **82**(6): 917-922.

Kinney, C. A., E. T. Furlong, et al. (2006). "Presence and distribution of wastewater-derived pharmaceuticals in soil irrigated with reclaimed water." Environmental Toxicology and Chemistry **25**(2): 317-326.

Klassen, N. V., D. Marchington, et al. (1994). "$H_2O_2$ determination by the $I_3^-$ method and by $KMnO_4$ titration." Analytical Chemistry **66**: 2921-2925.

Klavarioti, M., D. Mantzavinos, et al. (2009). "Removal of residual pharmaceuticals from aqueous systems by advanced oxidation processes." Environment International **35**(2): 402-417.

Koczura, R., J. Mokracka, et al. (2012). "Antimicrobial resistance of integron-harboring Escherichia coli isolates from clinical samples, wastewater treatment plant and river water." Science of The Total Environment **414**(0): 680-685.

Kolpin, D. W., E. T. Furlong, et al. (2002). "Pharmaceuticals, Hormones, and Other Organic Wastewater Contaminants in U.S. Streams, 1999−2000: A National Reconnaissance." Environmental Science & Technology **36**(6): 1202-1211.

Kümmerer, K. (2001). "Drugs in the environment: emission of drugs, diagnostic aids and disinfectants into wastewater by hospitals in relation to other sources – a review." Chemosphere **45**(6–7): 957-969.

LaPara, T. M., T. R. Burch, et al. (2011). "Tertiary-Treated Municipal Wastewater is a Significant Point Source of Antibiotic Resistance Genes into Duluth-Superior Harbor." Environmental Science & Technology **45**(22): 9543-9549.

Li, D., R. Qi, et al. (2011). "Bacterial community characteristics under long-term antibiotic selection pressures." Water Research **45**(18): 6063-6073.

Linden, K. G., O. S. Keen, et al. (2011). "Demonstrating advanced oxidation coupled with biodegradation for removal of carbamazepine." Water Environment Research Foundation final report for project INFR6SG09.

Linden, K. G., J. Thurston, et al. (2007). "Enhanced UV inactivation of adenoviruses under polychromatic UV lamps." Applied and Environmental Microbiology **73**(23): 7571-7574.

Lye, C. M., C. L. J. Frid, et al. (1997). "Abnormalities in the reproductive health of flounder *Platichthys flesus* exposed to effluent from a sewage treatment works." Marine pollution bulletin **34**(1): 34-41.

Ma, G. and N. G. Love (2001). "BTX Biodegradation in Activated Sludge under Multiple Redox Conditions." J Environ Eng (New York) **127**(6): 509-516.

Mack, J. and J. R. Bolton (1999). "Photochemistry of nitrite and nitrate in aqueous solution: a review." Journal of Photochemistry and Photobiology A: Chemistry **128**(1-3): 1-13.

Malik, A. and A. Aleem (2011). "Incidence of metal and antibiotic resistance in <b><i>Pseudomonas</i></b> spp. from the river water, agricultural soil irrigated with wastewater and groundwater." Environmental Monitoring and Assessment **178**(1): 293-308.

Mark, G., H.-G. Korth, et al. (1996). "The photochemistry of aqueous nitrate ion revisited." Journal of Photochemistry and Photobiology A: Chemistry **101**(2–3): 89-103.

McKnight, D. M., E. W. Boyer, et al. (2001). "Spectrofluorometric Characterization of Dissolved Organic Matter for Indication of Precursor Organic Material and Aromaticity." Limnology and Oceanography **46**(1): 38-48.

Metz, D. H., K. Reynolds, et al. (2011). "The effect of UV/H2O2 treatment on biofilm formation potential." Water Research **45**(2): 497-508.

Miller, M. P., D. M. McKnight, et al. (2006). "Hyporheic exchange and fulvic acid redox reactions in an alpine stream/wetland ecosystem, Colorado Front Range." Environmental Science & Technology **40**(19): 5943-5949.

Mopper, K. and C. A. Schultz (1993). "Fluorescence as a possible tool for studying the nature and water column distribution of DOC components." Marine Chemistry **41**(1-3): 229-238.

Neafsey, K., X. Zeng, et al. (2009). "Degradation of Sulfonamides in Aqueous Solution by Membrane Anodic Fenton Treatment." Journal of Agricultural and Food Chemistry **58**(2): 1068-1076.

Neta, P., P. Maruthamuthu, et al. (1978). "Formation and reactivity of the amino radical." The Journal of Physical Chemistry **82**(17): 1875-1878.

Ohno, T. (2002). "Fluorescence Inner-Filtering Correction for Determining the Humification Index of Dissolved Organic Matter." Environmental Science & Technology **36**(4): 742-746.

Painter, M. M., M. A. Buerkley, et al. (2009). "Antidepressants at environmentally relevant concentrations affect predator avoidance behavior of larval fathead minnows (Pimephales promelas)." Environmental Toxicology and Chemistry **28**(12): 2677-2684.

Paul, T., M. C. Dodd, et al. (2010). "Photolytic and photocatalytic decomposition of aqueous ciprofloxacin: Transformation products and residual antibacterial activity." Water Research **44**(10): 3121-3132.

Pomati, F., S. Castiglioni, et al. (2006). "Effects of a Complex Mixture of Therapeutic Drugs at Environmental Levels on Human Embryonic Cells." Environmental Science & Technology **40**(7): 2442-2447.

Pruden, A., R. Pei, et al. (2006). "Antibiotic Resistance Genes as Emerging Contaminants: Studies in Northern Colorado†." Environmental Science & Technology **40**(23): 7445-7450.

Rosario-Ortiz, F. L., S. P. Mezyk, et al. (2008). "Quantitative Correlation of Absolute Hydroxyl Radical Rate Constants with Non-Isolated Effluent Organic Matter Bulk Properties in Water." Environmental Science & Technology **42**(16): 5924-5930.

Rosario-Ortiz, F. L., S. A. Snyder, et al. (2007). "Characterization of the polarity of natural organic matter under ambient conditions by the Polarity Rapid Assessment Method (PRAM)." Environmental Science & Technology **41**(14): 4895-4900.

Rosenfeldt, E. J. and K. G. Linden (2004). "Degradation of Endocrine Disrupting Chemicals Bisphenol A, Ethinyl Estradiol, and Estradiol during UV Photolysis and Advanced Oxidation Processes." Environmental Science & Technology **38**(20): 5476-5483.

Rosenfeldt, E. J. and K. G. Linden (2007). "The ROH,UV concept to characterize and the model UV/H2O2 process in natural waters." Environmental Science & Technology **41**(7): 2548-2553.

Routledge, E. J., D. Sheahan, et al. (1998). "Identification of Estrogenic Chemicals in STW Effluent. 2. In Vivo Responses in Trout and Roach." Environmental Science & Technology **32**(11): 1559-1565.

Schmitt-Jansen, M., P. Bartels, et al. (2006). "Phytotoxicity assessment of diclofenac and its phototransformation products." Analytical and Bioanalytical Chemistry **387**(4): 1389-1396.

Sharma, V. K. (2008). "Oxidative transformations of environmental pharmaceuticals by Cl(2), ClO(2), O(3), and Fe(VI): Kinetics assessment." Chemosphere **73**(9): 1379-1386.

Sharpless, C. M. and K. G. Linden (2001). "UV photolysis of nitrate: Effects of natural organic matter and dissolved inorganic carbon and implications for UV water disinfection." Environmental Science & Technology **35**(14): 2949-2955.

Shuali, U., M. Ottolenghi, et al. (1969). "On the photochemistry of aqueous nitrate solutions excited in the 195-nm band." Journal of Physical Chemistry **7**: 111-122.

Snyder, S. A., S. Adham, et al. (2007). "Role of membranes and activated carbon in the removal of endocrine disruptors and pharmaceuticals." Desalination **202**(1–3): 156-181.

Stackelberg, P. E., E. T. Furlong, et al. (2004). "Persistence of pharmaceutical compounds and other organic wastewater contaminants in a conventional drinking-watertreatment plant." Science of The Total Environment **329**(1-3): 99-113.

Stedmon, C. A., S. Markager, et al. (2003). "Tracing dissolved organic matter in aquatic environments using a new approach to fluorescence spectroscopy." Marine Chemistry **82**: 239-254.

Steger-Hartmann, T., R. Länge, et al. (1999). "Environmental Risk Assessment for the Widely Used Iodinated X-Ray Contrast Agent Iopromide (Ultravist)." Ecotoxicology and Environmental Safety **42**(3): 274-281.

Storteboom, H., M. Arabi, et al. (2010). "Tracking Antibiotic Resistance Genes in the South Platte River Basin Using Molecular Signatures of Urban, Agricultural, And Pristine Sources." Environmental Science & Technology **44**(19): 7397-7404.

Sunkara, M. and M. J. M. Wells (2010). "Phase II pharmaceutical metabolites acetaminophen glucuronide and acetaminophen sufate in wastewater." Environmental Chemistry **7**: 111-122.

Ternes, T. A. and R. Hirsch (2000). "Occurrence and Behavior of X-ray Contrast Media in Sewage Facilities and the Aquatic Environment." Environmental Science & Technology **34**(13): 2741-2748.

Ternes, T. A., M. Meisenheimer, et al. (2002). "Removal of Pharmaceuticals during Drinking Water Treatment." Environmental Science & Technology **36**(17): 3855-3863.

Toze, S. (2006). "Reuse of effluent water—benefits and risks." Agricultural Water Management **80**(1–3): 147-159.

United States Environmental Protection Agency (2006). "Ultraviolet disinfection guidance manual for the final long term 2 enhanced surface water treatment rule." **EPA 815-R-06-007**.

Vajda, A. M., L. B. Barber, et al. (2008). "Reproductive disruption in fish downstream from an Estrogenic wastewater effluent." Environmental Science & Technology **42**(9): 3407-3414.

Vaughan, P. P. and N. V. Blough (1998). "Photochemical formation of hydoxyl radical by constituents of natural waters." Environmental Science & Technology **32**(19): 2947-2953.

Wammer, K. H., T. M. Lapara, et al. (2006). "Changes in antibacterial activity of triclosan and sulfa drugs due to photochemical transformations." Environmental Toxicology and Chemistry **25**(6): 1480-1486.

Warburg, E. (1918). "The energy conversion in photochemical procedures. VIII The photolysis of aqueous solutions and the equivalent photochemical law." Sitzungsberichte der Koniglich Preussischen Akademie der Wissenschaften **Part 2**: 1228-1246.

Watkinson, A. J., G. B. Micalizzi, et al. (2007). "Antibiotic-resistant Escherichia coli in wastewaters, surface waters, and oysters from an urban riverine system." Applied and Environmental Microbiology **73**(17): 5667-5670.

Weishaar, J. L., G. R. Aiken, et al. (2003). "Evaluation of specific ultraviolet absorbance as an indicator of the chemical composition and reactivity of dissolved organic carbon." Environmental Science & Technology **37**(20): 4702-4708.

West, B., P. Liggit, et al. (2011). "Antibiotic Resistance, Gene Transfer, and Water Quality Patterns Observed in Waterways near CAFO Farms and Wastewater Treatment Facilities." Water, Air, & Soil Pollution **217**(1): 473-489.

Westerhoff, P., G. R. Aiken, et al. (1999). "Relationship between the stucture of natural organic matter and its reactivity towards molecular ozone and hydroxyl radicals." Water Research **33**(10): 2265-2276.

Wu, C., A. L. Spongberg, et al. (2010). "Uptake of Pharmaceutical and Personal Care Products by Soybean Plants from Soils Applied with Biosolids and Irrigated with Contaminated Water." Environmental Science & Technology **44**(16): 6157-6161.

Yang, X., R. C. Flowers, et al. (2011). "Occurrence and removal of pharmaceuticals and personal care products (PPCPs) in an advanced wastewater reclamation plant." Water Research **45**(16): 5218-5228.

Zarifiou, O. C. and R. Bonneau (1974). "Wavelength-dependent quantum yield of OH radical formation from photolysis of nitrite ion in water." Photochemistry and Photobiology **45**(S1): 723-727.

Zellner, R., M. Exner, et al. (1990). "Absolute •OH quantum yields in the laser photolysis of nitrate, nitrite and dissolved H2O2 at 308 and 351 nm in the temperature range 278-353 K." Journal of atmospheric chemistry **10**: 411-425.

Zepp, R., J. Hoigné, et al. (1987). "Nitrate-induced photooxidation of trace organic chemicals in water." Environmental Science & Technology **21**(5): 443-450.

Zhang, X., K. D. Oakes, et al. (2010). "Tissue-Specific In Vivo Bioconcentration of Pharmaceuticals in Rainbow Trout (Oncorhynchus mykiss) Using Space-Resolved Solid-Phase Microextraction." Environmental Science & Technology **44**(9): 3417-3422.

Zhang, Y., C. F. Marrs, et al. (2009). "Wastewater treatment contributes to selective increase of antibiotic resistance among Acinetobacter spp." Science of The Total Environment **407**(12): 3702-3706.